Encapsulation of pancreatic beta cells

by

Niusha Nikravesh

A thesis submitted to the
University of Birmingham
for the degree of
DOCTOR OF PHILOSOPY

School of Chemical Engineering
College of Engineering and Physical Sciences
University of Birmingham
May 2017

UNIVERSITY^{OF} BIRMINGHAM

University of Birmingham Research Archive

e-theses repository

Abstract

Immunoisolation of pancreatic beta cells is a promising approach for the treatment of type I diabetes. In this thesis, a vibrating nozzle technology was utilised to reproducibly generate 1% alginate microparticles with an average diameter of 200 $\mu m\pm19$ S.D. This technology further enabled the application of fluidised bed bioreactor owing to high uniformity of particles, an important parameter for achieving homogeneous fluidisation. Experimental data collected from the cultivation of cells in fluidised culture was shown to provide a promising solution for handling encapsulated cells from manufacturing phase to clinical sites, which is currently a challenging issue for cell-based therapies. A reduction in beta cells insulin-secreting ability was observed after two weeks of static culture. This problem was addressed by investigating a 3-dimentional culturing technique and a novel polyelectrolyte multilayer (PEM) coating approach. Concave agarose micro-wells were used to culture robust pancreatic beta cell spheroids that enhanced cell-cell contact. Additionally, the novel PEM coating using Ca^{2+} pre-conditioning improved cell function while providing immunoisolation from cytokines, and reducing the total volume of the graft. This work presented an effective immunoisolation and culturing system to improve cells survival rate, which hopes to bring a closer step towards therapeutic transplantation.

To my beloved parents

Shirin and Hamid, who believed in me and offered me unconditional support

and to the memories of my grandfather Saleh Momayezi (1937-2016)

a kind-hearted man whom I miss every day.

Acknowledgments

First and foremost, I would like to express my sincere gratitude to my supervisor Professor Liam Grover, and to my co-supervisor Dr Sophie Cox, for their continuous support, guidance, and patience throughout my PhD. Thank you for providing me with the facilities to develop this project, and for advising me on how to approach research with an open mind.

Besides my supervisors, I would like to extend my appreciation to the other members of the tissue regeneration and interface lab, especially Dr Gurpreet Birdi who trained me in cell culture, and Dr Richard Williams for his assistance with confocal microscopy. Many thanks to Dr Marianne Ellis for the supply of fluidised system employed in this study.

I would like to acknowledge the University of Birmingham for providing me with a spectacular opportunity to perform my PhD project during the last three years.

Finally, I would like to thanks my wonderful parents for their encouragement through this process and for their unwavering support throughout my life.

Table of contents

List of Figures

List of Tables

List of abbreviations

3D three-dimensional

ALG alginate

APA alginate-poly amino acids-alginate

ATP adenosine triphosphate

BSA bovine serum albumin

Calcein AM calcein acetoxtmethylester

CLSM confocal laser scanning microscopy

DMEM Dulbecco's modified eagle medium

ECM extracellular matrix

ELISA enzyme-linked immunosorbent assay

FBS fetal bovine serum

G alpha-L-glucuronic acid

GLUT glucose transporter

GSIS glucose stimulated insulin secretion

HBSS Hank's balanced salt solution

hESCs human embryonic stem cells

IDF international diabetes federation

IEQ islet equivalent

ihPSCs human induced pluripotent stem cells

IL-1β interleukin-1-beta

INF-γ interferon- gamma

iNOS inducible nitric oxide synthase

KRBH Krebs-Ringer bicarbonate buffer

LBL layer-by-layer

M beta-D-mannuronic acid residues

NO nitric oxide

PAA polyacrylic acid

PAH polyallylamine hydrochloride

PAN-PVC polyvinyl chloride and polyacrylonitrile co polymer

PBS phosphate buffer saline

PEG polyethylene glycol

PEG-PLGA polyethylene glycol and poly-lactic-co-glycolic acid

PEM polyelectrolyte multilayer

PI propidium iodide

PLL poly-l-lysine

PLO poly-l-ornithine

PO$_2$ oxygen partial pressure

PSCs pluripotent stem cells

PSS polystyrene sulfonate

PVA polyvinyl alcohol

SI secreted index

STR stirred-tank reactor

T1D type 1 diabetes

T2D type 2 diabetes

TNF- α tumour necrosis factor- alpha

1 CHAPTER ONE

Introduction

The pancreas is a complex organ consisting of several different types of endocrine and exocrine cells, among which pancreatic beta cells are responsible for secreting insulin to maintain normoglycaemia throughout the individual's life [1]. Secretion of insulin plays a crucial role in the regulation of blood glucose levels after consumption of food. In patients with type I diabetes, however, immune cells start to destroy the insulin-secreting beta cells within the endocrine section of the pancreas, known as pancreatic islets [2]. Over a few years, this autoimmune reaction results in complete loss of beta cells mass and hence elevates the blood glucose level (> 7.0 mmol/L)[3].

Currently, insulin therapy is the most common treatment for type I diabetes. Maintaining normal blood glucose levels using exogenous insulin, however, requires several daily injections and frequent blood glucose monitoring [4-6]. Despite the relative success of insulin therapy to improve patient's quality of life, repeated incidents of hypoglycaemia and hyperglycaemia in these patients can lead to complications in many parts of the body later in life. The most common possible secondary complications associated with diabetes are kidney failure, leg amputation, blindness, and nerve damage [7, 8].

In the search for an alternative to insulin therapy, transplantation of isolated pancreatic islets from cadaveric donors was reported in 1974 [9, 10]. Major challenges facing the transplantation of the whole pancreas or isolated pancreatic islets are the invasive surgical procedure, the lack of sufficient donors, the reduced function of transplanted tissue within a short time post-transplantation, and the requirement for long-term immunosuppressive drugs. Since the administration of an immunosuppressant is a significant hindrance for type I

diabetes, currently pancreatic transplantation is only available for patients receiving kidney transplantation at the same time [4, 7].

To address the problem with the administration of immunosuppressant drugs, cell encapsulation has emerged to provide a strategy for immunoprotection of pancreatic islets [11, 12]. In the last two decades, significant interest has been developed in the application of microencapsulation technology for cell-based therapies [13]. Primarily, in an encapsulated system, a semi-permeable polymeric membrane surrounds a single or small group of cells [14, 15]. This approach could be a promising alternative to achieve real-time blood glucose regulation by transplanting microencapsulated insulin secreting cells within a polymeric microcarrier [5]. The semi-permeable membrane should allow bi-directional diffusion of oxygen, nutrients and cell products [10, 16]. It should also provide an immunoisolated environment for the protection of pancreatic beta cells from the host's cytokines and T-cells, which have been reported to be responsible for the destruction of pancreatic beta cells [17, 18].

The first reported encapsulation of pancreatic islets dates back to the 1980s to the work of Lim and Sun who encapsulated beta cells within alginate capsules [19]. Since then, the clinical application of this method has been impeded by several issues, including poor revascularisation of the encapsulated cells after implantation, and the large diameter of microcapsules typically within 400-800 μm, which results in the large graft volume compared with the size of transplantation site [10, 20]. Moreover, the large size of the capsules expressly leads to an unfavourable gap between encapsulated cells and the surrounding tissues,

followed by insufficient transfer of nutrients, the occurrence of hypoxia, and ultimately cell dysfunction and death [10, 13].

The challenges mentioned above in connection with encapsulated pancreatic beta cells are also linked to other cell-based encapsulation strategies. The future of transplantation using encapsulated cells appears assuring; however, their use as a regular therapeutic procedure requires a better understanding of cell responses within the encapsulated environment. These approaches include defeating host rejection by providing complete immunoisolation of encapsulated cells even from small molecules, such as cytokines. Furthermore, long-term viability and function of encapsulated cells might be obtained using engineering concepts to overcome mass transport limitations. Henceforward, the success of cell-based therapies massively depends on an eclectic mix of biological and engineering strategies to overcome the present obstacles within this field.

2 CHAPTER TWO

Type I diabetes

2.1 Diabetes

Diabetes is a chronic endocrine disease characterised by high glucose level in the blood (hyperglycaemia) [21]. According to the international diabetes federation (IDF), it has been estimated that by 2040, 642 million people will suffer from diabetes meaning that one in ten adults will be diagnosed with this disorder [22]. Diabetes can be categorised into two distinct diseases regarding their cause. Type 1 diabetes (T1D) is an autoimmune disease that is caused by the destruction of pancreatic beta cells by the host's immune cells [1, 8, 12]. On the other hand, type 2 diabetes (T2D) is generally associated with obesity and insulin resistance in tissues, such as fat, liver, and muscle. In this case, continuously high blood glucose level exceeds the capacity of pancreatic beta cells to secrete a sufficient insulin in response to the existing high demand and hence it leads to the failure of beta cells to function normally [2, 23, 24].

T1D mostly develops in childhood, and it is also known as juvenile's diabetes. The UK has the world's fifth-highest rate of children aged $0 - 14$ years diagnosed with T1D and it place a tremendous financial burden on both the government and individuals [1, 23, 25]. Up to now the exact aetiology of T1D has been remained elusive, and a combination of genetic vulnerability and environmental factors are believed to be responsible for the occurrence of this autoimmune disorder [12, 26].
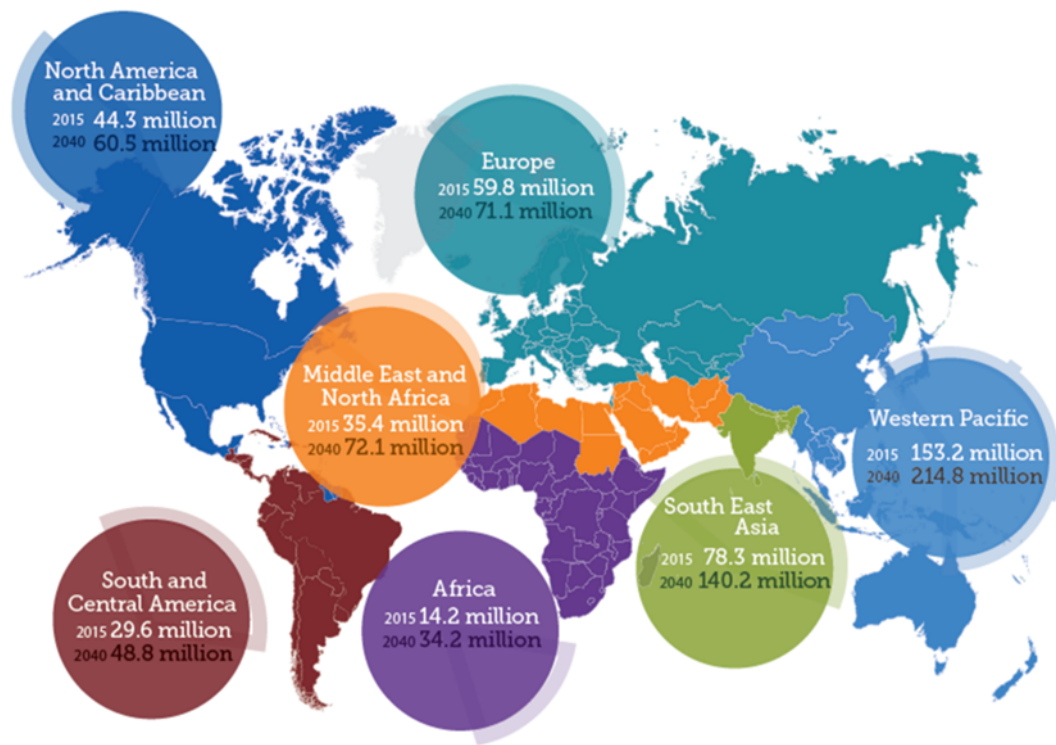
Figure 2-1
Estimation of people with diabetes, indicating the rapid prevalence of diabetes worldwide [27].

The life of T1D patients are completely dependent on the permanent administration of insulin and apart from recent achievements in formulating more effective exogenous insulin, maintaining normal blood glucose levels during the day remains a big challenge for patients. More importantly, frequent high blood glucose levels can lead to secondary complications, including cardiovascular and kidney disease, blindness, lower limb amputation, and even death [1, 12, 26]. Providing minute-to-minute blood glucose regulation can prevent such late complications and hence improve patients' quality of life. As a result, it has become a chief motivation for many researchers to find alternative treatments for T1D using approaches,

such as tissue engineering and pancreatic beta cell regeneration by renewable sources, including stem cells [18, 28].

2.2 Current treatments

Currently, there are two main therapeutic approaches for type I diabetics: **1)** insulin therapy, and **2)** pancreatic islet transplantation.

2.2.1 Insulin therapy

Prior to insulin therapy, T1D patients were placed on an extreme diet and consumed fewer than 500 calories per day, which resulted in a large number of deaths from diabetic coma and infectious diseases [29]. Treatment was revolutionised in 1921 after the discovery of insulin by Banting and Best. This discovery was followed by the first successful treatment of a T1D patient using insulin administration [29, 30]. Since then, insulin therapy has become the most common treatment, which typically involves 3-5 self-injections of insulin during the day. For T1D patients, a decision on the amount of insulin required to maintain normoglycaemia during the day depends on frequent monitoring of blood glucose level [4, 6].

Despite the success of insulin therapy to enhance the life expectancy of patients with T1D, it is still difficult to tightly control blood glucose level as many factors, such as diet, the level of physical activity can affect insulin requirement. Consequently, treatment based on insulin therapy is often complicated by incidents of hypoglycaemia and hyperglycaemia. Hypoglycaemia (low blood glucose) can cause reduced cognitive abilities, unconsciousness, and even death, while hyperglycaemia (high blood glucose) can lead to kidney disease, heart

attack, nerve damage and blindness [2, 7, 8, 12]. These abrupt changes in blood glucose level can increase the risk of diabetes complications. The severity of these complications emphasises the necessity of alternative treatments for patients suffering from T1D.

2.2.2 Pancreatic islet transplantation

Another treatment for T1D is pancreatic islet transplantation, which is currently only performed for T1D patients under severe conditions with frequent incidences of hypoglycaemia and those who have already received kidney transplantation [31, 32]. Since 2000, transplantation of pancreatic islets has been conducted according to the Edmonton protocol for collection, digestion, and purification of islets of Langerhans [5, 23, 33]. Isolated islets from cadaveric donors can then be infused into a vascularised organ, mostly through the hepatic portal vein in the liver [32] (Figure 2-2).
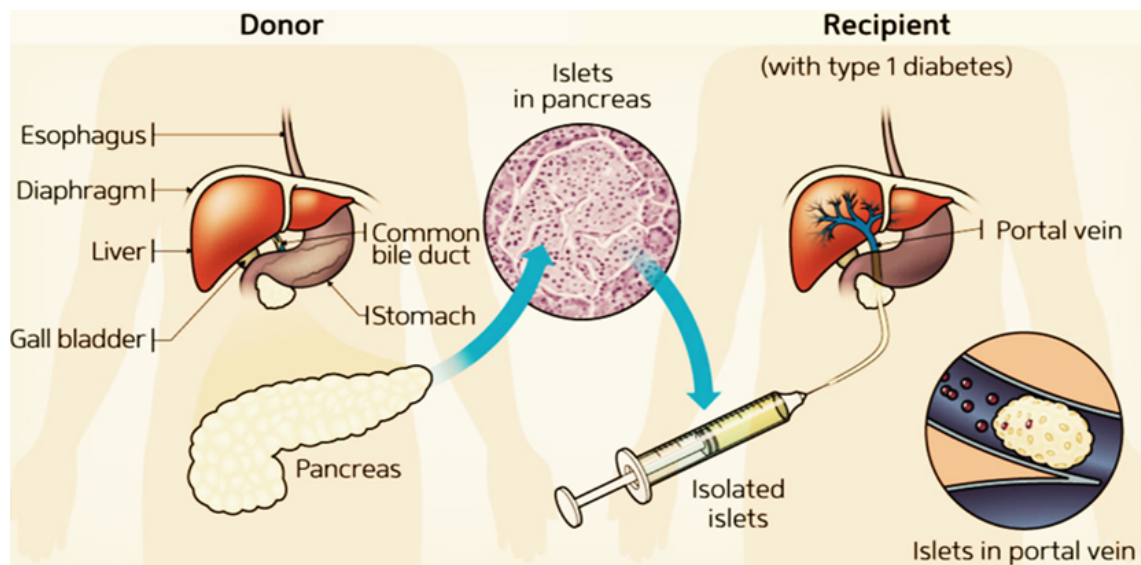
Figure 2-2
Schematic representation of pancreatic islets transplantation [34].

Even though islet transplantation can result in insulin independence for type I diabetics and requires less invasive surgery than other major transplantations, the successful clinical application of this approach has been limited by several major issues [18]. Notably, during isolation of pancreatic islets, cells lose their vascularised network as well as their extracellular matrix (ECM) connection with other cells and this reduces the levels of viability in the harvested cells. Therefore approximately 2-3 donors are required for each patient receiving an islet transplant [18, 23]. This places an upper limit on the number of patients that can receive this therapy, and hence more studies are required to increase the efficacy of islet isolation as well as regeneration of pancreatic beta cells using alternative approaches, such as stem cell administration [26]. Another major problem is the need for life-long immunosuppressive drugs, which can make patients more vulnerable to infectious disease. Moreover, studies have shown that immunosuppressive agents can affect islet functionality and revascularisation [23, 32]. To address these issues, immunoisolation of pancreatic islets

utilising encapsulation strategies, which is the primary focus of this thesis, can be a promising approach for protecting cells against immune responses and hence eliminating the need for immunosuppressive drugs [11, 12, 35]

2.3   Architecture of the pancreas

The pancreas is an abdominal organ surrounded by the liver, spleen, and small intestine. This organ with a size of approximately 15 cm consists of endocrine and exocrine compartments [36, 37] (Figure 2-3). The function of cells within the exocrine tissue, which connects to the small intestine through a system of ducts, is to synthesis and secrete digestive enzymes, such as trypsinogen, pancreatic lipase, and amylase [38]. While, the endocrine cells (pancreatic islets) comprises four main different cell types, each responsible for the secretion of a specific hormone, including glucagon producing α-cells, insulin producing β-cells, somatostatin producing γ-cells, and pancreatic polypeptide secreting PP-cells [39, 40]. Each islet contains approximately 1000-2000 single cells. After the discovery of pancreatic islets by Paul Langerhans in 1869, they have been named "islet of Langerhans" [36] and in diabetes research, an islet with an average diameter of 150 μm is regarded as a standard islet equivalent (IEQ) [40, 41]. Among different cells in pancreatic islets, beta cells are the only cells responsible for the secretion of insulin. Also, studies on pancreatic islets have shown that there is a difference in the morphology of islets between species. For instance, in rodents, beta cells are mostly located in the core of islets and surrounded by other non-insulin secreting cells, whereas, human islets are characterised by close contact between α and β cells [36, 39].
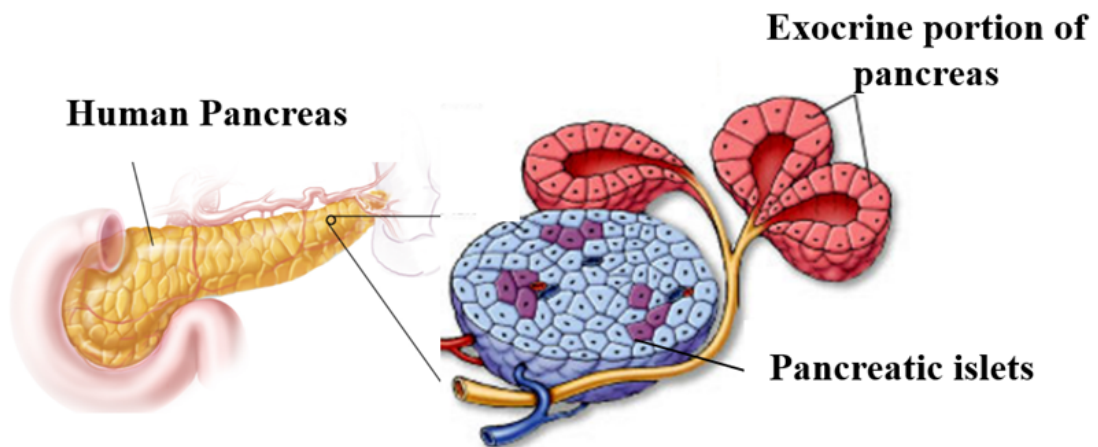
Figure 2-3
Schematic representation of pancreas, adapted from [42, 43].

Moreover, these specific three-dimensional (3D) islets contain dense fenestrated microvascular networks, and consequently the blood flow to the islets is nearly ten times more than the blood flow to the exocrine pancreas. This high level of vascularisation enables proper oxygenation and helps facilitate the ability of beta cells to sense changes in blood glucose levels [37, 44, 45]. Notably, the secretion of insulin from pancreatic beta cells relies on various factors, including the availability of nutrients, hormones, parasympathetic neurons (for activating specific receptors to induce glucose stimulated insulin response), sympathetic neurons (for prohibition of insulin secretion), and finally regulatory signals from other tissues, such as the liver, fat, endocrine intestine cells, and the gut [45-47].

2.4 Insulin structure

Insulin is a small polypeptide secreted from pancreatic beta cells and plays an important role in the regulation of blood glucose level [37]. In 1926, the 3D structure of insulin with a

molecular size of 5,805 Da was discovered by means of x-ray crystallography [37, 48]. An insulin molecule is composed of 51 amino acids divided between two chains. The "A chain" is made up from 21 amino acids, while the "B chain" contains 30 amino acids. The two chains are linked by two disulphide bonds [49]. Additionally, a third disulphide bond exists within the A chain (Figure 2-4). Insulin is stored in pancreatic beta cells within clusters known as "insulin granules". Mouse beta cells contain approximately 13,000 insulin granules. Among these granules, only a small portion of them (1%) is instantly accessible for release, whereas, the remaining insulin granules will be stored as a reservoir. [2, 37, 44].
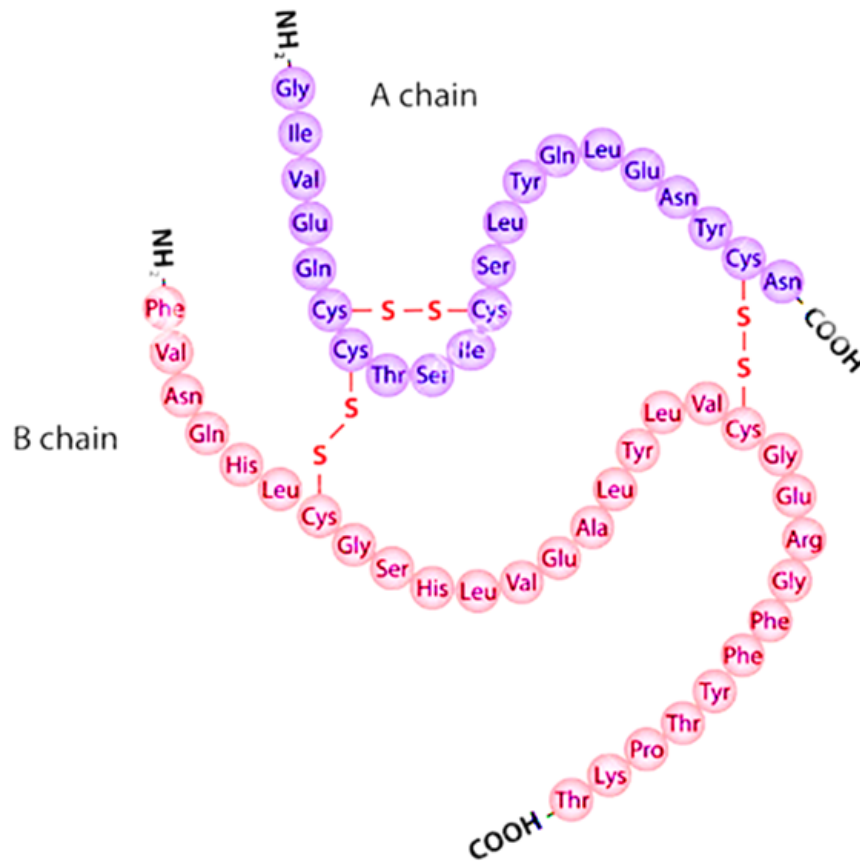
Figure 2-4
Structure of human insulin composed of 51 amino acids [50].

2.5   Insulin secretion mechanism

A rise in blood glucose level (> 7-10 mM) stimulates the secretion of insulin from pancreatic beta cells [49, 51]. The initiation of insulin secretion relies on various glucose sensors for measuring the level of circulating glucose. Notably, among several glucose transporters in different mammalian cells (GLUT 1- GLUT 13), glucose transporter 2 (GLUT-2) is the only transporter expressed in pancreatic beta cells for glucose entry [37, 49]. As illustrated in Figure 2-5, After uptake of glucose into beta cells, it is metabolised through glycolysis, and

mitochondria to produce adenosine triphosphate (ATP), which plays an important role in insulin secretion by controlling ATP-sensitive potassium channels (K_{ATP}) [49].

At high glucose concentrations (> 5 mM), rise in ATP leads to closure of K_{ATP} channels. This reaction is continued by depolarisation of the cell membrane, followed by an increase in Ca^{2+} influx through voltage-dependent calcium ion channels, and finally it results in the release of insulin from stored granules due to exocytosis [1, 37, 49]. On the contrary, at low blood glucose levels, K_{ATP} channels open and cause K^+ to flow out through the membrane, which then inhibits the influx of Ca^{2+} and insulin secretion (Figure 2-5). Therefore, the mechanism of insulin secretion at a cellular level mainly occurs by linking cell metabolism to the membrane potential [1, 22].
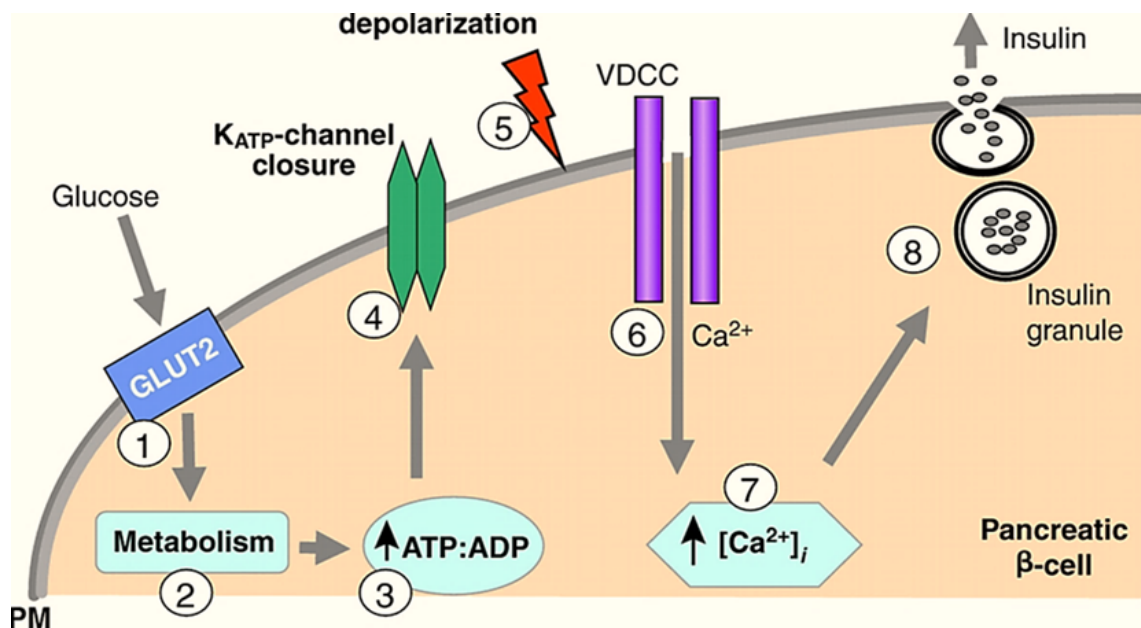
Figure 2-5
Secretion of insulin from pancreatic beta cells. (1) Uptake of insulin into beta cells through glucose transporter 2, (2,3) glucose is metabolised to generate ATP, (4,5) increase in ATP causes closure of the K_{ATP} channel, followed by depolymerisation of beta cell membrane, (6,7) initiation of Ca^{2+} channels, (8) release of insulin by exocytosis [22].

2.6   Inflammatory cytokines

Despite limited understanding of the T1D aetiology and its unknown triggers, in recent year further understanding has been developed as to the mechanism of pancreatic beta cell death [52]. At diagnosis of T1D, the majority of pancreatic beta cells are destroyed and total beta cells mass could reduce to nearly 70-80% of that in a healthy individual. Notably, studies have shown that in humans, beta cells dysfunction and death can be developed over several years, and this phase of T1D progression is known as insulitis [53, 54].

T1D as an autoimmune disease is mediated with the invasion of activated T-cells and macrophages [37]. In the early stage of T1D, immune cells penetrate into pancreatic islets and induce beta cells apoptosis and dysfunction as a result of secreting inflammatory cytokines [53]. Previous studies have shown that exposure of beta cells to three specific inflammatory cytokines: Interleukin-1- beta (IL-1β), Interferon- gamma (INF-γ), and tumour necrosis factor-alpha (TNF- α) could be the most important reason in beta cells death and thus insufficient secreted insulin [53, 55]. These inflammatory cytokines damage beta cells via certain receptors by activating signalling pathways, which result in expression of inducible nitric oxide synthase (iNOS). Consequently, the overexpression of iNOS leads to the production of nitric oxide (NO) [37]. Therefore, high concentrations of NO can reduce transcriptional factors that are known to be crucial to beta cells function and differentiation [52, 54, 55].

3 CHAPTER THREE

CELL-BASED REGENERATIVE MEDICINE

3.1 New treatments for type 1 diabetes

Based on the limits associated with the current pancreatic islets transplantation highlighted in section 2.2.2, and the inefficiency of insulin therapy in providing stable blood glucose regulation, various cell-based therapies for T1D have been investigated during the past three decades. This chapter reviews recent achievements and challenges in beta cell regeneration using cells, and polymeric immunoisolation devices for protecting transplanted cells from the host's immune response.

3.1.1 Regeneration of human pancreatic beta cells

Using the current Edmonton protocol, transplantation of pancreatic islets for one patient requires the isolation of islets from two to three donors. Consequently, the demand for human pancreatic donors vastly exceeds the supply, and this shortage impedes the clinical application of this treatment for all T1D patients. Therefore strategies that enable the regeneration of beta cells from other sources could become a promising approach to address the lack of donated pancreases [18, 56].

Pluripotent stem cells (PSCs) have been explored as an alternative to beta cells as a consequence of their capability to develop into any cell type [2]. Predominantly, differentiation of human embryonic stem cells (hESCs), human induced pluripotent stem cells (ihPSCs), and human pancreatic epithelial cells into beta cells have been studied [2, 57]. However, so far beta cells produced using stem cells typically lack complete function both *in vitro* and *in vivo*, and are unable to provide the exact granular ultrastructure of insulin [57]. In

addition, the clinical application of this approach has been hindered by the risk of tumour development after transplantation, and the current ethical issues in the application of embryonic stem cells [6].

In 2016, research by the Melton lab at Harvard stem cell institute led to the production of new beta cells, which compared with the previously reported studies, were closer to mature human pancreatic beta cells based on their ability to secrete insulin in response to glucose stimulation *in vitro* [58]. Although further progress in the current differentiation protocols is a requisite to achieve functional and reproducible human pancreatic beta cells, success in using this approach could provide an unlimited source for generation of insulin producing cells for transplantation. In the longer term, this could overcome a major obstacle in the clinical application of pancreatic transplantation as a standard treatment for T1D.

3.1.2 Beta cell immunoisolation

Even with the possibility of utilising stem cells to overcome the insufficiency of pancreatic donors, the requirement for life-long immunosuppressive drugs remains challenging. Immunosuppression increases the risk for the development of infectious disease, as well as reducing transplanted cell survival [12, 13]. An alternative approach to prevent graft failure and the need for toxic immunosuppressive drugs could be beta cell immunoisolation [5]. The immunoisolation of beta cells require that, a semi-permeable membrane be utilised to protect the encapsulated cells from direct contact with host's immune system. This enables the protection of cells from both allograft and xenograft rejection, as well as autoimmune rejection related to T1D [59]. Moreover, apart from protecting the encapsulated cells from

the surrounding environment by restricting their contact with cytotoxic T-cells and inflammatory cytokines, the encapsulated material should allow the free passage of oxygen, nutrients, insulin and other cell products and wastes [12, 18] (Figure 3-1). Since the first attempt in the 1960s to encapsulate cells in a semi-permeable polymeric membrane there have been many attempts to immunoisolate cells, which can be broadly divided into two approaches, macroencapsulation and microencapsulation [17, 59].
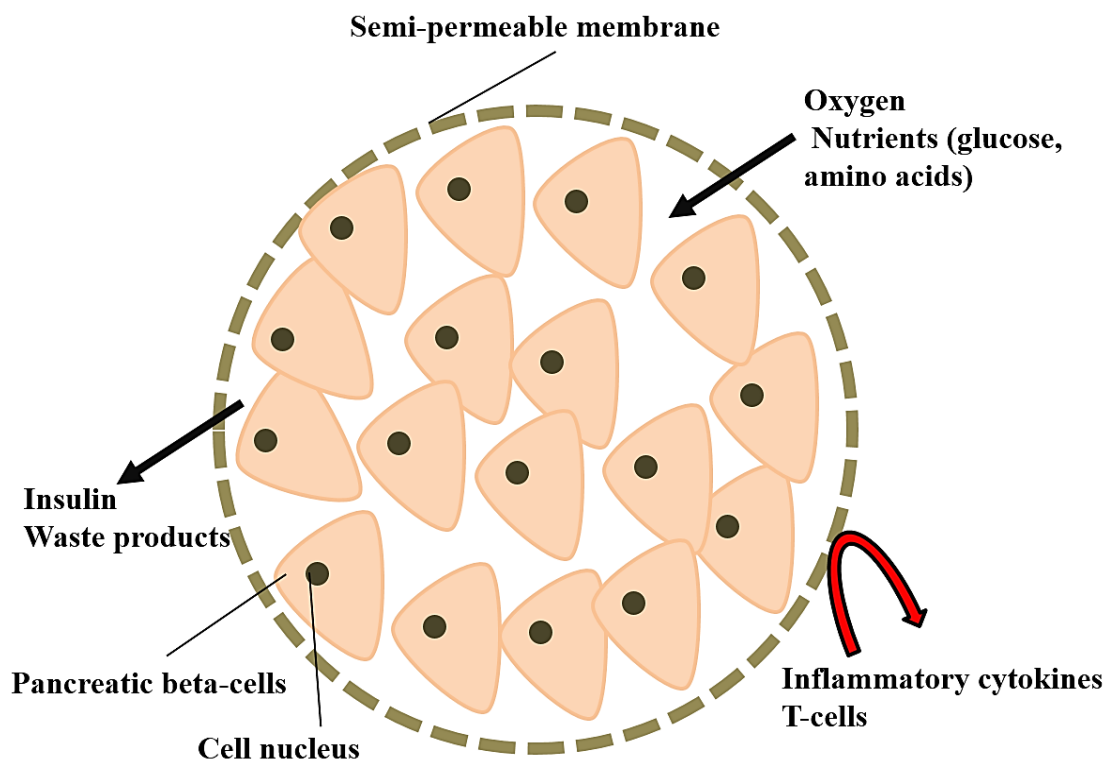
Figure 3-1

Schematic illustration of immunoisolated pancreatic beta cells within a semi-permeable membrane. The polymeric semipermeable membrane allows transfer of oxygen and nutrients, while protects the inner cells by restricting entry of immune cells.

3.1.2.1 Macroencapsulation

Macroencapsulation devices are relatively large capsules, which are typically a few millimetres to several centimetres in length [12]. The large size of the capsule means that, macro-devices have the potential to embed a large number of cells. These devices can be manufactured with various geometries, including, hollow fibres and hydrogel sheets [26]. An important advantage of these macro-carriers is the simple retrieval of encapsulated devices after implantation [12]. This allows for evaluation of viability and removal if they are failing to function. There are two classes of macro-encapsulation devices, which are classified on the basis of whether they are connected to the host's blood circulation: (**1**) extravascular, and (**2**) intravascular devices [12, 29].

3.1.2.1.1 Extravascular devices

Extravascular devices are implanted outside the vasculature, which reduces surgical risk during implantation in comparison with intravascular devices [12]. For implantation of extravascular devices in both human and animal models (rats, and monkeys), the peritoneal cavity and subcutaneous sites have been most commonly used [29]. So far, different natural or synthetic materials including, a copolymer of sodium methyl sulfonate and acrylonitrile (AN69) [59], a copolymer of polyvinyl chloride and polyacrylonitrile (PAN-PVC) [26], agarose, and polyvinyl alcohol have been used for manufacturing these macro-devices [12].

Despite partial success in using extravascular devices in maintaining normoglycaemia (between 2 to 9 weeks) without immunosuppressive drugs, several major drawbacks remain which make their application less favourable. These limitations are mainly related to the occurrence of large pancreatic islet clusters within the macro-capsule. These large clusters are

prone to cell necrosis due to limited diffusion of nutrients and oxygen to the islets located at the centre of the clusters. Moreover, the relatively slow response of pancreatic beta cells to changes in glucose concentration (>20 min), linked to the size of this extravascular devices, is another obstacle for their clinical application [12, 26].

3.1.2.1.2 Intravascular devices

Intravascular devices were created to overcome the mass transport limitations associated with extravascular devices. As the name suggests, intravascular macro-devices are implanted directly into the arterial vessel, hence they have the advantage of being connected to the patient's blood circulating system [29]. This results in increased diffusion of oxygen and glucose to the encapsulated islets when compared with extravascular macro-devices [12, 18, 26].

In 1977, Chick, *et al*. developed the first PAN-PVC hollow fibre intravascular device for transplantation of pancreatic beta cells in a diabetes-induced rat [59]. Their studies showed the potential of intravascular devices to reduce blood glucose level due to an increase in the concentration of plasma insulin for 14 days before the development of blood coagulation [59]. Since then, similar results have been reported, which demonstrate that the majority of technologies are not efficacious because of surgical risk during implantation and the occurrence of thrombosis, especially at the interface between the implanted membrane and the host's blood vessel [17]. Consequently, using this method requires anticoagulation therapy drugs, which are not recommended for people with type I diabetes [26].

3.1.2.2 Microencapsulation

The advent of micro technology for encapsulating enzymes in 1964, led to the broader application of this technology for cell-based therapeutic research [5]. In general, microcapsules provide a semipermeable polymeric structure with the size of 200-1500 μm for enveloping single or small clusters of cells [60]. The spherical shape and small dimension of microcapsules present several advantages compared with the macrocapsules mentioned earlier [11]. Firstly, microparticles have a large surface area to volume ratio that enhances the transport of nutrients and oxygen to the encapsulated cells [29]. Secondly, the small diameter of these particles require less invasive surgery and even for particles in the range of 200-600 μm, the transplantation of encapsulated microcapsules could be achieved through injection of particles to the desired transplantation site [17]. Finally, in the case of any microcapsule rupture, only a small group of encapsulated cells will become exposed to the host's immune cells, meaning that only a few cells will be destroyed and the remaining encapsulated cells would be unaffected. This makes these cell carrier devices more favourable compared to macroencapsulated devices [29].

The first relatively successful attempt in encapsulating pancreatic beta cells in alginate microparticles and their transplantation into the peritoneal cavity of a diabetic rat was reported by Lim and Sun in 1980 [19]. Since then, the application of microcapsules for protecting pancreatic beta cells in search of an alternative treatment for T1Ds has become a promising technique [17, 61]. Up to now, a range of materials and methods have been investigated for microencapsulation. In addition to several studies on animal models, there have been reports of short-term clinical success in humans. For instance, in 1994 Soon-Shiong

et al. [62] reported transplantation of encapsulated pancreatic islets within alginate microcapsules for a patient with T1D who had already received kidney transplantation. Their study resulted in nearly 9 months of insulin independence, however, this result was achieved while the patient was on a low dose of immunosuppressive drugs [62]. More examples of pancreatic islet microcapsules for transplantation in both human and animal models is presented in Table 3-1.

Table 3-1: Summary of human and animal trials in transplantation of encapsulated pancreatic islets.

Biomaterial	Particles size (μm)	Cell source (donor-recipient)	Site	Outcomes	Refs
Alginate-PLO-alginate	500	Allograft (human-human)	Peritoneum	- study duration: 6 months - increase in C-peptide levels - reduction in exogenous insulin administration	[63]
Ba^{2+}-alginate	340	Allograft (human-human)	Peritoneal cavity	- study duration: 30 months - detectable increase in C-peptide after 3rd islets infusion - no difference in insulin requirement - the occurrence of fibrosis and islets necrosis after 16 months	[64]
Ba^{2+}/Ca^{2+}-alginate	-	Xenograft (human-mice)	Peritoneal cavity	- study duration: 3 months - responsiveness of retrieved particles to changes in glucose and glucagon - clustering of microcapsules in transplantation site	[65]
Ca^{2+}-alginate	450	Allograft (rat-mice)	Bone marrow (femur)	- study duration: 1 month - risk of pulmonary embolism - retrieved encapsulated cells maintained positive for insulin - the difficulty in transplanting proper amount of islets owing to insufficient space provided by transplantation site	[66]
Alginate-PLL	650	Allograft (rat-rat)	Peritoneal cavity	- study duration: 1 week - application of positively charged PLL increased induced immune responses - high-G alginate capsules were reported to increase inflammatory responses compared to intermediate-G alginate particles	[67]
Alginate-Collagen-alginate	300	Allograft (rate-mice)	Intraperitoneal cavity	- study duration: 4 weeks - maintenance of the blood glucose level < 200 mg/ml - no obvious change in microparticles morphology - loss of cells function overtime	[68]
Alginate	800	Xenograft (pig-monkey)	Kidney capsules	- study duration: 6 months - detection of C-peptide up to 1 month - no fibrosis or cellular overgrowth - partial islets survival	[69]

3.2 Biomaterials for microencapsulation

Biomaterials play an important role in providing an appropriate environment for cells in tissue engineering. In general, their application can be categorised into two areas. They can either be used as carriers in drug delivery systems, for the release of encapsulated reagent at the desired therapeutic site, or as a semi-permeable membrane for the protection of transplanted cells from the host immune system [60, 70]. A biomaterial for the latter application should provide high cell viability while allowing optimal cell function [71]. It is shown in chapter four of this thesis that high cell survival does not always imply optimum function of encapsulated cells. Furthermore, non-toxicity of encapsulation biomaterial and its manufacturing procedure is an important requirement for successful encapsulation [26]. This becomes more critical to cells with low proliferation capacities, including pancreatic islets isolated from cadaveric donors, as these cells are more susceptible to toxicity during encapsulation [70]. Moreover, the chosen biomaterial should allow the relatively long-term immunoisolation of the encapsulated cells compared with the drug delivery systems, which makes biomaterials with low degradation rates of high interest, especially in the case of cell-based therapies for chronic diseases such as diabetes [71].

During the last 30 years, various natural and synthetic materials have been evaluated for cell encapsulation, including hyaluronic acid [72], gelatin [72], alginate [60, 72-74], polyethylene-glycol (PEG) [73], polyvinyl alcohol (PVA) [73], alginate-poly amino acids-alginate (APA) [5], agarose [17, 73, 74], sol-gel silica [17], chitosan [17, 73], poly-l-lysine (PLL) [60], poly-l-ornithine (PLO) [60], polyethylene-glycol and poly-lactic-co-glycolic acid (PEG-PLGA) [74],

polyether sulfone [72], polyethyleneimine [60], and cellulose [72]. Among these, natural

polysaccharides are the most studied biomaterial for cell encapsulation, as a consequence of

their ability to form hydrogels in mild conditions [71]. Hydrogels possess many advantageous

properties for cell encapsulation, specifically owing to the similarity between the structure of

these polymers and the macromolecular-based components of the body [75]. These soft

three-dimensional structures are capable of absorbing large volumes of biological fluids owing

to the presence of hydrophilic groups, such as hydroxyl (-OH), amide ($CONH_2$), and sulfonyl

hydroxide (SO_3H) in their chemical structure [76, 77].

Application of various gelation techniques and polymer concentration can lead to the

formation of hydrogel microparticles with different levels of homogeneity. The gel polymer

can be evenly distributed through the particle or alternatively may form a shell with a

polymer-free core. This feature of hydrogels is another important reason for their growing

application in cell-based approaches, which allows controllable permeability and stability of

the carrier system [17, 78]. Hydrogels from natural polymers have so far generally been

reported to initiate less host inflammatory response, when compared with synthetic polymers

[25], which often require the addition of toxic solvents during the manufacturing procedure

[74].

3.2.1 Alginate structure

Since the application of alginate for microencapsulation of cells in 1980 [19], it has become

widely studied biomaterial in wound healing, drug delivery, and tissue engineering [8, 75].

Alginate is an anionic polysaccharide extracted from fast-growing brown algae or certain

bacterial species, including *Pseudomonas* and *Azotobacter* [74, 76]. This linear unbranched polymer is composed of consecutive beta-D-mannuronic acid residues (M), consecutive alpha-L-glucuronic acid (G) residues, and blocks of alternating M and G residues [74] (Figure 3-2). Extraction of alginate from different species affects both the fraction of G and M monomers and the length of each block, which also results in batch-to-batch variation of commercially available alginate [75, 76].

Among alginates with different composition, those of higher molecular weight typically form gels that are more robust; however, this can also lead to high viscosity of the alginate sol. This, in fact, is less desirable during processing and formation of microcapsules owing to the higher shear forces generated using viscous solutions compared with the alginate solutions with lower viscosity. [75].

M-block

G-block

MG-block
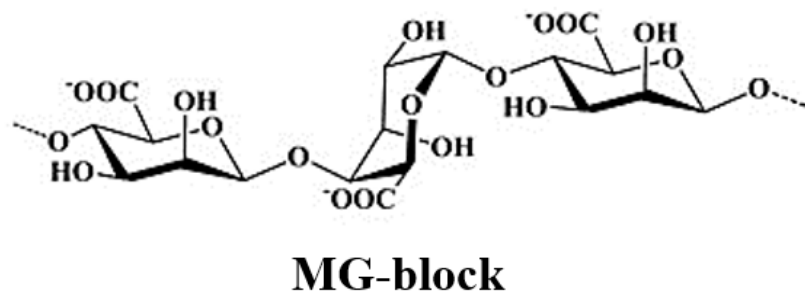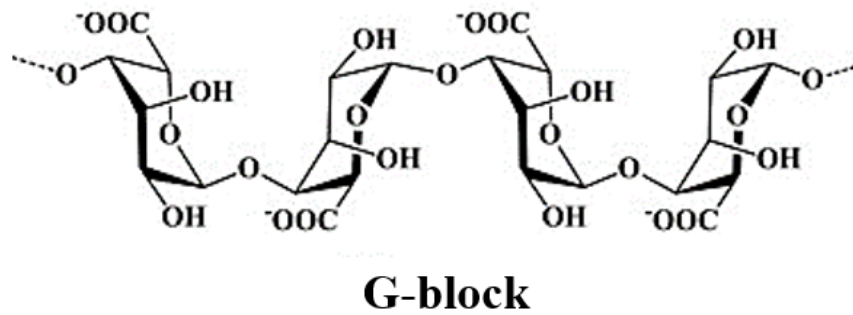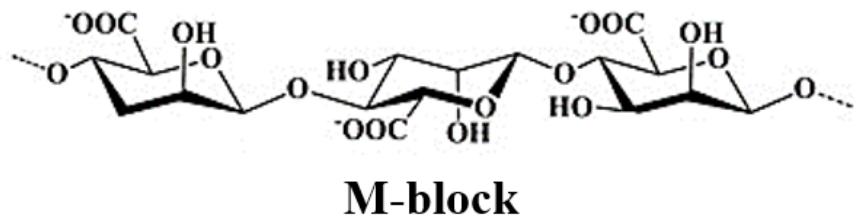
Figure 3-2
The molecular structure of alginate composed of M (mannuronic acid) and G
(glucuronic acid) residues [79].

3.2.2 Gelation mechanism of alginate

Alginate is a polyelectrolyte, which carries a net negative charge. An important characteristic of alginate is its ability to form gels in the presence of divalent cations [75]. Although alginate itself is soluble in water, cross-linked alginate is an insoluble complex as the charged groups within the polymeric structure of alginate are shielded and can no longer attach to water molecules [8].

Formation of alginate gel occurs by ionic bonding between the divalent cations and the polymer chains [76]. The degree to which alginate tends to bind with different cations varies according to the following trend: $Mg^{2+}< Ca^{2+}< Sr^{2+}< Ba^{2+}$ [80]. Despite Ba^{2+} having the greatest affinity to the polymeric chain, its application is restricted due to the toxicity of barium, especially in the case of *in vivo* studies. So far, Ca^{2+} has been the most widely used cross-linker for cell encapsulation owing to its minimal effect on cell viability. Similar to other divalent cationic mentioned earlier, Ca^{2+} can only bind to G and GM blocks of alginate structure with a fast gelling kinetics based on the established egg-box model [80, 81] (Figure 3-3). Although Ca^{2+} cannot bind to M-blocks, which makes alginate with a larger proportion of G residues more desirable for bead generation. Several studies have shown that choosing alginate with high-G blocks is also more likely to trigger inflammatory response than alginate with lower G/M ratios [60].
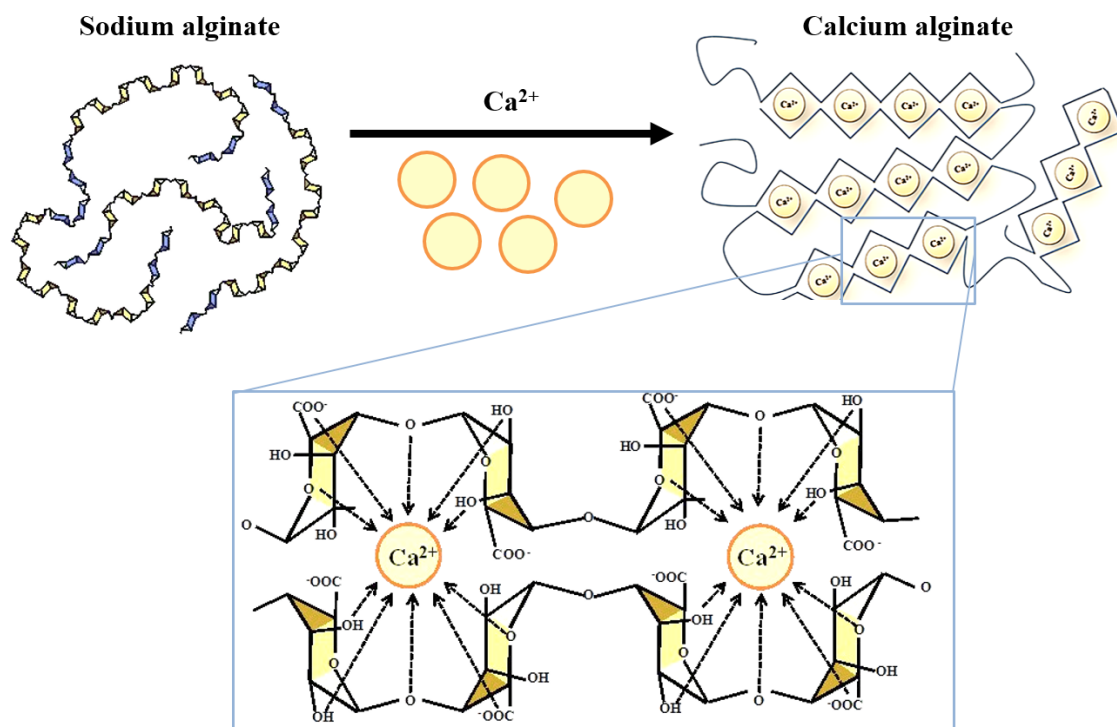
Figure 3-3
Schematic of egg-box model: ionic binding between calcium ions and alginate G residues; adopted from [72, 82]

3.2.3 Methods for producing alginate microcapsules

The simplest method for the formation of alginate beads is extrusion into a solution of the cross-linking cation. This technique is based on dripping alginate droplets from a syringe with a needle of desirable size (the smaller the needle diameter – the smaller the particles), and when the gravitational force overcomes the surface tension on the edge of the needle, the polymeric drop is released into the cross-linking medium [83]. Despite the simplicity of extrusion, in recent years studies have been devoted to replacing this approach with technologies capable of producing beads with smaller size and higher uniformity [84].

The coaxial airflow dripper, electrostatic bead generator, jet cutter, and vibrational nozzle technology are among the existing strategies for the formation of alginate microparticles with higher uniformity [85, 86]. All of these techniques are solely based on mechanical processes to either increase the velocity of droplet formation at the nozzle head or breaking up the alginate liquid jet while it is passing through the nozzle [83].

In the coaxial airflow dripper, the formation of alginate droplets is enhanced by the addition of airflow through a concentric nozzle, while in electrostatic bead generator an electric field boosts droplet formation. Jet cutter bead generators, as the name implies, are designed with rotating cutting wires for breaking the polymeric liquid jet while it detaches from the nozzle head. Finally, in vibrational nozzle technology, at a specific wavelength, the laminar liquid stream breaks apart into droplets under vibrational force [5, 84] (Figure 3-4). Although all these devices are superior to the conventional extrusion technique by allowing the formation of smaller particles with narrower size distribution, recent studies have shown that the processes are all very sensitive to variation in environment and material [84, 87].
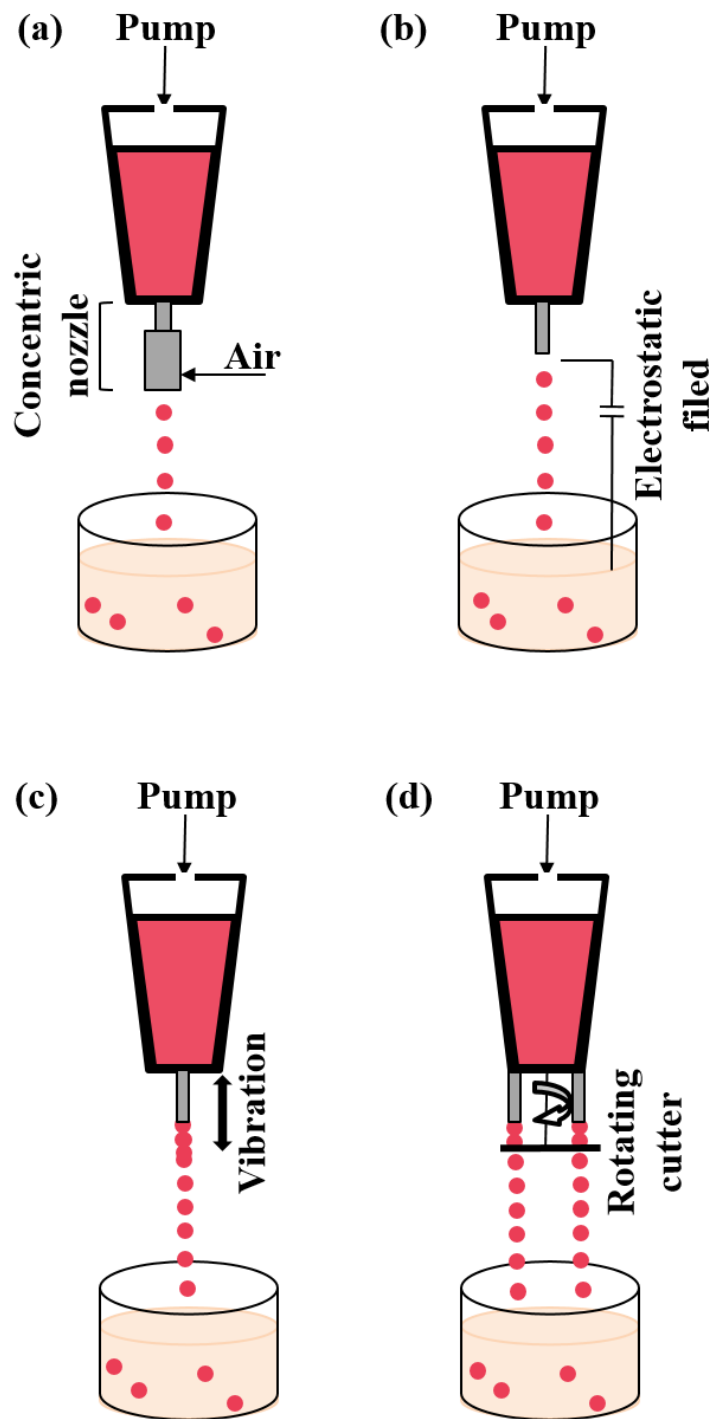
Figure 3-4
Schematic of different technologies for production of alginate microparticles using external cross-linking gelation. (a) Coaxial airflow dripper, (b) electrostatic bead generator, (c) Vibrational nozzle technology, (d) Jet cutter bead generator.

In 2008, Prüsse, *et al.* published a comprehensive report comparing the ability of these four devices in generating alginate microparticles. Coaxial airflow and electrostatic bead generators were shown to be more applicable to produce alginate particles using both low and high alginate concentrations compared with the other two technologies. On the other hand, the application of the vibrational nozzle technology and jet cutter can increase the production rate of microparticles 20-40 times in comparison to coaxial airflow and electrostatic bead generator [84]. An increase in the rate of particle generation has the major benefit of enhancing the efficiency of the cell encapsulation process.

3.3 Current challenges in islets microencapsulation

Apart from tremendous achievements in cell encapsulation technology especially within the last decade, further evaluation is required to address remaining challenges before stepping forward to clinical transplantation of encapsulated pancreatic islets. Poor function and reduced viability of encapsulated islets in the first few weeks after transplantation mainly occur due to limited diffusivity and poor revascularisation of these micro-devices.

3.3.1 Limited mass transport

Mathematical models indicate that pancreatic islets transplanted to the intraperitoneal cavity are in contact with oxygen partial pressure (PO_2) of 0.05-0.06 atm, while encapsulated microparticles with an average size of 500 μm can only be exposed to a $PO_2 < 0.03$ atm [18]. This could even result in harsher conditions for the cells located at the centre of microparticle

compared to those near the surface owing to the limited transfer of oxygen, nutrients, and cellular wastes [7, 88].

Access to sufficient oxygen is crucial for the mitochondria of pancreatic beta cells. PO_2 less than 0.01 atm can affect the amount of secreted insulin from beta cells because of a reduction in mitochondrial ATP production (Section 2.5) [61]. Additionally, void space created within the current typical manufactured microcapsules with the size range of 400-800 μm lead to a time lag while glucose and insulin are diffusing in or out of the immunoisolated membrane [88]. Although limited mass transport can cause lower survival rate for any encapsulated cells, this is of more importance for pancreatic insulin secreting cells. The resulted time lag created by the microcapsules semi-permeable membrane affects physiological kinetics of insulin secretion in respond to abrupt changes in glucose concentrations [4]. Consequently, improvement in the design of encapsulated pancreatic islets to provide better mass transportation is vital to overcome the current cell necrosis occurring within a few weeks after transplantation.

3.3.2 Search for an optimum transplantation site

In accordance with the current standard for the clinical transplantation of non-encapsulated pancreatic islets, the liver has been the most successful site and cells are usually administered through the portal vein. The liver is an organ in which insulin is naturally metabolised, and it provides a nutritionally rich environment for the transplanted cells [4]. However, the major disadvantage of using the liver is the lack of a sufficiently well vascularised network in the immediate vicinity of transplanted islets. After transplantation of pancreatic islets,

revascularisation of graft usually occurs after 1-2 weeks. Therefore, lack of rapid development of vascularisation can result in cell dysfunction and hypoxia due to low oxygenation. As discussed earlier, this could be even more problematic for cells encapsulated within a semipermeable membrane [18, 89]. For encapsulated pancreatic islets, which are of larger volume compared with the non-encapsulated islets, the intraperitoneal site has been the most studied site. The intraperitoneal site can provide easy access to the transplanted system; however, it still lacks sufficient vascularisation. Previous trials have also shown that transplanted microcapsules in the intraperitoneal space have the tendency to float in the cavity or even adhere to the abdominal organs [4, 60].

Up to now, several other transplantation sites including, the spleen, the brain, the eye, the pancreas, the renal subcutaneous space, and the small intestine have been investigated for transplantation of both encapsulated and non-encapsulated pancreatic islets [60]. So far, reports have shown that these transplantation sites suffer from various drawbacks. For instance, the eye and brain can be regarded as immunologically-privileged sites, meaning that they can tolerate antigens without evoking inflammatory responses, but both sites lack sufficient space for the transplantation of a relatively large amount of encapsulated cells with an average size of 500 μm [12, 60]. Therefore, convincing clinical transplantation of pancreatic beta cells within microparticles still relies on finding an optimum site, which is highly vascularised, provides sufficient space for the graft volume, and needs the minimum surgical procedure.

3.4 Polyelectrolyte multilayer coating

Polyelectrolyte multilayer (PEM) coating also known as layer-by-layer (LBL) self-assembly technique is a recent strategy with the potential to protect cells from immune responses [90, 91]. In general, LBL self-assembly technique involves an alternate deposition of oppositely charged materials, such as polymeric electrolytes, nanoparticles, and proteins on a charged surface [91, 92] (Figure 3-5). Importantly, each deposition step is followed by a washing step to remove any remaining un-bonded or weakly bonded polymeric chains from the previous deposition step [93].
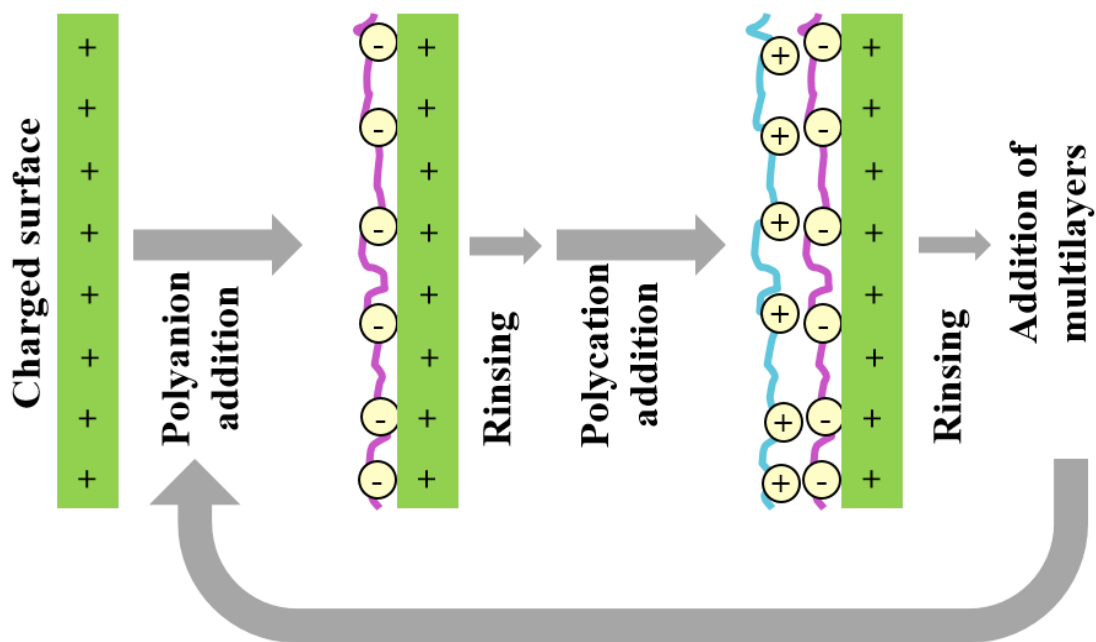
Figure 3-5
Schematic of polyelectrolyte multilayer coating procedure on a surface with initial positive charge, the addition of polymeric bilayers can be repeated until a desirable coverage of the surface is achieved.

The discovery of PEM coating method in 1997 has opened up new horizons in the modification of both biological and non-biological substrates [94], especially for biomedical applications. Examples include biosensors, drug delivery systems, cell surface modifications, and membranes such as wound healing films [90, 93, 95].

Apart from the presence of relatively weak Van der Waals interactions and hydrogen bonding between the polyelectrolytes, the formation of the multilayers dominantly relies on electrostatic interactions between the oppositely charged polymers [92]. Selective permeability of polyelectrolyte multilayers can be manipulated by choosing a different number of bilayers, as well as varying polyelectrolyte combinations [93]. Two main mechanisms have been reported regarding the growth of bilayers on a charged surface. The first mechanism is based on a linear relation between thickness and number of deposited bilayers, while in the second mechanism an exponential relation exists between thickness and number of bilayers. The latter mechanism occurs when the polyelectrolytes attraction is less strong. In this case, the two oppositely charged polymers could diffuse between layers and become involved in the formation of multilayers. Hence a desirable thickness can be achieved by the addition of fewer bilayers compared to the linear growth mechanism [92, 93].

3.4.1 Advantage of PEM coating for cell encapsulation

Among various biomedical applications attributed to PEM coating, this robust coating method particularly possesses several advantages for encapsulating mammalian cells compared to the conventional microparticles [92, 96]. Overall, PEM coating procedure is a simple and cost effective method [95]. In terms of compatibility with cell survival, the alternate deposition of

bilayers is achievable under mild temperature and pH conditions. Often during the PEM coating, there is no requirement for cross-linker or toxic solvents [92].

The PEM coating was first developed for flat charged surfaces; however, later on, its application was extended to three-dimensional geometries [96]. The deposition of thin polyelectrolyte bilayers around a single or clusters of cells can, to a great extent, reduce the diffusion distance between the encapsulated cells, and surrounding tissues and vasculature systems. Consequently, PEM coating could enhance cell survival by increasing the transfer rate of oxygen and nutrients compared to conventional microcapsules [95-97].

3.4.2 Materials used in PEM coating

As discussed earlier in section 3.4, the thickness of the PEMs relies on the growth mechanism between oppositely charged polyelectrolytes. Therefore, achieving a desirable thickness and physical property depends highly on the polyelectrolyte layer composition. Up until now several synthetic and natural polyelectrolyte pairs have been investigated in cell-based studies, such as PEG-lipid and PVA, PLL-g-PEG-(biotin) and streptavidin [97], polystyrene sulfonate (PSS) and polyallylamine hydrochloride (PAH), PSS and polyacrylic acid (PAA), collagen and heparin, collagen and chitosan [93, 98].

In 2012, encapsulated mouse pancreatic islets using PEM coating was reported by Zhi, *et al*. [97]. In this study, they have encapsulated islets within multilayers of alginate and modified phosphorylcholine chitosan to maintain cells insulin secretory ability, as well as minimising inflammatory response triggers by the cationic polymer. Apart from encapsulation of cells

using PEM coating, this method has also been applied in surface modification studies. An example includes the formation of PAA/PAH multilayers with linear growth by Moussallem, *et al.* [99]. This work investigated the cellular behaviour of A7r5 rat smooth muscle cells on culture substrates made from PEMs with different stiffness, and mechanical properties. In summary, a vast variety of polyelectrolyte has been utilised in PEM coating, however, further investigation into the biological impact of PEMs on both cell survival and immunoprotection is required.

3.5 Application of bioreactors in cell-based therapies

In vitro mammalian cell culture dates back to 100 years ago. However, since then modern biotechnological approaches in cell culture methods has been investigated to keep up with high demand for biological products [100]. One important example is the large-scale production of pharmaceutical reagents from mammalian or plant cells cultured within bioreactors. Examples of such products include enzymes, hormones, monoclonal antibodies, vaccines, cytokines, and recombinant proteins [100, 101].

By the advent of tissue engineering technology in recent years, application of bioreactors has gained attraction for the cultivation of tissue cells and artificial organs in a three-dimensional environment. Compared to conventional static culture, bioreactors could provide a culturing environment more similar to *in vivo* [102]. In general, bioreactors are devices that can offer a controlled culture environment in parallel with providing a desirable sterile condition. These devices are often provided with a continuous flow of culture medium. This could effectively

enhance the supply of nutrients to cells, as well as removal of waste products in a controllable manner compared with static culture [100, 103].

Reactors for biological applications can be categorised into main six types: (**1**) stirred-tank bioreactors, (**2**) pneumatically agitated bioreactors, (**3**) rotary bioreactors, (**4**) hollow fibre bioreactors, (**5**) fixed-bed bioreactors, and (**6**) fluidised bed bioreactors [103].

In stirred-tank bioreactors and pneumatically agitated bioreactors, sufficient mixing of nutrients and oxygen throughout the medium is induced by impellers and aeration, respectively. While rotary bioreactors overcome diffusion limitations provided by a dynamic flow of culture medium within a rotational vessel [100]. Hollow fibre bioreactors could provide low shear levels by penetration of medium through semi-permeable membrane hollow fibres and are mostly desirable for adherent cell types [104]. Fixed-bed bioreactors are usually preferred for cells being immobilised on the surface of microcarriers. In this case, fixed-bed comprises of immobilised cell carriers in contact with a continuous low velocity of culture medium [101], while in fluidised-bed, an upward flow of medium enhances the fluidisation of cellular microcarriers within the bioreactor column [105].

The application of a bioreactor with a specific design largely depends on the characteristic of the biological system, especially their sensitivity to shear forces. As an example, stirred-tank bioreactors are more common for scaled-up production of therapeutic proteins from plant cells owing to their low shear sensitivity. While hollow fibres have been successful in seeding and cultivating adherent mammalian cells [103]. Up to now, several mathematical studies using computational fluid dynamic have been reported for different types of bioreactors

mentioned earlies [105, 106]. However, there are fewer studies in connection with their feasibility for the cultivation of immunoisolated endocrine cell-based carriers.

3.6 Aims and Objectives of thesis

The principle aim of the work presented here is to develop and investigate techniques for the encapsulation of pancreatic beta cells. During this thesis, assessments were concentrated on viability and insulin secretion ability of encapsulated beta cells within two different encapsulating strategies, as well as cultivation of encapsulated cells in static versus fluidised system. For both encapsulating systems investigated in this thesis, generation of immunoisolated systems with less than 250 μm was aimed to enhance cell survival through facilitated diffusion of oxygen and nutrients. In this regard, vibrational technology with a high production rate, as well as its potential for producing microcapsules with narrow size distribution was preferred compared to the other encapsulation technologies. Specific objectives were:

Chapter 4: Encapsulation of pancreatic beta cells using the vibrating nozzle method

- Optimisation of influential parameters in generating uniform alginate microcapsules with a desirable size of <250 μm using vibrational technology.

- Investigation of cells distribution within the alginate matrix.

- Evaluation of encapsulated cells insulin secretion under glucose-stimulated condition.

Chapter 5: Cultivation of encapsulated cells in a fluidised bed bioreactor

- Investigation of the effect of fluidised cultivation on the viability and function of endocrine cells.

- Study of the feasibility of fluidised bed bioreactor as a short-term solution for the storage and handling of cell-embedded micro-carriers.

Chapter 6: Encapsulation of beta cell spheroids using polyelectrolytes

- Establishment of the optimal cell concentration to generate harvestable and robust pancreatic beta cell spheroid utilising 3D concave agarose micro-wells.

- Examining the biological impact of polyelectrolyte multilayers using layer-by-layer assembly technique on beta cell spheroids.

- Development of a non-cytotoxic novel approach for the enhancement of viability and metabolic activity of cells coated with bilayers of alginate and poly-l-lysine.

- Evaluating the effect of the polyelectrolyte multilayer coating on immunoisolation and insulin secretion of beta cells.

4 CHAPTER FOUR

Encapsulation of pancreatic beta cells using the

vibrating nozzle method

4.1 Introduction

Cell encapsulation is a promising strategy to provide immunoprotection for transplanted islets [11, 12]. In recent times, important advances within this field have been made through microstructural manipulations leading to larger surface area to volume ratio, increased oxygen and nutrient diffusion rate, and also access to more implantation sites by injection [5, 16].

There is a range of methods for the encapsulation of living cells in alginate microparticles. Successful cell encapsulation, however, requires that the resulting capsules be of homogeneous size and distribution. It is also important to use a method of manufacture that is mild and rapid to reduce the loss in potency of the pancreatic beta cells [83, 107-109].

In this study, a vibrating nozzle system was utilised to obtain alginate microcapsules with uniform size and spherical shape. Microparticle size was manipulated by changing processing parameters, including frequency of the vibrating nozzle, polymer concentration, nozzle size, and pump flow rate. β-TC-6 cells were embedded in optimised alginate microparticles with an average diameter of 200 ± 19 μm. Cell viability, mitochondrial activity and microcapsule stability were evaluated *in vitro*. Finally, the functionality of encapsulated pancreatic beta cells was tested using a glucose stimulated insulin secretion assay.

4.2 Materials and methods

4.2.1 Construction of vibrating nozzle encapsulator

A B-395 pro (Buchi, UK) encapsulator was used for the preparation of alginate microparticles (Figure 4-1). The vibrating instrument consists of a feed line connected to a syringe and a nozzle. The internal diameter of the nozzles used in this study was 80-120 µm. A receiving cross-linking solution (100 mM $CaCl_2$) was placed at a distance of 20 cm from the nozzle head. In vibrating nozzle technology, a laminar fluid jet will naturally break into droplets at a particular frequency, resulting in jet breakup to nearly double the internal diameter of the nozzle [5]. Moreover, the geometry and size of the drops formed are dependent on nozzle diameter, polymer flow rate, frequency, and viscosity of the extruded liquid.
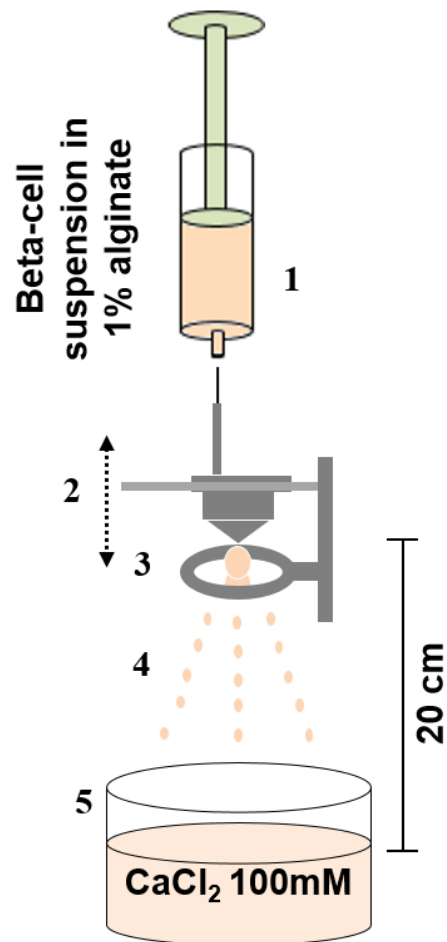
Figure 4-1
Schematic of alginate microparticle production using vibrating nozzle technology: (1) Pumping of alginate and cell suspension with syringe pump, (2) Mechanical vibration of the nozzle at set frequency, (3) Droplet formation from the nozzle head, (4) Formation of uniform spherical drops due to the controlled break-up of the liquid jet and electrostatic charge, (5) cross-linking solution.

4.2.2 Cell culture

Mouse pancreatic beta cells (β-TC-6) were obtained from the ATCC and cultured in Dulbecco's

modified eagles medium (DMEM) (Sigma, UK) supplemented with 10% fetal bovine serum

(FBS), 2.5% HEPES, 1% penicillin/streptomycin, and 2.5% L-glutamine. Cells were grown and maintained in culture medium at 37°C in a humidified tissue culture incubator at 5% CO_2. All experiments were conducted using cells between passages 26-40.

4.2.3 Preparation of solutions for cell encapsulation

Medium viscosity alginate ($\geq$ 2000 cP, M/G ratio= 1.56) from brown algae (Sigma, UK) was dissolved in sterile deionised water (1%w/v). The cross-linking solution was prepared by dissolving granular calcium chloride (Sigma, UK) in deionised water (100 mM). All solutions were sterile filtered using 0.22 μm syringe filter (Millipore, USA) and were UV sterilised overnight.

4.2.4 Optimisation of alginate particle diameter

The shape and size distribution of alginate microparticles were optimised by adjusting the alginate concentration (0.5-2%w/v), cross-linking solution concentration (0.05-1 M), vibration frequency (800-1800 Hz), and particle hardening time (5-20 min). Alginate microparticles were prepared by attaching a 10 mL syringe filled with the polymer solution to the nozzle head (nozzle size: 120 μm). Furthermore, the electrode and pump flow rate were adjusted to 500 V and 21 mL/min, respectively throughout the first part of the experiments. After washing the samples twice using deionised water, the size distribution of samples was calculated from a random sampling of 20 individual microspheres. An optical microscope and a digital camera (Olympus Co., Germany) were used to obtain images of the microparticles, which were evaluated using Image J software (NIH, Bethesda, MD, USA).

4.2.5 Cell encapsulation

β-TC-6 cells were grown in T-75 flasks to ≥80% confluency prior to harvesting. The cells were then detached from the culture flask using Trypsin-EDTA solution (Sigma, UK). After being washed in phosphate buffered saline (PBS) (Fisher scientific, UK), 1×10^6 cells were suspended per 1 mL of the sterile alginate solution. The formation of microcapsules was carried out with the vibrational encapsulator using the optimised processing parameters (frequency=3000 Hz, Alginate conc. =1w/v%, $CaCl_2$ conc. =0.1 M, and pump flow rate=15 ml/min, nozzle size=120 μm). Formed microparticles were then incubated in a 100 mM $CaCl_2$ bath for 10 min. After gelation, the capsules were washed twice with PBS and DMEM to remove any remaining calcium ions from the encapsulated particles.

4.2.6 Evaluation of microcapsules size over time

Alginate microparticles with and without cells were prepared (section 4.2.5) and kept in supplemented DMEM at 37°C, and 5% CO_2. To investigate the change in diameter of the microparticles over a period of 32 days, and to further determine the effect of cells on alginate particle morphology in comparison to void particles, 60 microcapsules were chosen randomly from each sample. The diameter of each microparticle was measured at day 4, 10, 18, and 32 of culture with bright field light microscopy and analysed using Image J software.

4.2.7 Microcapsules resistance to rupture

The integrity of alginate microcapsules through the injection process was examined using needles of different gauges. Briefly, 200 µL of alginate microcapsules suspended in DMEM were injected through an 18G, 21G, and 23G needle. For each needle size, the injection of microcapsules was repeated three times. Following injections, the stability of the microcapsules was visualised using an optical microscope connected to a digital camera.

4.2.8 Confocal laser scanning microscopy

Confocal microscope (Olympus FV1000, Multiple Ar laser, Germany) was used for visualisation of fluorescently stained samples. Compared with the conventional microscopes, confocal laser scanning microscopy (CLSM) enable one depth-level image at a time. The laser passes through a light source, and it reflects by a dichroic mirror towards the detection system. The pinhole aperture within the detection system enables the exclusion of most of the out-focus fluorescent from the acquired focal plane. Finally, by scanning sequential focal planes a point-by-point optical scanning of a 3D object is achievable (Figure 4-2). This allows reconstruction of a 3D fluorescently labelled construct by assembling these optical sections in a z-stack [110-112]. Here, 10x magnification was chosen for all samples. Detector gain and laser intensity were set with regulation using signals from both background and stained cells based on visual observation. Reconstruction of raw z-stack images of 3D microcapsules were then achieved using Imaris software (Bitplane, UK).
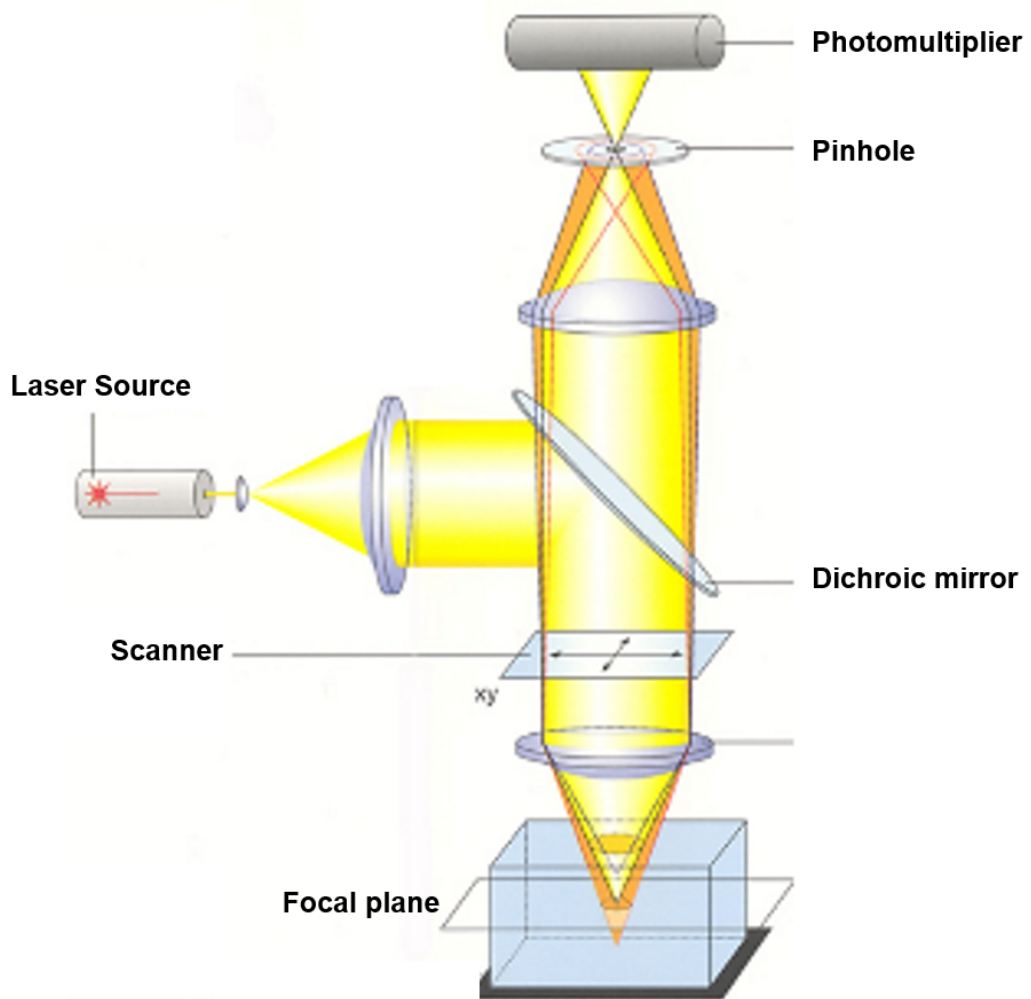
Figure 4-2
Schematic illustration of light pass on a confocal laser scanning microscope, adopted from [113].

4.2.9 Live/ dead assay

The viability of β-TC-6 cells encapsulated in alginate microparticles was assayed using a live/dead cytotoxicity kit (Invitrogen, UK). Two-colour fluorescence method involving

propidium iodide (PI) (indicator for dead cells), and calcein acetoxymethylester (calcein AM) (indicator for viable cells) were chosen. Upon addition of non-fluorescent calcein AM ($C_{46}H_{46}N_2O_{23}$), it converts to calcein ($C_{30}H_{26}N_2O_{13}$) with a green fluorescence owing to the cell's intracellular activity (peak excitation= 495 nm, peak emission= 515 nm). In contrast to calcein AM, PI ($C_{27}H_{34}I_2N_4$) cannot diffuse through the cell and nuclear membranes of live cells. Therefore, it only stained DNA of non-viable cells with a red fluorescence (peak excitation= 488 nm, peak emission= 617).

Briefly, 5 μL of calcein AM and 25 μL of PI were added to 2 mL of capsules suspension in DMEM, followed by incubation at 37°C for 40 min. After staining, the cells were imaged using CLSM. Multi-line Ar laser (488 nm) and HeNe laser (543 nm) were utilised for the detection of calcein and PI signals, respectively.

4.2.10 Cell mitochondrial activity

β-TC-6 metabolic activity in alginate matrix was analysed with the Alamar Blue assay (Invitrogen, UK), according to the manufacturer's protocol, at days 4, 9, 11, 15, 18, 23, and 25 of culture. Alamar Blue is a compound that, when reduced by cellular metabolism, changes from a non-fluorescent blue colour to a fluorescent red form. The amount of reduction of the assay reagent is proportional to the cell mitochondrial activity. Alamar Blue reagent (10%v/v) was added to microcapsules suspended in supplemented DMEM for 4 h under growth conditions. Fluorescence was read at 570 nm excitation and 600 nm emission using a microplate reader (GloMax-Multi+Mictoplate Multimode reader, Promega, USA). The

morphology of encapsulated cells was also visualised with bright-field microscopy, in order to determine any deformation or cell protrusion from the hydrogels over time.

4.2.11 Permeability of alginate capsules to FITC-mouse antibody

To investigate the permeability of the 1%w/v alginate microcapsules to immunologically relevant molecules, an anti-mouse major histocompatibility antigen (MHC class II) (ebioscience, UK) [114] was used. Sixty microcapsules with embedded β-TC-6 cells were picked randomly. 200 μL of 2% Bovine serum albumin (BSA) (Sigma, UK), and Hanks' Balanced salt solution (HBSS) (Sigma,UK) (blocking buffer) was added to the particles, followed by addition of 2 μL of antibody solution. The suspension was then incubated at 37°C for 1h. Capsules were then washed three times with HBSS to remove any excess antibody remaining in the solution [114]. For the control sample, non-encapsulated cells were also exposed to the mouse antibody with the same procedure. Samples were then observed using confocal microscopy.

4.2.12 Glucose-stimulated insulin secretion (GSIS) assay

To evaluate the functionality of beta cells (MIN-6 cells), the secreted amount of insulin from non-encapsulated and encapsulated cells in response to changes in glucose was measured [115, 116]. Briefly, samples with $1x10^6$ cells/mL were washed and pre-incubated in Krebs-Ringer bicarbonate buffer (KRBH: 125 mM NaCl, 1.2 mM $MgSO_4$, 1.2 mM $CaCl_2$,22 mM $NaHCO_3$, 10 mM HEPES, 1.19 mM KH_2PO_4) + 0.1% BSA for 2 h. Then, samples underwent a static incubation for 1 h with low (2 mM) glucose concentration in KRBH+ 0.1% BSA followed by the addition of high (20 mM) glucose concentration in KRBH+ 0.1% BSA as the stimulator

and samples incubated for another hour. For each incubation period, the cultured supernatant was collected for the insulin assay. The supernatant obtained by centrifugation of the dissolved particles was then diluted to the appropriate range based on the assay standard curve. The secreted insulin was measured using a rat/mouse insulin enzyme-linked immunosorbent assay (ELISA) kit (Millipore, USA), and the colorimetric reaction was quantified using a plate spectrophotometer (GloMax-Multi+Mictoplate Multimode reader, Promega, USA) at a wavelength of 450 nm. According to the manufacturer, for the standard curve, a sigmoidal four parameter logistic equation was fitted (Equation 4-1).

$$Y=d+ (a-d)/ (1+(X/c)^{b})$$ **Equation 4-1**

Here, X indicates absorbance and Y is insulin concentration (ng/ml) of a standard sample. The constant values were calculated as follow (R^2 value= 0.99934):

Table 4-1
Constant parameters of sigmoidal logistic equation.

a= 8.4652595	b= -1.1983119
c= 21.9761095	d= 0.1665466

Results were normalized by measuring the number of encapsulated cells in each sample using a CyQUANT cell counting kit (Invitrogen, UK), which expresses strong fluorescence after binding to the cellular nucleic acid (maximum excitation= 480, maximum emission= 520). Moreover, the data were expressed as a stimulated index (SI), which indicates the ratio of insulin secreted with high glucose over insulin secreted with low glucose stimulation.

4.3 Statistical analysis

All data were expressed as mean ± standard deviation (S.D.). The student's t-test assuming equal variance was used to identify a significant difference between the individual groups of the GSIS assay. One-way analysis of variance (One-way ANOVA) was used to identify any significance difference between the means of the independent groups. Furthermore, Bonferroni correction in conjugation with ANOVA was performed to find means that were significantly different within groups. A p-value < 0.05 was determined as significant.

4.4 Results

4.4.1 Optimised alginate microparticles

In the production of alginate beads with the vibrating nozzle technology, an increase in alginate concentration from 0.5 to 2%w/v resulted in an increase in average bead diameter from 220 to 800 µm (P-value <0.01) (Figure 4-3: a). Increasing alginate concentration beyond this resulted in the nozzle becoming blocked and the spraying process being halted. An increase in vibration frequency from 800 to 1800 Hz was shown to reduce particle diameter from 600 to 300 µm (P-value <0.01) (Figure 4-3: b). Statistically no significant differences in microparticle diameter were observed as a result of changing the concentration of the $CaCl_2$ cross linking solution between 0.05 and 1 M (P-value =0.88) or increasing the gel hardening time from 5 to 20 min (P-value =0.85) (Figure 4-3: c, d).
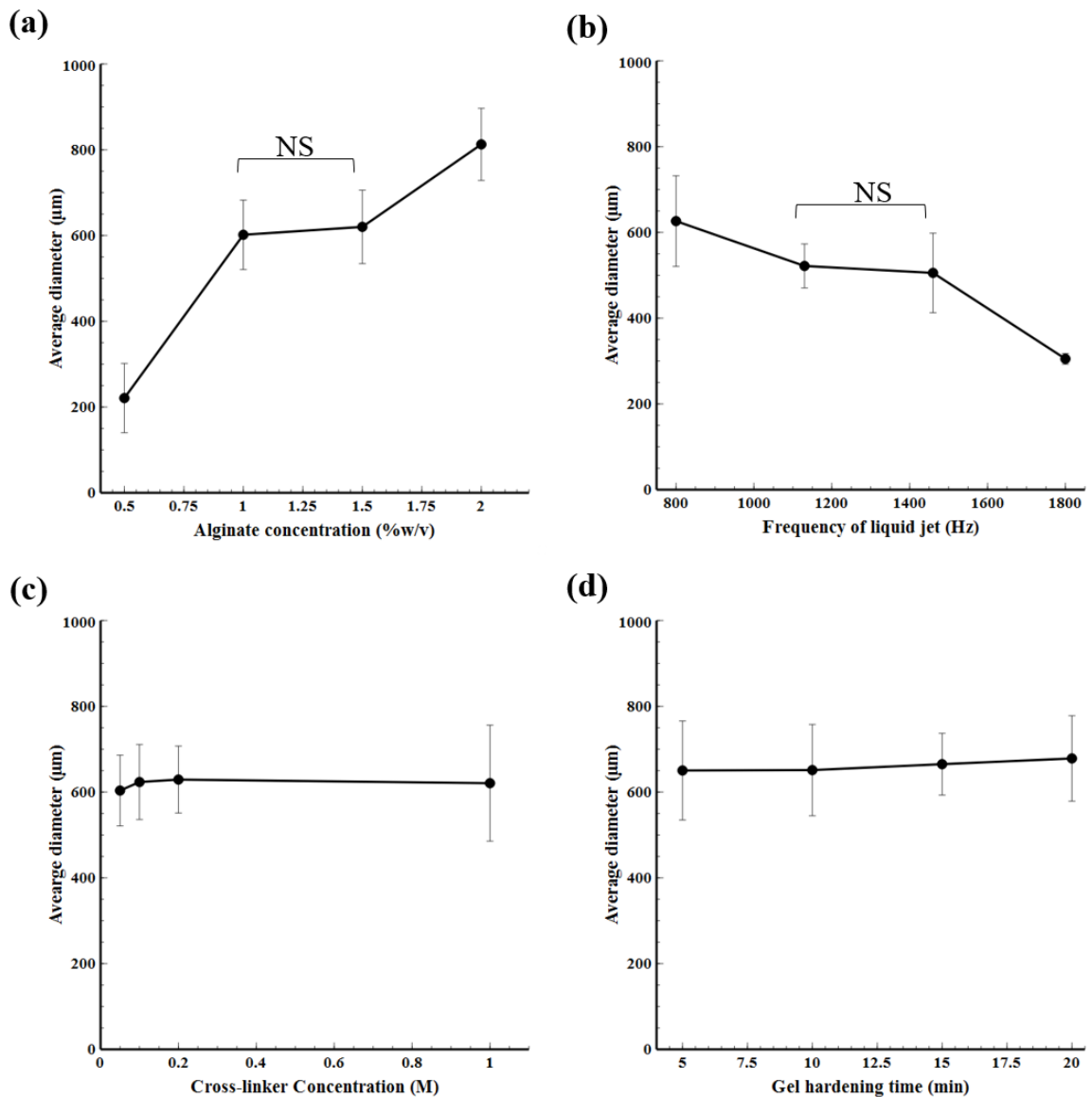
Figure 4-3
Effect of individual processing parameters on average diameter and size distribution of alginate microparticles, produced by vibrating nozzle technology (nozzle inner diameter: 120 μm). (a) Alginate concentration 0.5-2% w/v (P<0.01) (frequency=1000 Hz, CaCl$_2$=0.1 M, hardening time=10 min), (b) Frequency of vibrating nozzle 800-1800 Hz (P<0.01) (alginate concentration=1%, CaCl$_2$=0.1 M, hardening time=10 min), (c) Cross-linked solution concentration 0.05-1 M (P>0.05) (alginate concentration=1%, frequency=1000 Hz, hardening time=10 min), (d) Gel hardening time 5-20 min (P>0.05) (alginate concentration=1%, frequency=1000 Hz, CaCl$_2$=0.1 M). Results are presented as means± S.D. (number of microparticles= 20). In each experiment, a single processing diameter was varied and all others were constant, NS=non-significant.

These outcomes, in parallel with visual observation suggested that an interdependent behaviour between the mentioned parameters and polymer flow rate exist during bead production, which needed to be adjusted simultaneously to achieve particles with higher uniformity in both their size and shape. Moreover, during the whole encapsulation process the voltage was set at 500 V. Excessive voltage (>1 kV) resulted in unstable and multi-jet spray of the polymer solution from the nozzle head, which hampered particle uniformity. Due to frequent blockage of the nozzle with 80 μm diameter (minimum available size within the device) with the polymer solution, the 120 μm nozzle was chosen for generation of microparticles throughout this chapter. Figure 4-4 shows the results from optimised acellular alginate particles with an average diameter of 200 μm and less than 9% relative standard deviation.
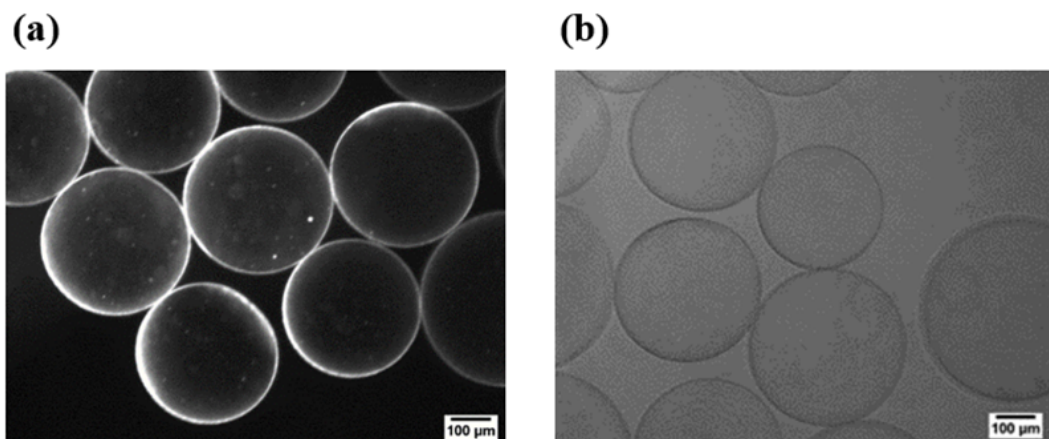
Figure 4-4
Production of alginate microcapsules utilising vibrational nozzle technology (a) and (b) Phase contrast and optical micrographs of optimised void alginate microparticles, respectively (frequency=3000 Hz, Alginate conc. =1w/v%, CaCl$_2$ conc. =0.1 M, and pump flow rate=15 ml/min, nozzle size=120 μm), scale bar shows 100 μm.

Comparison between size distribution of microcapsules generated with vibrational technology versus extrusion of alginate droplets from a needle (31G) was further investigated. Using vibrational nozzle allowed narrow size distribution of particles mostly within the size range of 180-220 µm. While the conventional method resulted in a broader size distribution ranging from 180-1140 µm (Figure 4-5).
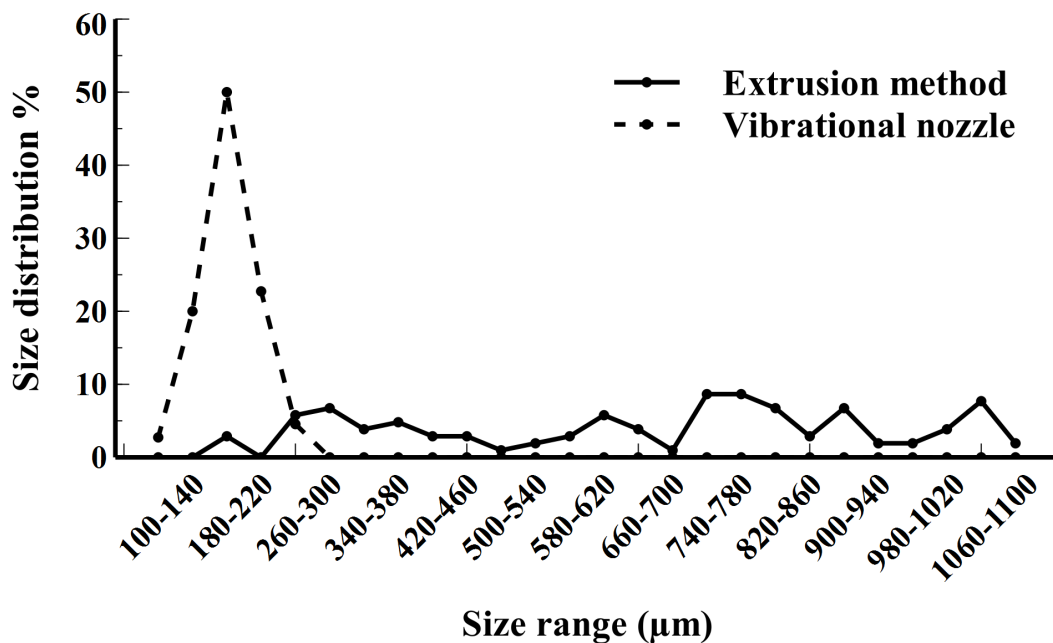
Figure 4-5
Comparison between size distributions of alginate microparticles prepared with vibrational nozzle and conventional extrusion technique, respectively (n=110 microcapsules).

4.4.2 Stability of alginate microparticles

Any changes in size of the alginate microcapsules (with or without cells) was monitored by capturing images of the particles 4, 10, 18, and 32 days after encapsulation. In general, an increase of 15 µm in average size of the alginate particles was observed followed by a decrease after day 18 for acellular particles (Figure 4-6: a). The maximum change for acellular alginate microparticles in supplemented DMEM was observed on day 18 with an average diameter of 202 µm± 29 S.D. Unlike the void microcapsules, the changes in the diameter of particles with encapsulated cells was not significantly different over time (Figure 4-6: b). Additionally, differences in microparticle morphology over time was observed in micrographs, and cells did not show any protrusion from the alginate capsules (Figure 4-6: c, d, and e).
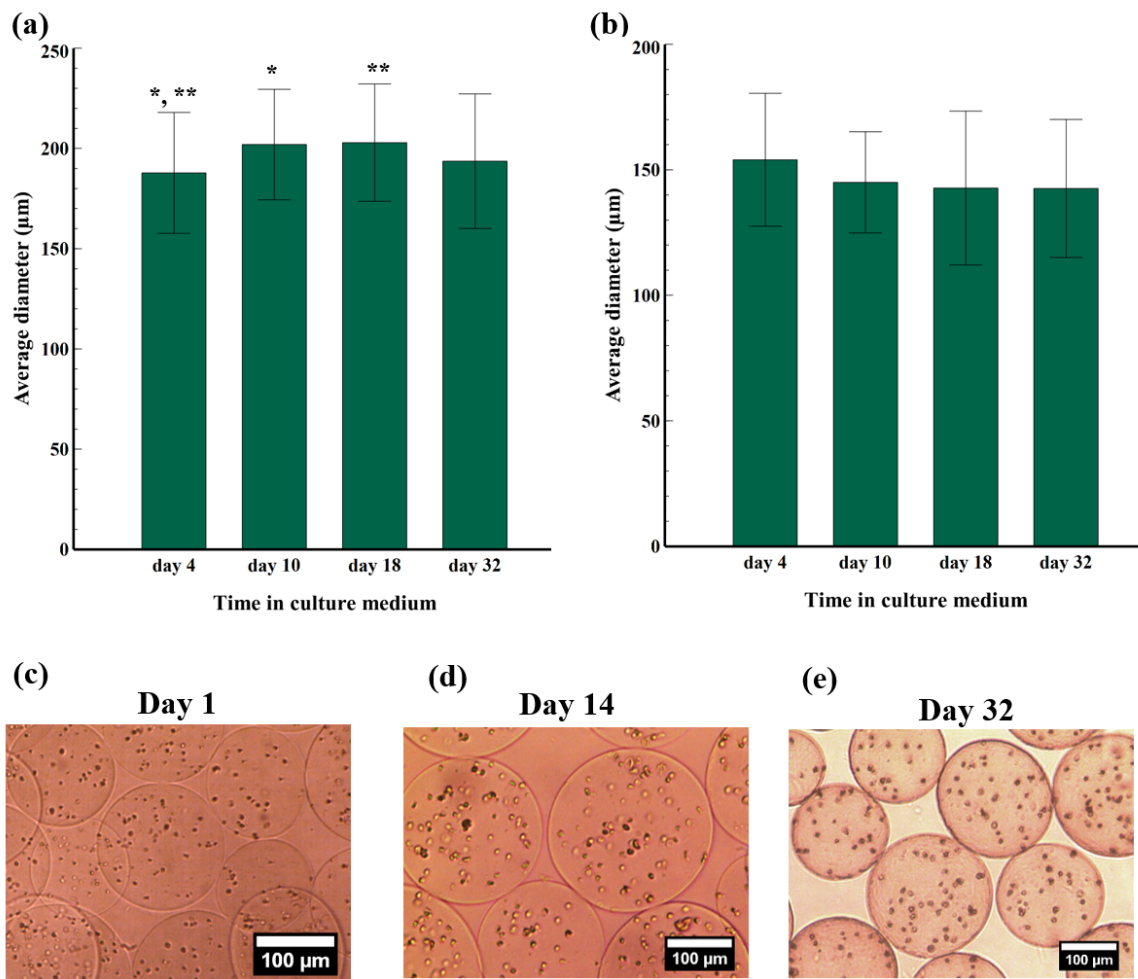
Figure 4-6
Diameters and morphologies of microparticles produced with the vibrating nozzle technology. Change in alginate microparticle diameter with time, (a) Alginate microparticles without cells, and (b) Alginate microparticles with cells; (n=60), (*, ** P<0.05). (c), (d), and (e) Light micrographs of encapsulated β-TC-6 cells cultured over time. All scale bars represent 100 μm.

The stability of 1% alginate microcapsules in response to shear forces create during the injection of microcapsules was also examined to evaluate whether it was possible to inject them into transplant sites. Notably, the choice of needle size was based on those used mostly within *in vivo* studies [117, 118]. Application of 18G and 21G needles enabled the injection of

particles without any observable effect on the morphology of alginate microparticles. Whereas, a few broken and/or deformed alginate particles was observed under the optical microscope when a 23G needle was utilised (Figure 4-7).
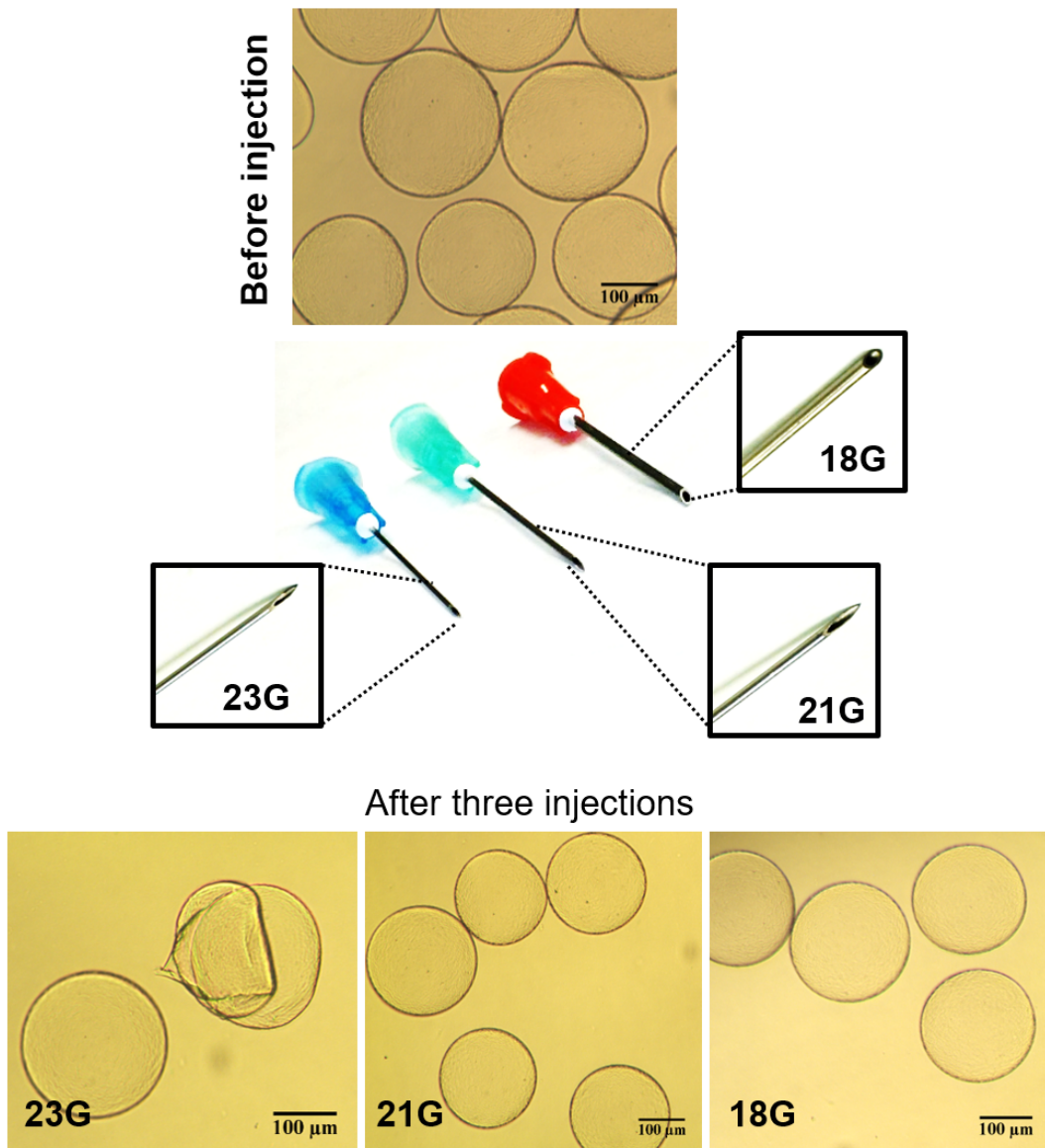
Figure 4-7
Light micrographs of 1% alginate microcapsules to indicate their integrity after being injected through needles of different gauges. All scale bars represent 100 µm.

4.4.3 β-TC-6 cell viability in the alginate hydrogels

The viability of beta cells embedded within 1%w/v versus 2%w/v alginate microcapsules was examined on day 7 of culture. Cells within 1% alginate exhibited a higher viability of 98%± 3 (p= 0.03) when compared with the same concentration of cells encapsulated within 2% alginate microcapsules (Figure 4-8).
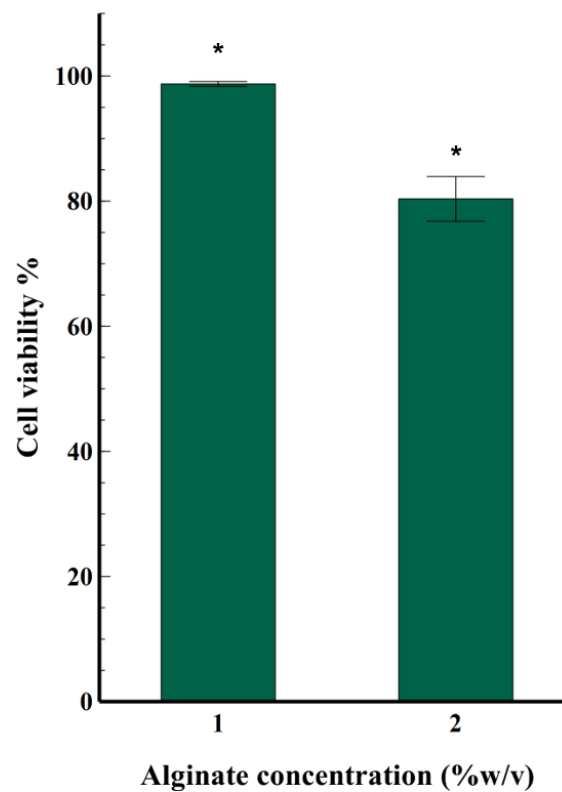
Figure 4-8
Quantitative evaluation of live/dead analysis of encapsulated cells on day 7, cell density=1 x 10^6 cells/mL (n=10 microcapsules) (*, P<0.05).

The encapsulated cells in 1%w/v alginate were monitored at days 4, 10, 18, and 32 to assess the viability of encapsulated cells using Live/dead fluorescent staining and microscopy. Encapsulated cells showed high viability during the *in vitro* study, and at all-time points, more than ~80% of the encapsulated cells were positive for calcein AM (Figure 4-9).
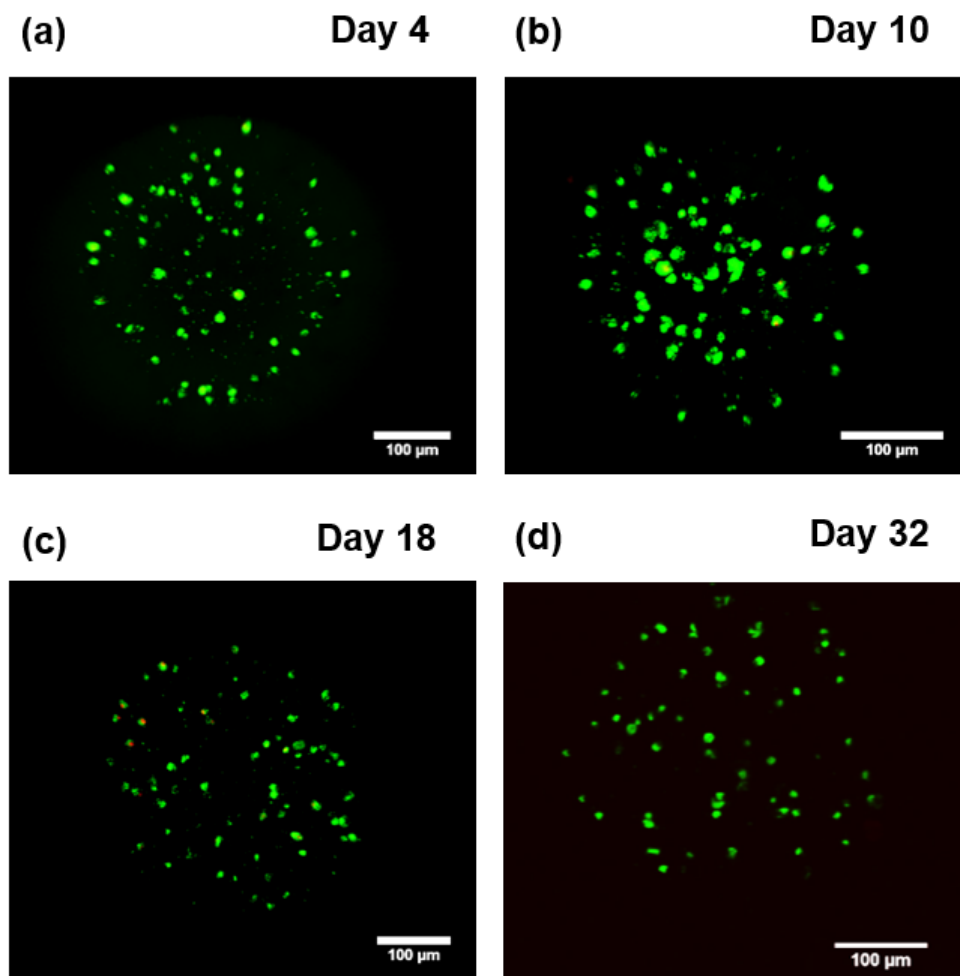
Figure 4-9
Evaluation of encapsulated cells viability. (a, b, c, and d) confocal micrographs of live/dead (calcein-AM/ PI) encapsulated β-TC-6 cells in alginate hydrogel after 4, 10, 18, and 32 days of culture (Viable cells: green and non-viable cells: red). All scale bars represent 100 μm.

In order to provide more insight in to the distribution of cells within the hydrogel network, a z-stack analysis using CLSM was performed allowing for 3D identification of encapsulated cell location in the alginate matrix. Promisingly, cells were observed to be distributed uniformly between the core and the inner surface of alginate hydrogels (Figure 4-10).
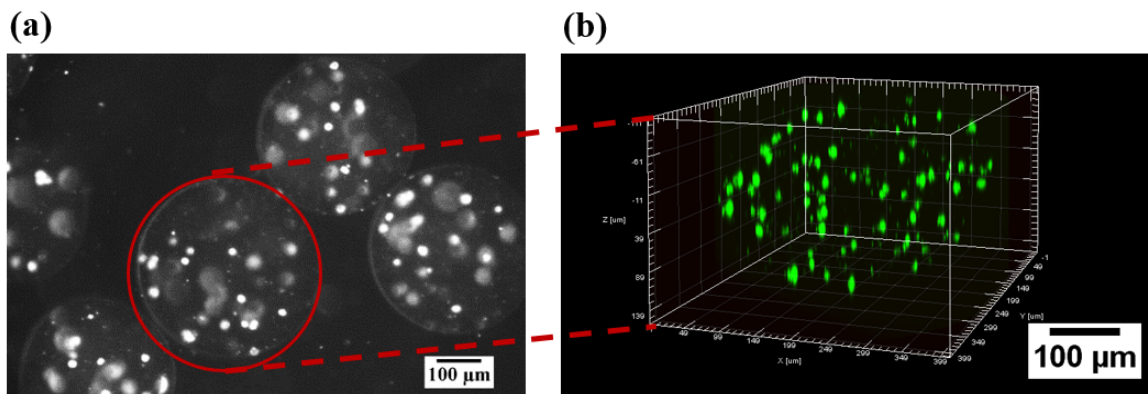
Figure 4-10
Distribution of encapsulated cells within the alginate microcapsules. (a) Phase contrast microscopy of a group of microcapsules with embedded pancreatic β-TC-6 cells. (b) Image showing the three-dimensional distribution of encapsulated cells within an alginate microparticle using confocal laser scanning microscopy, and Z-stack imaging (stacks of 2-D images, occupying the same x-y position but varying along z-axis). All scale bars represent 100 μm.

4.4.4 Microencapsulated β-TC-6 cell metabolic activity

The metabolic activity of cells within the alginate hydrogels was assessed by the Alamar blue assay with a colourimetric signal proportional to cell number at days 4, 9, 11, 15, 18, 23, and 25 post-seeding. At 18 days of culture (Figure 4-11), the reduction of Alamar blue reagent due to metabolic activity of encapsulated cells reached a maximum value of 55%; corresponding to an approximate 20% increase in cell mitochondrial activity from day 4 to 18 *in vitro*. While

after day 18, encapsulated β-TC-6-cells demonstrated a slight decrease in their mitochondrial

activity, with a reduction of 53% on day 25. However, when statistical analysis was performed,

no significant differences between the means of metabolic activity of cells on day 18 and day

25 were identified.
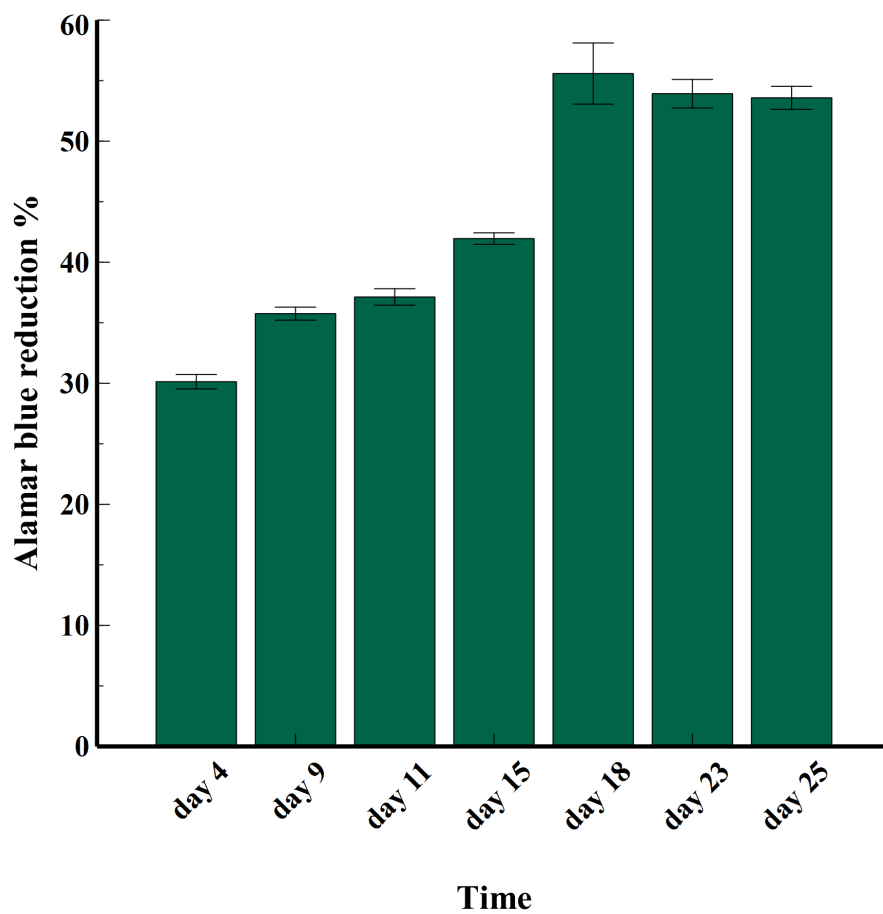
Figure 4-11
Metabolic activity of β-TC-6 cells within alginate matrix using the Alamar blue assay; results are presented as means± S.D. (n=3).

4.4.5 Antibody exclusion

To investigate the permeability of 1%w/v alginate microcapsules to immunologically relevant molecules, encapsulated cells were exposed to FITC-mouse antibody, which target the MHC class II antigens on the surface of beta cells. Compared with the control sample, cells encapsulated in alginate were successfully protected from the antibody. No fluorescence was detectable in the encapsulated samples using confocal microscopy; however, non-encapsulated cells showed a high fluorescence signal after being exposed to the FITC-linked antibody (Figure 4-12).

(a)

(b) **(c)**

(d) **(e)**
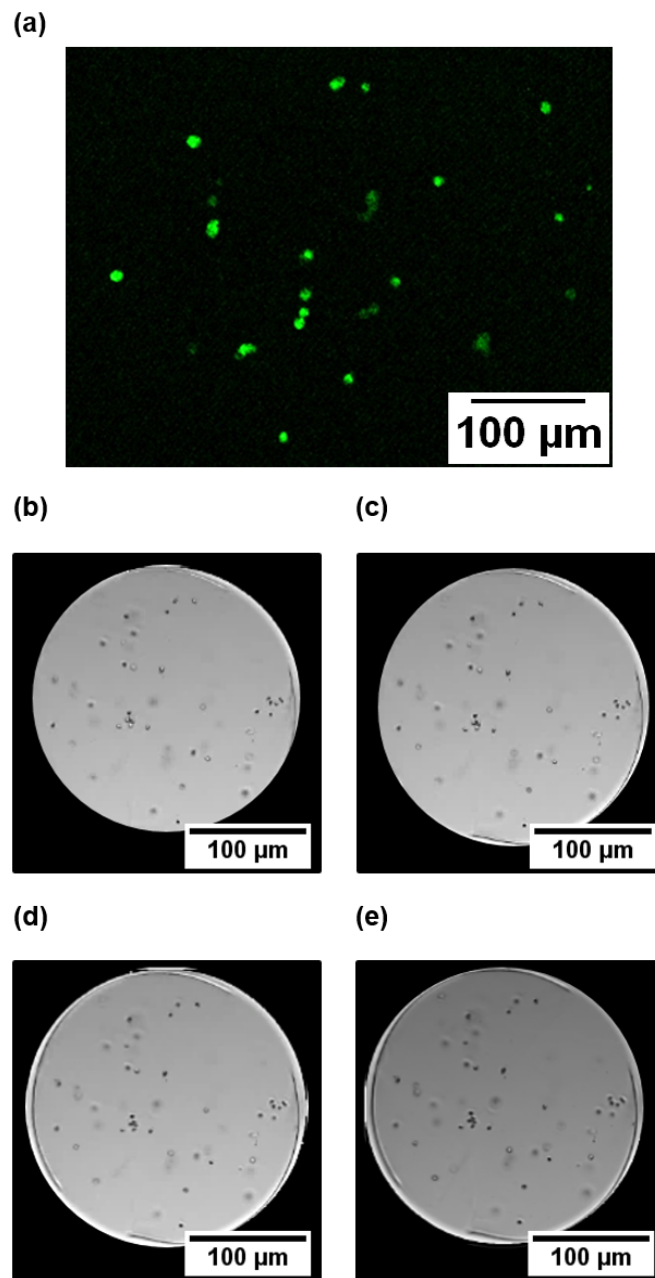
 Figure 4-12

Confocal images of cells after being exposed to FITC-mouse antibody. (a) Non-encapsulated cells. (b, c, d, and e) Z-stack merged-images of β-TC-6 cells embedded in alginate microparticle at thickness of 24 µm, 36 µm, 48 µm, and 60 µm from centre of the alginate particle, respectively (The merged images were acquired by transmitted imaging and FITC channel). All scale bars represent 100 µm.

4.4.6 *In vitro* assessment of beta cells function

Insulin secretion of pancreatic beta cells (MIN-6) in response to glucose was investigated on days 7 and 14 by culturing samples in a series of low (2 mM), and high (20 mM) glucose concentration. After 7 days, cells encapsulated in the alginate microcapsules showed an insulin secretion index (SI) greater than 1. Moreover, cells secreted 15.2 and 39.3 insulin (ng/mL) under low and high glucose conditions, respectively, which was similar to the amount of insulin secreted from the non-encapsulated cells (17.8 and 37.6 insulin (ng/mL) at low and high glucose condition (Figure 4-13: a). However, after 2 weeks the encapsulated cells displayed an unrepresentative insulin secretion response to glucose by showing lower SI value (Figure 4-13: b). Static analysis of quantitative data obtained on day 14 from the rat/mouse insulin enzyme-linked immunosorbent assay revealed a significant reduction in encapsulated cells insulin secreting functionality compared to encapsulated cells on day 7.
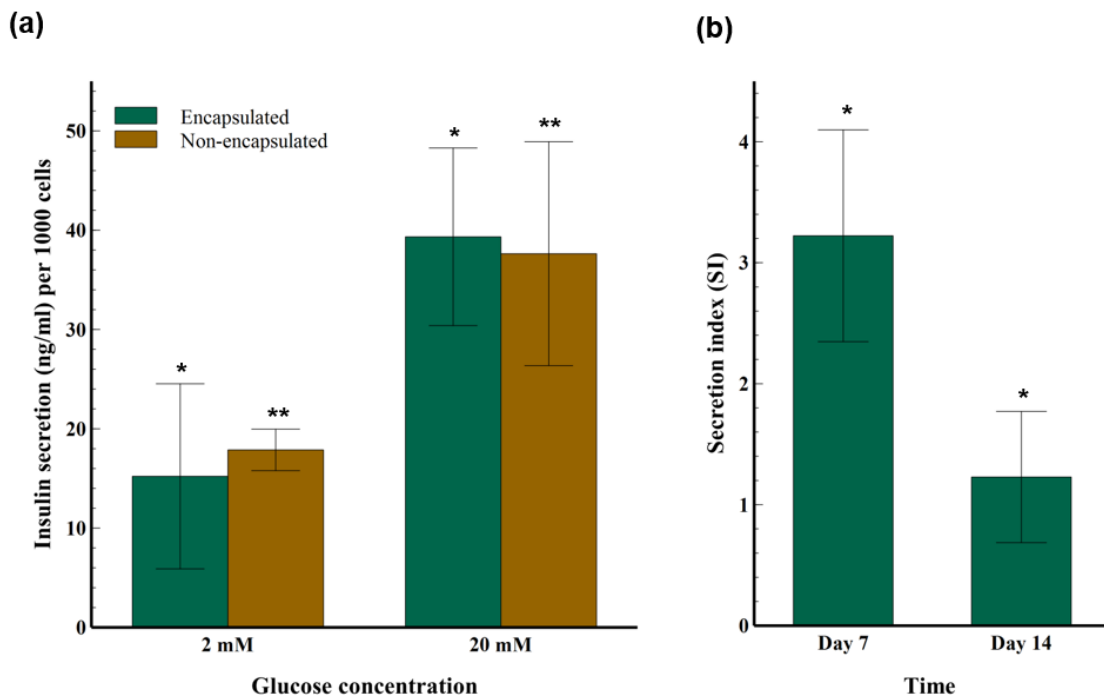
Figure 4-13
**Beta cell function in response to changes in glucose concentration using the GSIS assay.
(a) Insulin release of non-encapsulated (control) and encapsulated pancreatic cells on day
7; Insulin release was normalized against 1000 cells. (n=3), (*, ** $P<0.05$). (b) Stimulation
index of encapsulated cells on days 7, and 14; SI value shows the ratio between high
glucose and basal glucose (*, $P<0.05$).**

4.5   Discussion

Encapsulation of living cells in polymeric carriers has long promised to enable cell-based
therapies by camouflaging the encapsulated cells from the host's immune system. In this
work, β-TC-6 cells were encapsulated in alginate microparticles utilising a vibrating nozzle
technology. In comparison to conventional encapsulation techniques that often fail to
generate repeatable alginate microparticles with a narrow size distribution, the whole
vibrating nozzle encapsulation process was a simple, quick (~5 min for encapsulating 10 ml of

cell suspension in polymer), and in situ method for production of microcapsules with the capability of generating relatively uniform micro-droplets with a well-defined diameter.

Herein, the entire encapsulation process was conducted at room temperature under physiological pH. Preliminary observations showed that for the optimisation of the experimental parameters several factors, such as the nozzle, vibration frequency, polymer concentration, pump flow rate, and electric field strength, influence the final average diameter and size distribution of the generated particles. Optimisation of these parameters resulted in the generation of spherical microparticles with average diameter of 200 $\mu m \pm 19$ S.D when using a 1%w/v alginate solution. The resulting microcapsules were transparent with liquid core, as shown in bright field and dark field microscopy (Figure 4-4).

Investigation of alginate microparticle size change over time showed that initially the average diameter of particles increased as a result of hydrogel swelling behaviour (Figure 4-6: a). However, the particles showed a decrease from day 18, possibly due to the degradation process, as has been reported by previous studies [76]. Moreover, during this study no obvious changes in the surface morphology of alginate microparticles were observed. Overall, no obvious difference in diameter of microcapsules overtime with and without encapsulated cells was found, demonstrating that the encapsulated cells had no significant effect on the degradation rate of alginate microparticles.

Cell viability analysis demonstrated no significant effect of vibration frequency on viability of encapsulated beta cells. Cultures remained highly viable after 32 days (Figure 4-9). Most alginate encapsulation systems do not meet the important criteria of avoiding protrusion of

cells from capsules, which is associated with a fibrotic response and graft failure [108, 119]. 3D visualisation of alginate capsules revealed a uniform distribution of cells in the matrix without leakage of cells from capsules until 32 days of post-seeding (Figure 4-10. Notably, cells encapsulated within 2% alginate particles showed a reduction in their viability (Figure 4-8). Therefore, the low concentration of alginate (1%w/v) used here has possibly allowed sufficient perfusion of oxygen and nutrients, thus enhancing their long-term in vitro viability.

To get a more complete image of cell survival and the metabolic activity of β-TC-6 cells embedded in alginate hydrogel, a spectrophotometric-Alamar blue assay was performed at several time intervals. This analysis provided evidence that 1%w/v alginate hydrogels supported cell metabolic activity (Figure 4-11).

In the present study, we demonstrated that encapsulated cells were able to sense the changes in glucose concentration during the GSIS assay by showing secretion index of more than 1. On the other hand, our long-term *in vitro* study revealed a significant reduction in insulin secretion ability of encapsulated cells after 2 weeks (Figure 4-13).

In an attempt to further monitor endocrine pancreatic cells reduced capacity in secreting insulin after being cultivated for 14 days, microcapsules with double cell density (2 x 10^6 cells/mL) were also investigated with the GSIS assay. However, cells exhibited the same trend after being cultured in vitro for 2 weeks.

Despite the fact that encapsulated cells retained high viability and metabolic activity during the in vitro study, it was concluded that for endocrine cells, such as pancreatic insulin secreting

cells, reduction in their insulin functionality might be related to the low interaction between single cells dispersed in an alginate microcapsule in comparison to their physiological structure within the pancreatic islets. In the pancreas, beta cells function also depends on several regulatory signals from other tissues, including the liver, intestinal endocrine cells, fat, and the gut. Furthermore, interactions with glucagon releasing α-cells and sympathetic neurones enhance the ability of beta cells to stimulate insulin secretion and achieve normoglycaemia [23-25]. Therefore, in chapter 6 of this thesis, a detailed study was performed by the application of 3D cell culture plate, as a possible solution to increase cell-cell interactions within a novel encapsulated system.

5 CHAPTER FIVE

Cultivation of encapsulated cells in a fluidised bed

bioreactor

5.1 Introduction

Despite several studies on cell-based transplantation via microencapsulating technology, their clinical application has been hindered by several issues, including the insufficient transfer of nutrients [10], and the lack of a storage method for the cultivation of encapsulated cells prior to transplantation [13]. A promising methodology to address the issues with storage and distribution of a therapeutically relevant number of encapsulated cells between laboratory and clinical site could be through storage and expansion in bioreactors [13]. Bioreactors not only provide clinical accessibility but also lower the contamination risk associated with conventional culturing methods. Economically, these devices are regarded as a more cost effective approach for cell-based therapeutic studies compared to standard cell culture flasks, owing to less frequent media changes [13, 101, 102].

Stirred tank bioreactors (STR) [100], pneumatically agitated bioreactors (such as bubble column, and air-lift column) [100], membrane bioreactors (such as hollow fibres) [120], fixed-bed bioreactors [101], and fluidised bed bioreactors [105] are the most typical reactors that have been used for both plant and mammalian cell culture. Of these systems, hollow fibres are the most studied bioreactors for the cultivation of mammalian cells. Primarily, they have been investigated to treat liver failure as a bio artificial liver assist device [121].

The mechanism of hollow fibre bioreactors is based on the cultivation of adherent therapeutic cells on the outside of the fibres, and then the flow of fluid or blood can pass through the hollow fibres to nourish the cells [104, 120]. Apart from hollow fibres advantage in eliminating the need for any mechanical mixing compared to stirred-tank bioreactors and pneumatically

agitated bioreactors, their application for the cultivation of encapsulated cells has been hampered since they cannot be used for encapsulated cells. The non-applicability of hollow fibre bioreactors for microcapsules is mainly due to the existence of a semi-permeable membrane (fibre wall) between the encapsulated cells and the fluid, resulting in relatively low diffusion of nutrients [121]. Alternatively, fluidised bed bioreactors can provide direct contact between encapsulated cells and cell culture medium or physiological fluids. In these bioreactor systems, the difference between the density of encapsulated particles and the medium enables the suspension of particles with an upward flow of the medium and hence encapsulated cells will float throughout the column without the need for aeration or mechanical agitation [105, 121].

The present work investigates the feasibility of applying a fluidised bed bioreactor design for the cultivation of pancreatic insulin secreting beta cells encapsulated in uniform alginate microcapsules. The performance of the fluidised bed bioreactor was studied by evaluating beta cell viability, insulin secretion ability, microcapsule breakage, and swelling degree. Results from the bioreactor system were compared to that of conventional cell culture flasks.

5.2 Materials and methods

5.2.1 Cell culture

MIN-6 cells (AddexBio, San Diego, USA) were cultured in DMEM (4500 mg/L glucose) supplemented with 15% FBS, 2 mM L-glutamine and 0.05 mM 2-mercaptoethanol (Sigma, UK) [37]. Since mouse pancreatic beta cells have limited ability to tolerate oxidative stresses, 2-

mercaptoethanol was added to the cell culture medium to aid in maintaining a reducing environment; limiting toxic oxygen radicals. All cultures were incubated at 37°C with 5% CO_2 until they reached 70-80% confluency.

5.2.2 Cell encapsulation

Alginate solution (1%w/v) and cross-linking solution ($CaCl_2$) was prepared as mentioned in section 4.2.3. MIN-6 cells were grown in T-75 flasks to ≥80% confluency before harvesting. The cells were then detached from the culture flask using Trypsin-EDTA solution. After being washed in PBS, 2×10^6 cells/mL were suspended in the sterile polymer solution (total volume= 10 mL). The formation of microcapsules was carried out with the vibrational encapsulator (A B-395 pro); more details regarding the encapsulation procedure is provided in section 4.2.4. Formed microcapsules were then incubated in a 100 mM $CaCl_2$ bath for 10 min. After gelation, alginate microcapsules were washed with PBS and DMEM, respectively to remove any remaining calcium ions. Cellular microcapsules were then cultured in the bioreactor (fluidised culture) and T-75 culture flasks (Sarstedt, Germany) (static culture) for further studies.

5.2.3 Fluidised bed bioreactor

The fluidised bed bioreactor consists of a cylindrical vessel, and a feeding vessel containing the culture medium. A bioreactor (provided by Dr. Ellis at the University of Bath) with the following dimensions was used in this study: cylinder height=100 mm (with attached heading=80 mm), cylinder diameter= 15 mm, total volume= ~ 15 mL. To prevent alginate microcapsules escaping the column, PTFE frits with 100 µm pore size (Kinesis, UK) were added

to the bottom and top of the system. While the encapsulated cells were retained in the bioreactor column, the culture medium was pumped axially by a peristaltic pump through the cylindrical vessel via a circulating loop (Figure 5-1). The bioreactor set up was then incubated at 37°C with 5% CO_2. All bioreactors sections were autoclaved at 121°C for 30 minutes before experimental setup.
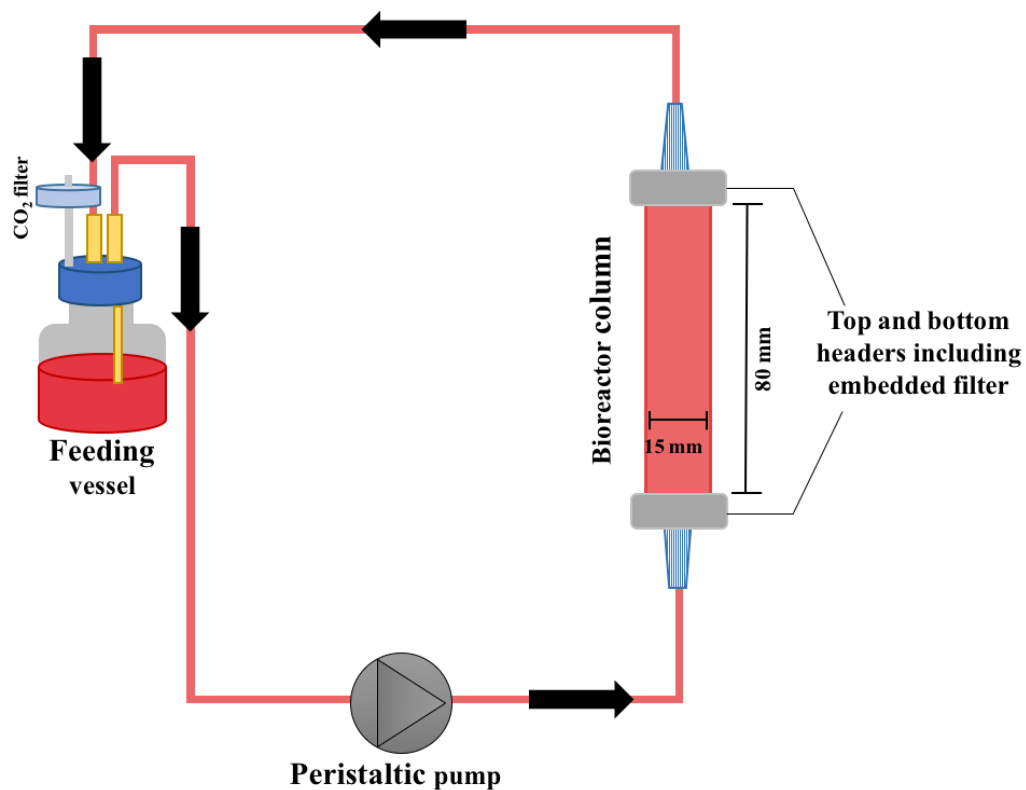
Figure 5-1
Schematic diagram of the fluidised bed bioreactor for the cultivation of encapsulated MIN-6 cells; closed sterile circulating loop includes bioreactor glass column, tubing with plastic connectors, bioreactor headers attached to frits with 100 µm pore size, cell culture feeding bottle, and a peristaltic pump.

5.2.4 Performance of fluidised bed bioreactor

The fluidisation performance of the bioreactor was quantitatively evaluated by measuring the bed expansion parameter. The pump flow rate was increased until particles reached within 1 cm vicinity of the filter located at the top end of the bioreactor column, and the height of the fluidised bed within the column was measured at each flow rate. Expansion of encapsulated acellular microparticles versus different flow rates was then calculated using Equation 5-1. Images of fluidised microcapsules were imaged using a USB digital microscope (Veho, UK).

$$H/H_0 = (1-\varepsilon_0)/(1-\varepsilon) \qquad\qquad \textbf{Equation 5-1}$$

Where H_0 and ε_0 indicate initial bed height and porosity, and H indicates achieved bed height [122].

5.2.5 Microcapsules degree of swelling

After 1 and 7 days of culture, 500 µL of DMEM media containing encapsulated MIN-6 cells was collected from the fluidised bed bioreactor and T-75 cell culture flask (control). Fifty microcapsules were randomly captured using light microscope connected to a digital camera, and their diameter was evaluated using Image J software. To indicate the effect of fluidisation on encapsulated particles, the degree of swelling of both samples in static versus fluidised culture was calculated using Equation 5-2.

$$S_w = [(D_t/D_0)^3 - 1] \qquad\qquad \textbf{Equation 5-2}$$

Where D_0 indicates average diameters of alginate microparticles on day 0, and, D_t indicates average diameter on day 1 or 7 [123].

5.2.6 Encapsulated microparticle stability

Microparticles cultured in both fluidised bed bioreactor and cell culture flask were randomly selected and observed under a light microscope (n= 200 microcapsules). The number of damaged and/or broken microparticles were noted on the day of encapsulation (day 0) and after 1 and 7 days of culture in both static and fluidised culturing conditions.

5.2.7 Cell viability

The viability of MIN-6 cells encapsulated in alginate microparticles from both the fluidised bioreactor and culture flask were assessed using a two-colour fluorescence method involving PI (indicator for dead cells), and calcein AM (indicator for viable cells). Briefly, 5 µL of calcein AM and 25 µL of PI was added to 2 mL of capsules suspended in DMEM, followed by incubation at 37℃ for 40 min. After staining, the cells were imaged using confocal laser scanning microscopy, and raw data from z-stack was analysed with Imaris software, more details was provided in section 4.2.9.

5.2.8 Insulin secretion

To investigate the functionality of encapsulated MIN-6 cells cultured in both the fluidised bed bioreactor and static condition, the secreted amount of insulin in response to changes in glucose was measured using the GSIS assay (section 4.2.12). Briefly, collected samples from

both groups were washed and pre-incubated in KRBH + 0.1% BSA for 2 h. Samples were then statically incubated for 1 h with low (2 mM) glucose concentration in KRBH+ 0.1% BSA followed by the addition of high (20 mM) glucose concentration in KRBH+ 0.1% BSA as the stimulator and samples incubated for another hour. For each incubation period, the samples were collected during GSIS for quantitative evaluations. The collected samples were then diluted to the appropriate range based on the assay standard curve (1:100 ratio). Secreted insulin was measured using a rat/mouse insulin ELISA, and the colorimetric reaction was quantified using a plate spectrophotometer at 450 nm. CyQUANT cell counting kit was utilised to normalise the ELISA results to the number of encapsulated cells in each sample. The insulin-stimulated index (SI) was calculated from the ratio of insulin secreted under high and low glucose stimulation.

5.3 Statistical analysis

Results are presented as mean ± standard error of the mean unless otherwise stated. Student's t-test, assuming equal variance, was used to identify any significant differences between pairs of groups. A p-value < 0.05 was determined as significant.

5.4 Results

5.4.1 Fluidisation of microparticles

Fluidisation of cell embedded microcapsules within the bioreactor was initiated by the passage of an upward flow of cell culture medium through the fixed bed of accumulated

microcapsules located at the bottom of the column (H_0= 1cm). Further increase in fluid flow

rate, forced upward movement of alginate particles, followed by the horizontal and

homogenous rise of the bed height until particles reached the top filter. Quantitative

evaluation of bed expansion versus fluid flow rate was determined as an important parameter

in evaluating fluidisation quality (Figure 5-2). For fluid flow rates up to 100 µL/min particles

were partially distributed within the column and complete suspension of particles within the

entire length was achieved at 2000 µL/min (Figure 5-3).

(a)

Flow rate=0.0011 × pump rpm+0.177

R^2= 0.9998

(b)
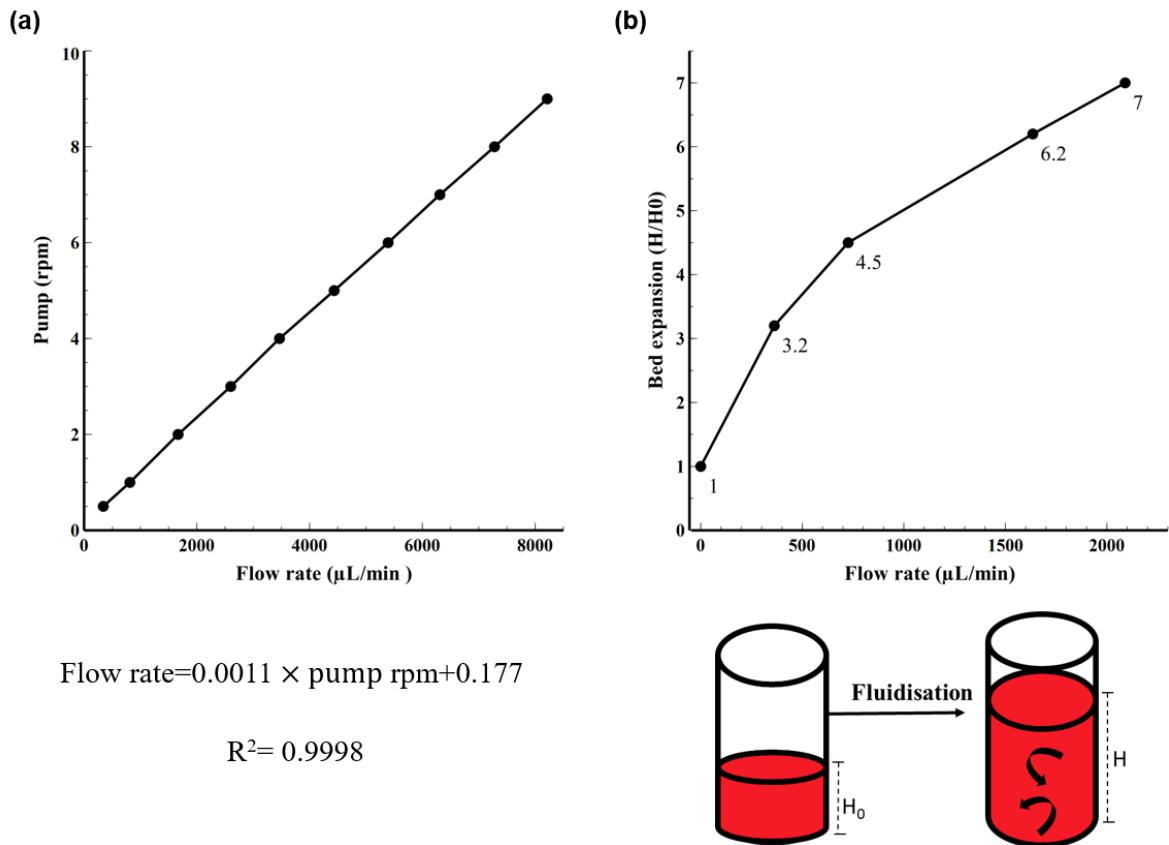
Figure 5-2
Quantitative evaluation of fluidisation using bed expansion parameter. (a) Calibration curve of the peristaltic pump utilised for pumping the cell culture medium through the bioreactor column. (b) Quantitative characterisation of fluidisation quality using bed expansion parameters (H_0 and H indicate initial bed height, and achieved bed height versus flow rate, respectively).
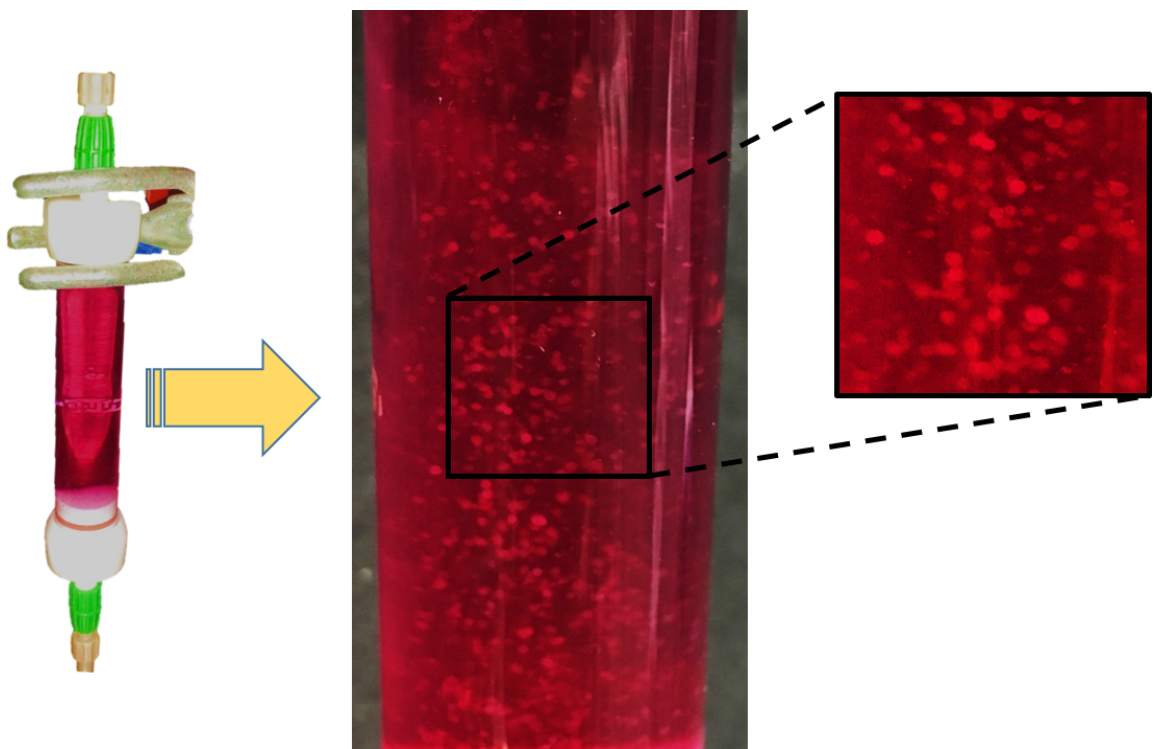
Figure 5-3

Visual observation of fluidised cellular alginate microcapsules within fluidised bed bioreactor at the fluid flow rate of 2000 µL/min.

5.4.2 Stability of alginate microcapsules

A comparison of cellular microcapsule stability in fluidised versus static culture was investigated at the maximum flow rate of 2000 µL/min (Figure 5-4). The difference in swelling degree of cellular microparticles 24 h post-encapsulation was not significant (P=0.69) between particles cultured in the fluidised bed bioreactor and T-75 culture flask. After 7 days of culture, the same trend was observed between the two groups (p=0.053) and encapsulated cells exhibited a similar morphology under both culturing conditions.
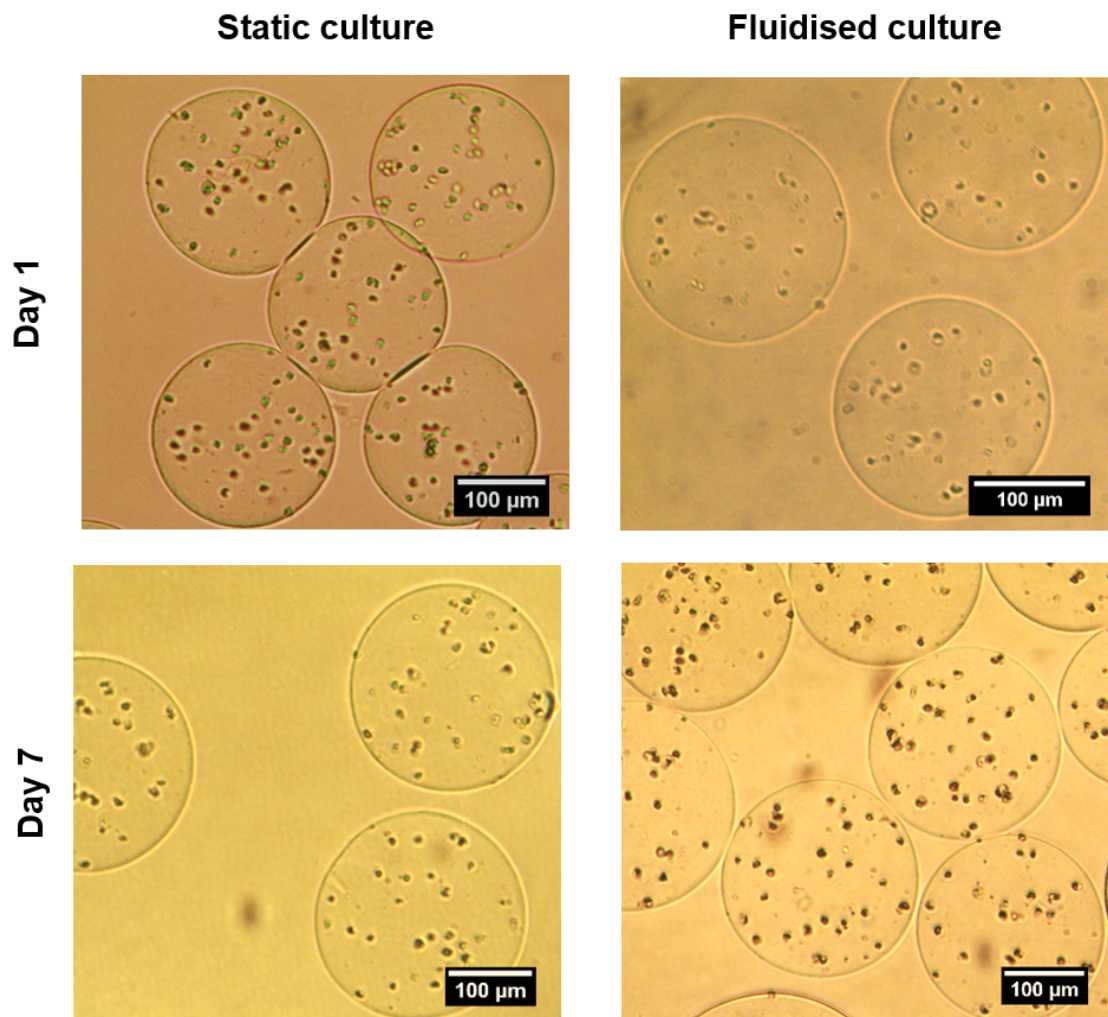
Figure 5-4
Optical micrographs of MIN-6 pancreatic cells (2 x 10^6 cells/mL) embedded within alginate microcapsules cultured for 7 days in a fluidised bed bioreactor and T-75 cell culture flask. Scale bars are 100 μm.

In addition, an increase in the diameter of microcapsules was observed over time within both fluidised (from 271.26 ±5.4 μm to 299.24 ±5.3 μm) and static culture (from 275.57 ±5.1 μm to 341.66 ±7.8 μm) (Figure 5-5).
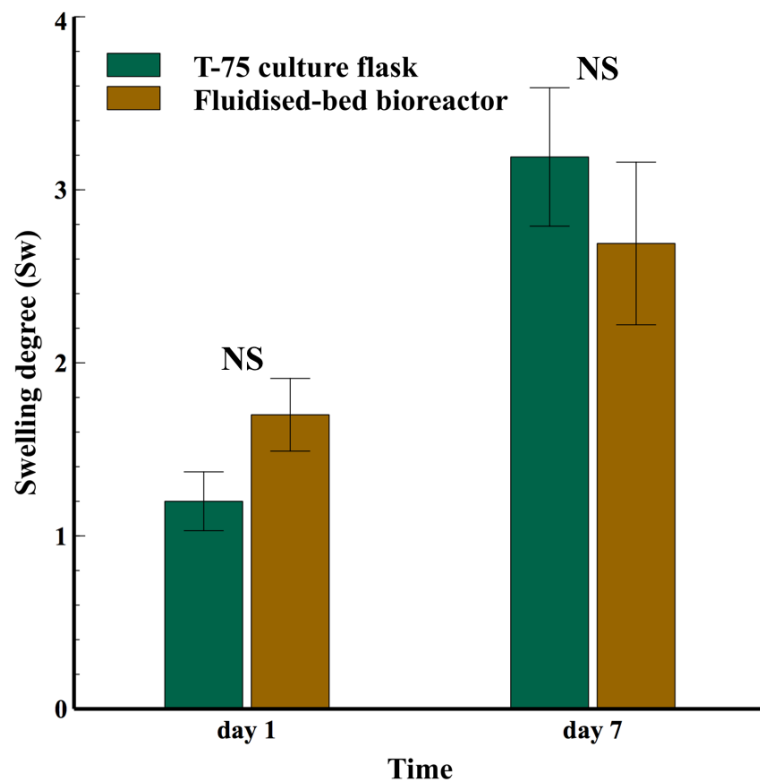
Figure 5-5

Comparison between swelling degree of cultured cellular alginate microcapsules under static and fluidised (flow rate= 2000 µL/min) conditions on days 1 (NS, P=0.053) and 7 (NS, P=0.69), (particles number= 50). NS=non-significant.

To further investigate the effect of fluidisation (flow rate= 2000 µL/min) on the resilience of the cellular microparticles to fracture, alginate capsules from both fluidised and static culture were optically observed in search of any ruptured microcapsules (Figure 5-6: a). The percentage of damaged cellular microcapsules from both fluidised and static culture differed

less than 1.2% and 2% on day 1 and 7, respectively (Figure 5-6: b). Overall, among the entire randomly selected microcapsules (n = 200), only 4% damaged capsules were found in fluidised condition on day 7.
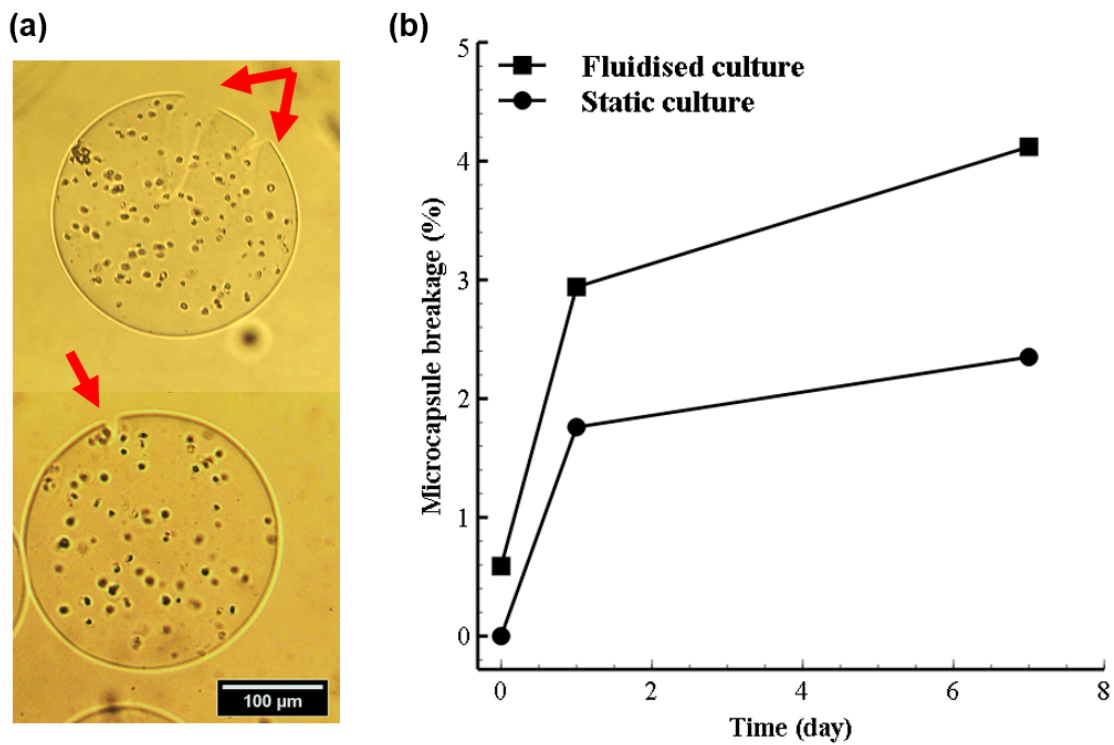
Figure 5-6
Light micrograph of damaged alginate microcapsules captured on day 7 in fluidised bed bioreactor. (d) Comparison of fluidisation impact on cellular alginate microcapsules breakage under static and fluidised culture (particles number= 200). Scale bar shows 100 μm.

5.4.3 Evaluation of cell viability

Besides 2-dimensional micrographs of groups of live/dead fluorescently stained cells in alginate capsules (Figure 5-7), confocal laser scanning microscopy enabled 3-dimensional reconstruction of an individual microcapsules using the z-stack imaging technique (Figure 5-8). In both static and fluidised culture, there were very few dead MIN-6 cells within the group of encapsulated microparticles. Therefore, qualitative observation exhibited high viability of cells cultivated in the fluidised bed bioreactor versus T-75 culture flask conditions after 1 and 7 days of *in vitro* studies.
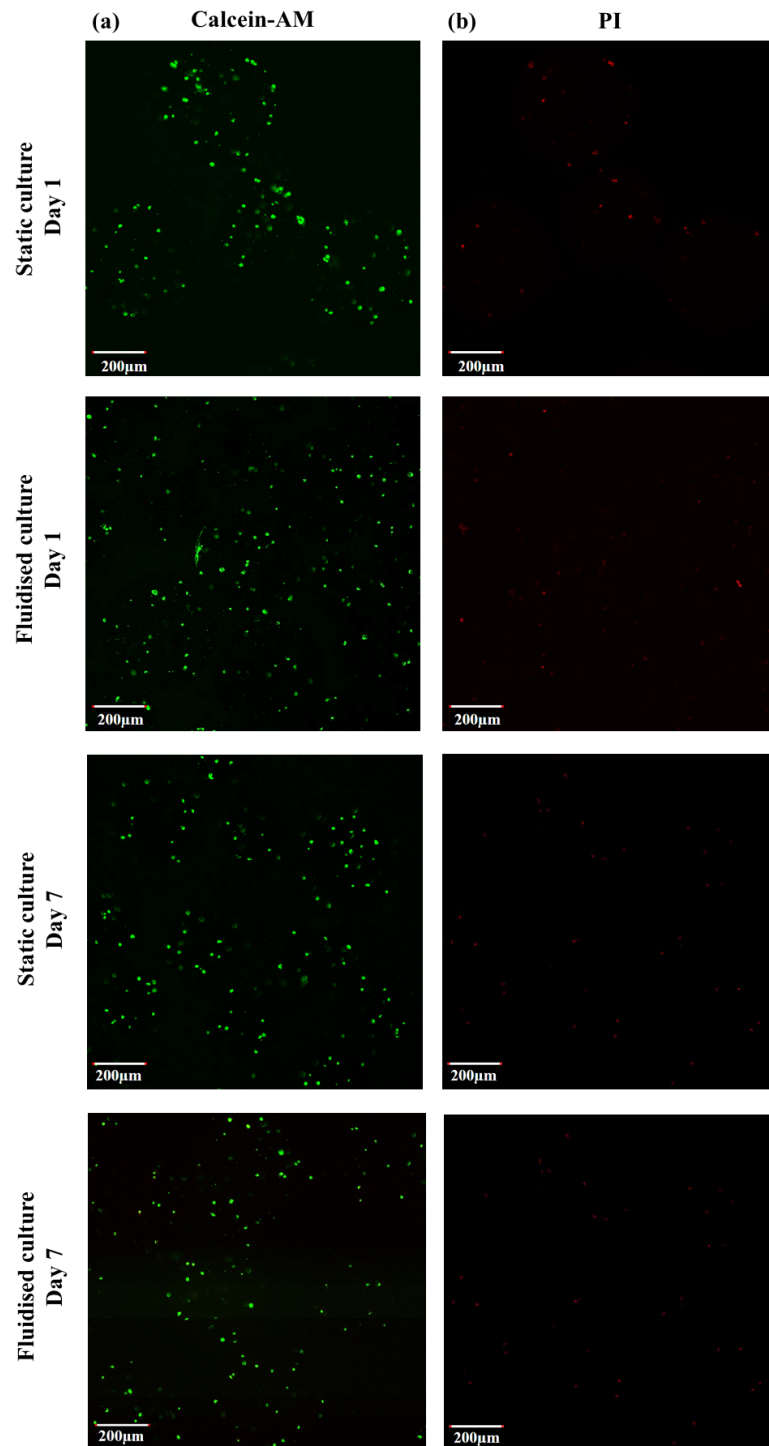
Figure 5-7

Evaluation of encapsulated cell viability in fluidised versus static culture. (a) Unmerged two-dimensional confocal micrographs of live cells (calcein AM marker: green channel) within a group of alginate microcapsules. (b) Unmerged two-dimensional confocal micrograph of dead cells (PI marker: red channel) within a group of alginate microcapsules. Scale bars represent 200 μm.
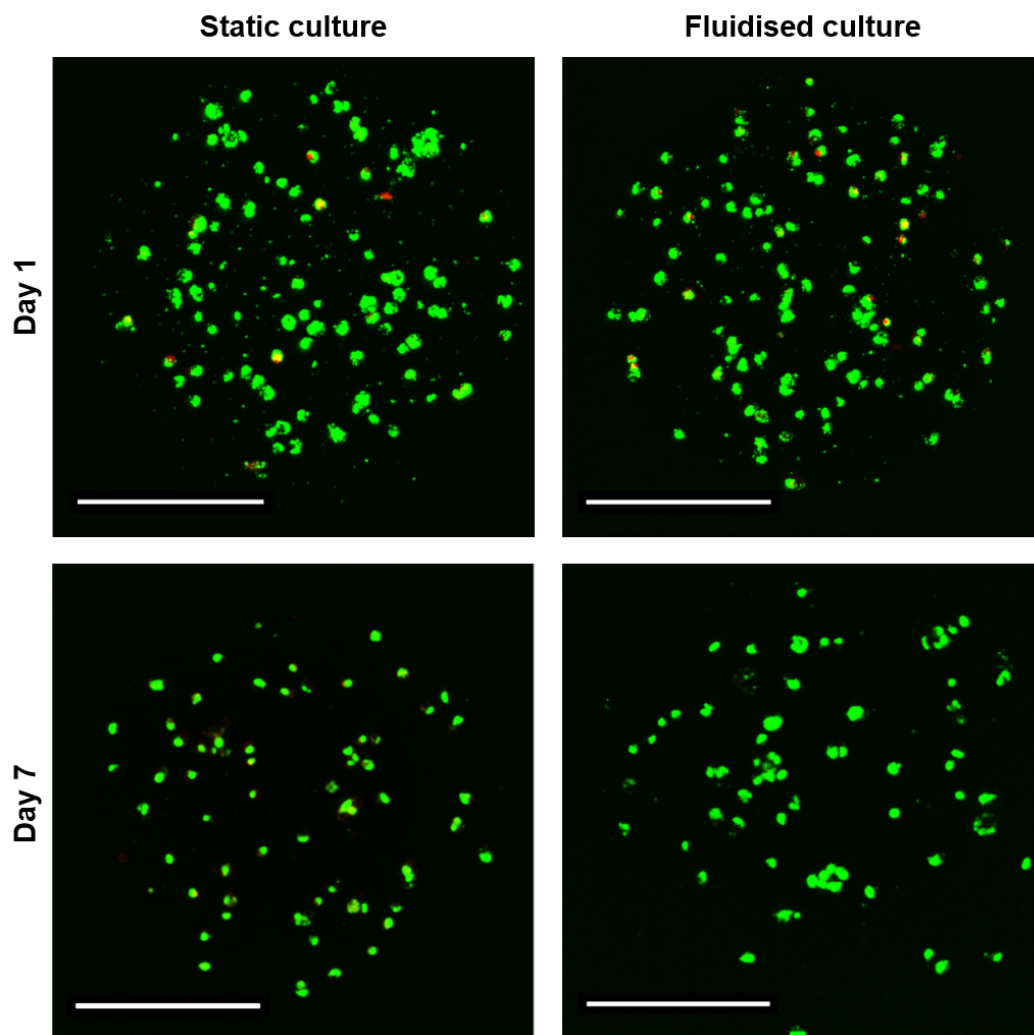
Figure 5-8
3-dimensional reconstruction of one cellular alginate microcapsule with merged green (calcein AM) and red (PI) channels. Scale bars represent 200 μm.

5.4.4 Insulin secretion in response to glucose

The secretion of insulin in response to changes in glucose concentration, which is essential to assess the functionality of encapsulated cells *in vitro*, was evaluated using GSIS assay.

Obtained results confirmed that encapsulated MIN-6 cells within 1% alginate were able to show a significant increase in amounts of secreted insulin when transferred from low to high glucose concentration (P<0.001), regardless of the culture condition.

On day 1, encapsulated MIN-6 cells cultivated in fluidised bed bioreactor secreted 30.2 ± 5.1 ng/mL and 103.1 ± 14.4 ng/mL in response to 2 mM and 20 mM glucose concentration, respectively (SI= 3.4). In contrast, cells cultured in static culture secreted 20.7 ng/mL± 3.5 in low and 50.3 ng/mL± 1.9 in high glucose concentration (SI= 2.4). Statistical analysis confirmed cells response to glucose stimulation were significant (P= 0.002) for fluidised bed bioreactor compared to the static culture condition in a T-75 flask (Figure 5-9).
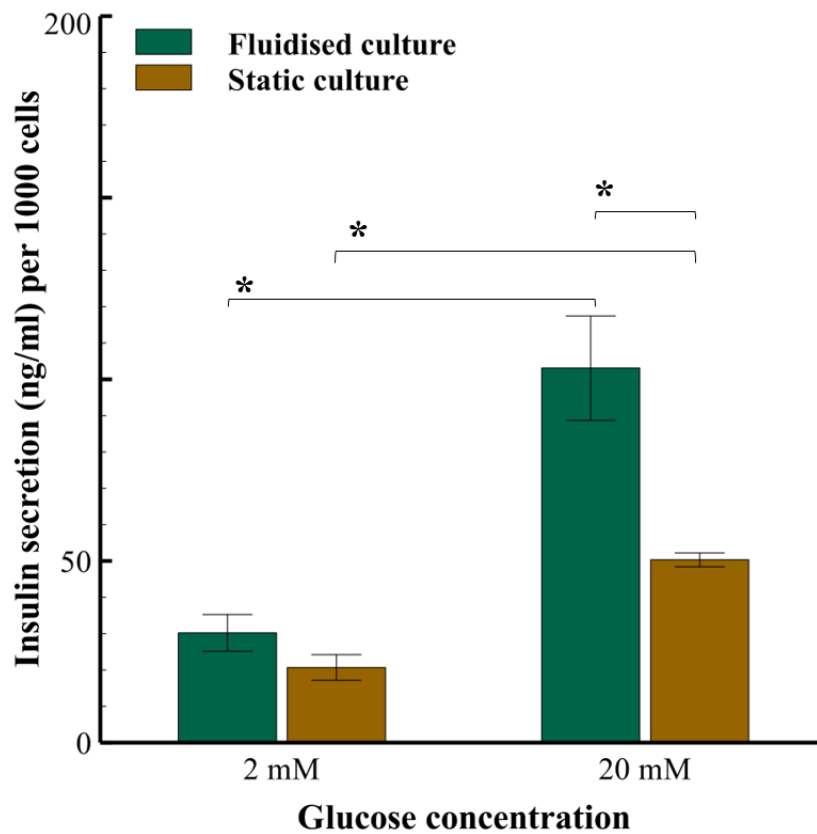
Figure 5-9

Insulin secretion of MIN-6 cells in response to glucose stimulation on day 1; insulin release from encapsulated cells cultivated in static culture versus fluidised bioreactor was normalised against 1000 cells. Results are represented mean ± SEM (n= 4), (*P<0.05).

The same trend was observed on day 7 post-encapsulation; MIN-6 microcapsules cultivated in the fluidised bed bioreactor secreted significantly more (P< 0.001) insulin when exposed to higher glucose concentration compared to the static condition. Figure 5-10 showed that samples from fluidised bed bioreactor secreted 46.6 ng/mL± 12.3 and 170.7 ng/mL± 13.9 in high and low glucose concentration (SI= 3.7), respectively. While samples from static culture

secreted 32.6 ± 6.6 ng/mL in 2 mM glucose solution, and 74.3 ± 0.2 ng/mL in response to 20

mM glucose concentration (SI= 2.3).
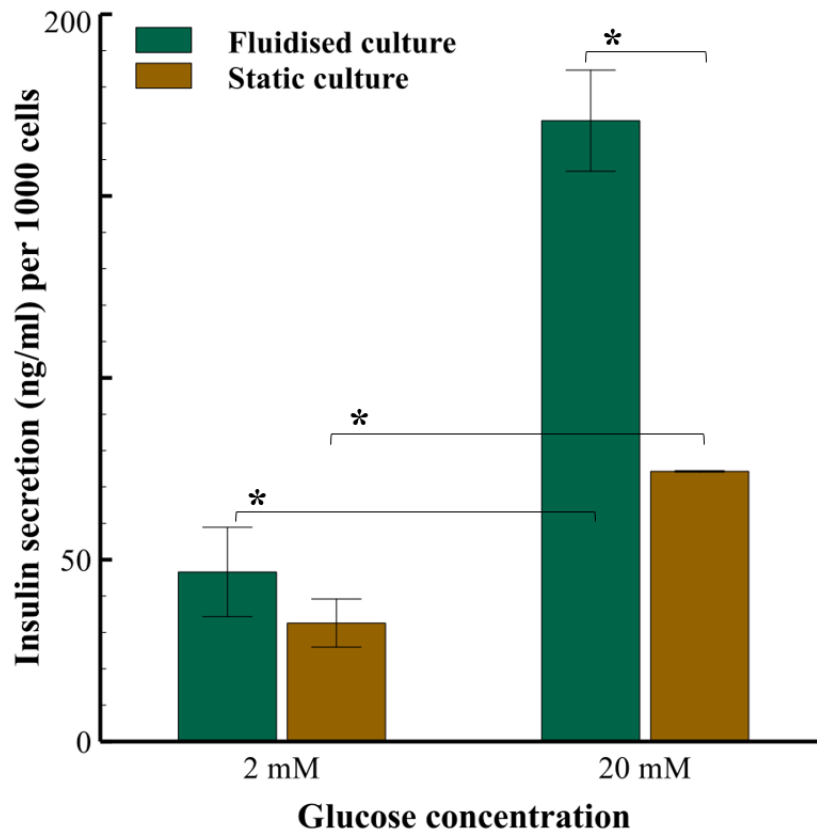
Figure 5-10
Insulin secretion of MIN-6 cells in response to glucose stimulation on day 7; insulin release was normalised against 1000 cells. Results are represented mean ± SEM (n= 4), (*P<0.05).

5.5 Discussion

A variety of bioreactors has been studied for a broad range of applications, including biopharmaceutical, bacteria and yeast culture, enzyme production, scaffolds, and mammalian cell culture (mainly for hepatocytes, and bone marrow stromal osteoblasts) [106, 124, 125]. However, there are fewer published studies regarding the experimental application of bioreactors for cell-based microencapsulated systems. Herein, a simple fluidised bed bioreactor was studied to cultivate pancreatic MIN-6 cells encapsulated within alginate. The use of fluidised bed for mammalian cells has several advantages compared to other types of bioreactors. This mainly includes their ability to allow sufficient mass transfer, owing to the perfusion of cell culture medium through the bioreactor column, which provides direct contact between the encapsulated cells and the medium for the exchange of nutrients and oxygen [126].

Unlike plant cells, mammalian cells do not have cell wall [127], which make them more vulnerable to shear forces imposed by mechanical mixing in pneumatically, and stirred-tank bioreactors. Hence, application of a fluidised bioreactor, based on the upward flow of the medium and its circulation through the column, completely removes the need for mechanical mixing with impeller or aeration, and this improves survival of cells with higher shear sensitivity [100, 128]. Fluidised bioreactors have a very simple design (Figure 5-1) with low manufacturing cost, especially compared to the more complex hollow fibre bioreactors. This chapter introduced a new application of fluidised bioreactors to overcome the existing transplantation challenge by providing a handling method between manufacturing and clinical site. This approach could also be beneficial to minimise loss and damage prior to

transplantation, especially for transplantation of cells with insufficient donor supply, such as pancreatic beta cells obtain from cadaveric donors [26].

Herein, characterisation of fluidisation quality within bioreactor column was evaluated by measuring bed expansion versus medium flow rates (Figure 5-2). The application of the vibrational encapsulator, discussed in more detail in Chapter four, allowed the generation of reproducible, and uniformly shaped and sized alginate microcapsules with the average diameter of 200 ± 19 μm S.D. The value of bed expansion is in connection with factors, such as fluid velocity, micro-carriers diameter, and fixed-bed height (H_0) [129]. Consequently, the formation of microparticles with high uniformity enhanced homogenous mixing of particles throughout the entire bioreactor column (Figure 5-3). This was also confirmed evaluating encapsulated cell viability and insulin secretion sensitivity.

Additionally, the feasibility of applying a fluidised bed bioreactor for the cultivation of cells primarily relies on the ability of the fluidised system to provide the least damage to the stability of the immunoisolated semipermeable membrane. As was shown in Figure 5-5, at a maximum flow rate of 2000 μL/min to achieve expansion of particles throughout the entire column, no statistically significant difference was observed between the swelling degree of cellular microparticles cultured in fluidised bed bioreactor or T-75 flask. In Figure 5-5 the increase observed in the average diameter of alginate microcapsules from day 1 to day 7 was expected due to the swelling behaviour of alginate hydrogel, which has been reported both in chapter four of this thesis and previous studies [76]. This result in parallel with low microcapsule breakage (Figure 5-6) suggested the promising performance of fluidised bioreactor used in here for the cultivation of encapsulated MIN-6 cells within 1% alginate

transplantation, especially for transplantation of cells with insufficient donor supply, such as pancreatic beta cells obtain from cadaveric donors [26].

Herein, characterisation of fluidisation quality within bioreactor column was evaluated by measuring bed expansion versus medium flow rates (Figure 5-2). The application of the vibrational encapsulator, discussed in more detail in Chapter four, allowed the generation of reproducible, and uniformly shaped and sized alginate microcapsules with the average diameter of 200 ± 19 µm S.D. The value of bed expansion is in connection with factors, such as fluid velocity, micro-carriers diameter, and fixed-bed height (H_0) [129]. Consequently, the formation of microparticles with high uniformity enhanced homogenous mixing of particles throughout the entire bioreactor column (Figure 5-3). This was also confirmed evaluating encapsulated cell viability and insulin secretion sensitivity.

Additionally, the feasibility of applying a fluidised bed bioreactor for the cultivation of cells primarily relies on the ability of the fluidised system to provide the least damage to the stability of the immunoisolated semipermeable membrane. As was shown in Figure 5-5, at a maximum flow rate of 2000 µL/min to achieve expansion of particles throughout the entire column, no statistically significant difference was observed between the swelling degree of cellular microparticles cultured in fluidised bed bioreactor or T-75 flask. In Figure 5-5 the increase observed in the average diameter of alginate microcapsules from day 1 to day 7 was expected due to the swelling behaviour of alginate hydrogel, which has been reported both in chapter four of this thesis and previous studies [76]. This result in parallel with low microcapsule breakage (Figure 5-6) suggested the promising performance of fluidised bioreactor used in here for the cultivation of encapsulated MIN-6 cells within 1% alginate

microparticles. Notably, the bioreactor utilised in this particular study was designed for microcarriers with >150 μm in diameter, owing to the inserted frits filters within both top and bottom headers of the bioreactor column. It is worth mentioning that loading particles with larger size within the fluidised bioreactor used here will increase the initial bed height (H_0). Therefore, affecting the bed expansion rate, which may then require the application of column with larger dimensions compared to the one used in this study. This could then provide enough free space within the column for achieving efficient mixing between the encapsulated cells and the cell culture medium.

The fluidised bed bioreactor outcome on the biological activity of MIN-6 cells was another important aspect evaluated in this study. Confocal laser scanning microscopy, shown in Figure 5-7 and Figure 5-8 established the high viability of encapsulated cells cultivated in fluidised culture. Results suggest that fluidisation achieved in the bioreactor column did not have any harmful effect on cell viability. Additionally, determination of MIN-6 cells ability to remain functional in fluidised culture revealed that encapsulated cells cultivated within the bioreactor exhibited higher insulin sensitivity compared to the control group. Notably, comparison of results obtained from GSIS assay on day 1 (Figure 5-9) versus day 7 (Figure 5-10), showed the insulin-stimulated index of encapsulated MIN-6 cells in static culture was slightly reduced from 2.4 to 2.3. Whereas, in the case of the fluidised bed bioreactor, in conjugation with encapsulated cells ability in secreting more amount of insulin on day 7, the value of the insulin-stimulated index was also exhibited an increasing trend from 3.4 to 3.7.

An explanation for enhanced insulin sensitivity of pancreatic MIN-6 cells in the fluidised culture could be described as follows: during static culture of encapsulated particles,

microcapsules accumulate at the bottom of cells culture flask. Therefore, nutrients and oxygen have to diffuse through the capsules on upper layers to reach the cell embedded in microcapsules at the bottom of the culture flask. Gradually, cells at the bottom of the culture flask could suffer from lack of nutrients and oxygen compared to the other encapsulated cells. On the other hand, fluidised culture provides an equal chance for all cells to be exposed to the cell culture medium within the entire length of the column. Based on above, homogenous nourishing environment achieved here using fluidised culture resulted in enhanced function of endocrine insulin-secreting beta cells versus static culture.

Moreover, during 7 days of in vitro culture, the fluidised bed was connected to 20 ml of cell culture medium container without the addition of fresh culture medium through the in vitro fluidisation, which to a great extent can reduce the risk of contamination owing to the lower requirement to open the sterile bioreactor circulating loop. Whereas, in the case of encapsulated cells within the static cell culture flask, the medium needed to be diluted with fresh DMEM every other day to provide essential nutrients, and prolong the microparticles hydration. This, in fact, shows the ease of application of fluidised bioreactor for maintaining encapsulated cells viability and functionality in the clinical sites, even if there are unexpected delays in surgical transplantation, which currently with conventional static cell culturing methods cannot be easily maintained [13].

6 CHAPTER SIX

Encapsulation of beta cell spheroids using

polyelectrolytes

6.1 Introduction

Encapsulation of pancreatic beta cells within polymeric microcapsules prior to transplantation can protect the cells from the host immune system, which would eliminate the need for immunosuppressant drugs. Critically immunoisolation should be balanced with the need for the diffusion of oxygen, signalling molecules, nutrients, and secreted products, such as insulin [2, 61]. An excellent encapsulation system, which could meet all the characteristics mentioned above, seems to be a major requirement to enhance the efficacy of cell transplantation for T1D. Up until now, the relatively large diameter of microcapsules (400-800 μm) in comparison to the transplantation site, results in an unfavourable ratio between encapsulated cells volume and overall capsule volume [10, 20]. Consequently, the large distance between the encapsulated cells and the surrounding environment results in a limited mass transfer, hypoxia, and ultimately cell dysfunction and death [8].

A possible solution may be to coat cells with polyelectrolytes rather than embedding cells in a polymeric matrix. This coating could be achieved using a technique known as PEM, which is based on the alternate deposition of anionic and cationic polyelectrolytes onto a charged surface, and was discussed in more detail in chapter three of this thesis [130, 131]. This approach limits the gap between the cells and the surrounding environment resulting in a shorter response time to external stimulation [132], while retaining a coating that may prevent immune response. In the case of pancreatic beta cells, this may allow rapid response to changes in blood glucose and thereby better regulation of insulin and glucose levels.

Apart from alginate's ability to form into microcapsules using divalent cross-linkers, it can form polyelectrolyte complexes in the presence of polycations, such as PLL and chitosan [133-135]. In this chapter, alginate (anionic polyelectrolyte) and PLL (polyelectrolyte with a positive charge) were applied to build polyelectrolytes bilayers. Owing to the negative charge of cells, PEM coating is typically initiated by the deposition of a cationic polymer. However, previous studies have shown that when cationic polymers are used in direct contact with cells, it increases the possibility of host inflammatory responses and cytotoxic behaviour [8, 98]. Therefore, here a novel pre-coating step was introduced into a conventional PEM coating method to minimise the influence of PLL on cell viability by conditioning the surface of cell aggregates with $CaCl_2$, before exposure to PLL. The resulting spheroids were analysed with respect to viability, functionality, and immunoisolation.

In chapter four, it was hypothesised that the reduced ability of the pancreatic beta cells to function over time could be associated with the low cell-cell interactions between individual cells encapsulated within the matrix of one microparticle. This was addressed in here by evaluating the effect of utilising 3-dimensional cell culturing technique to create beta cell spheroids in search of higher cell-cell interactions prior to PEM coating. Then, the possible effect of this approach on the function of endocrine insulin-secreting beta cells was investigated using the GSIS assay.

6.2 Materials and methods

6.2.1 Cell culture

MIN-6 cells were cultured in supplemented DMEM (section 5.2.1). All cultures were incubated at 37°C with 5% CO_2 until they reached 70-80% confluency. Culture medium was changed every other day to enhance cell growth and viability.

6.2.2 Seeding beta cells within micro-wells

Micro-molds (Sigma-Aldrich, UK) were used for casting 3D culture plates by adding 500 µL of 2 w/v% agarose (Sigma-Aldrich, UK) solution into each mold. The final transparent agarose culture plate with 400 µm diameter micro-wells (number of micro-wells per mold: 256) were removed from the mold after being cooled (Figure 6-1).
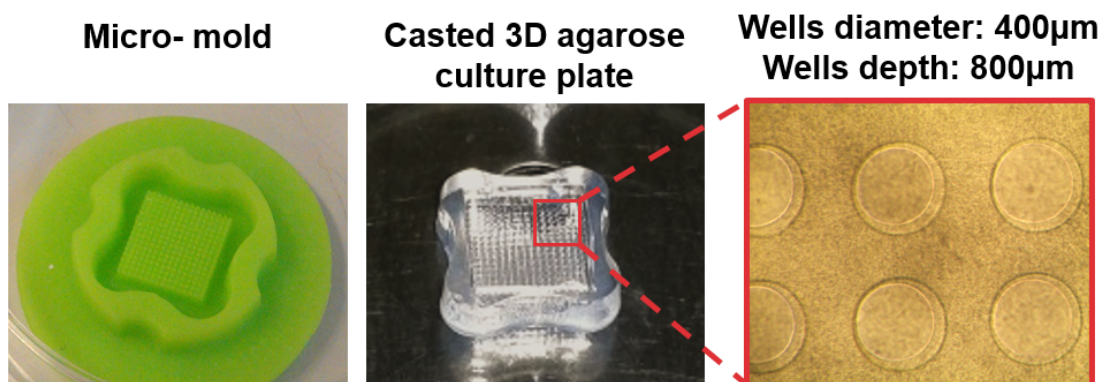
Figure 6-1
3D culture plate cast using 2 w/v% molten agarose. The final agarose culture plate contains 256 micro-wells with a concave bottom.

Cells were first trypsinized with trypsin-EDTA and counted with a haemocytometer. MIN-6 cells suspended in supplemented DMEM, at different densities of 2 x 10^5, 3 x 10^5, and 5 x 10^5 cells/200 µL (each agarose 3D culture plates can contain the maximum volume of 200 µL of cell suspension in DMEM), were seeded on top of the concave agarose micro-wells. Different cell densities were investigated to achieve robust and uniform beta cell spheroids. Spheroid formation was observed daily using an inverted microscope, and formed spheroids were used for further studies after being cultured for 4-5 days.

6.2.3 Comparison between 2D and 3D culture plates

The size of the MIN-6 cell spheroids formed in micro-wells were compared with the same concentration of cells 5 x 10^5 cells/200 µL (2.5 x 10^6 cells/mL) seeded on flat-bottomed non-attachable 35 mm cell culture plates (ThermoFisher Scientific, UK). The average diameters of the two groups were determined on day 7 of culture from thirty randomly selected samples, which were observed using a light microscope. Quantitative data was determined using Image J software.

6.2.4 Coating MIN-6 spheroids with multi-polyelectrolyte layers

After 4-5 days of culture, cell spheroids were retrieved from the micro-wells by inverting the 3D agarose culture plates under 450 rpm for 5 min using a plate shaker (Grant-bio, PMS-1000i, UK). Solutions of alginate (1 mg/mL) (ALG, medium viscosity ($\geq$ 20,000 cP, M/G ratio= 1.56) and PLL (1 mg/mL) (MW: 30,000-70,000, Sigma, UK) were prepared in deionised water and PBS, respectively. All solutions were sterile filtered using a 0.22 µm syringe filter and UV

sterilised overnight. Contrary to the conventional layer-by-layer polyelectrolyte deposition, before starting the coating process cell spheroids were first suspended in 200 μL of CaCl$_2$ (100 mM) (Figure 6-2). After washing with PBS, 200 μL of alginate was added to minimise the potential toxicity of direct contact between cells surface and cationic polymer (PLL). Alternating layers of PLL and alginate were then applied according to conventional PEM methods [92, 136]. Briefly, 200 μL of PLL was added to the pre-coated spheroids, after 4 min deposition time, cells were washed twice in 500 μL PBS to remove any unbound PLL, followed by the addition of the anionic polymer (alginate) with the same procedure. The last two steps were repeated to achieve the desired number of layers. Finally, cells were washed three times with DMEM and were incubated at 37°C for further studies.

Conventional PEM

Uniformly aggregated pancreatic beta cells with negative charge

Deposition of cationic polymer (PLL) as the initial coating layer

Deposition of anionic polymer (ALG) and formation of first bilayer due to electrostatic forces

Addition of the alternate bilayers can be repeated several times to achieve immunoisolation

Beta Cells
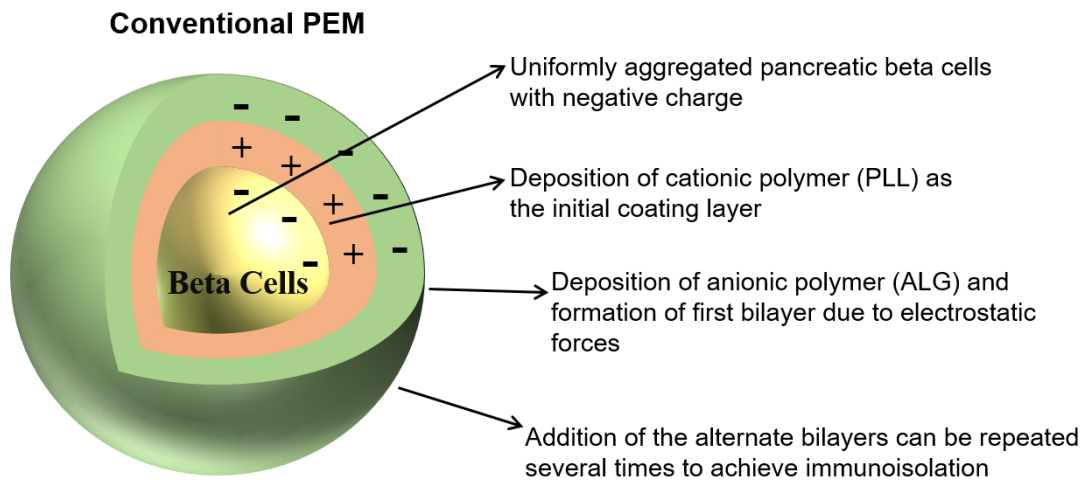
PEM with Ca^{2+} pre-conditioning

Aggregated cells were pre-conditioned in 100 mM CaCl$_2$

Ca^{2+} enhances deposition of anionic polymer by providing positive charge on cells

Indirect contact of cationic polymer with cells

Beta Cells
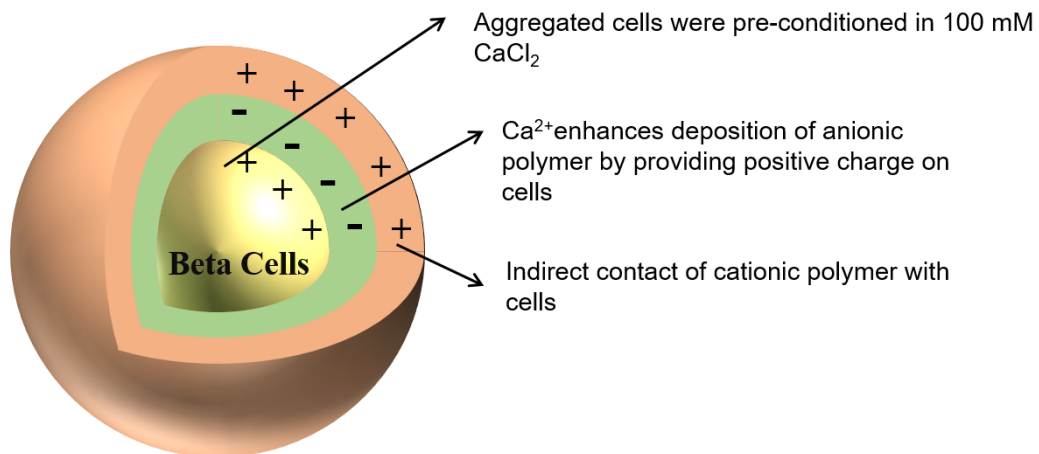
Figure 6-2
A schematic illustration representing the difference between a novel PEM coating approach using calcium pre-conditioning, reported in this study, compared with the conventional PEM coating method.

6.2.5 Fluorescent labelling of PLL

To prepare the fluorescently labelled PLL, 0.1 mg of Alexa Fluor 647NHS ester (Succinimidyl Ester) (Thermo Fisher, UK) was dissolved in 1 mL of dimethyl sulfoxide (DMSO, Sigma, UK) according to the manufacturer's instructions. 100 µL of the dye was added to 1 mL of PLL stock solution with a concentration of 2 mg/mL. The solution was incubated at room temperature for 6 h under continuous stirring. To remove the excess dye, the solution was then dialysed for 24 h against deionised water. The final PLL solution was then kept in the dark at $4°C$ until needed.

6.2.6 Assessment of cell viability and metabolic activity

The viability of coated MIN-6 cells using different coating deposition sequences was evaluated using a live/dead staining kit. Briefly, on the day of experimentation, 1 µL of Calcein AM (662 Da, an indicator for live cells) and 5 µL of PI (668 Da, an indicator for dead cells) were added to a 200 µL suspension of coated spheroids in cell culture medium. Cells were incubated in the dark at $37°C$ for 15-30 min. Stained cells were then visualised using confocal laser scanning microscopy, and images were analysed using ImageJ and Imaris software.

The metabolic activities of coated and non-coated (control) MIN-6 cells were assessed using the Alamar Blue cell proliferation assay. More details about the mechanism of this assay were provided in section 4.2.10. Briefly, 20 µL of Alamar Blue reagent were added to 200 µL of cell spheroids suspension in DMEM, followed by incubating for 4 h at $37°C$. The fluorescence was then read (590 nm emission and 560 nm excitation) using a microplate reader. The results

were reported as percentage reduction between the coated and the control sample using Equation 6-1.

% difference between coated and control sample=

$$\left[\frac{\text{Fluorescent intensity of sample at 590 nm}}{\text{Fluorescent intensity of control at 590nm}} \right] \times 100$$

Equation 6-1

6.2.7 Direct immunofluorescent staining

An immunofluorescent assay was used for visualising F-actin protein within the intracellular structure of MIN-6 spheroids. This technique is based on binding of a specific antibody, which has been conjugated with a fluorescent dye, to the target protein. The fluorescent signals can be visualised with fluorescent microscopy techniques, such as CLSM. As shown in Figure 6-3 the immunofluorescent assay can be categorised into two different methods depending on the type of antibody used for the experiment (direct or indirect assay) [137].
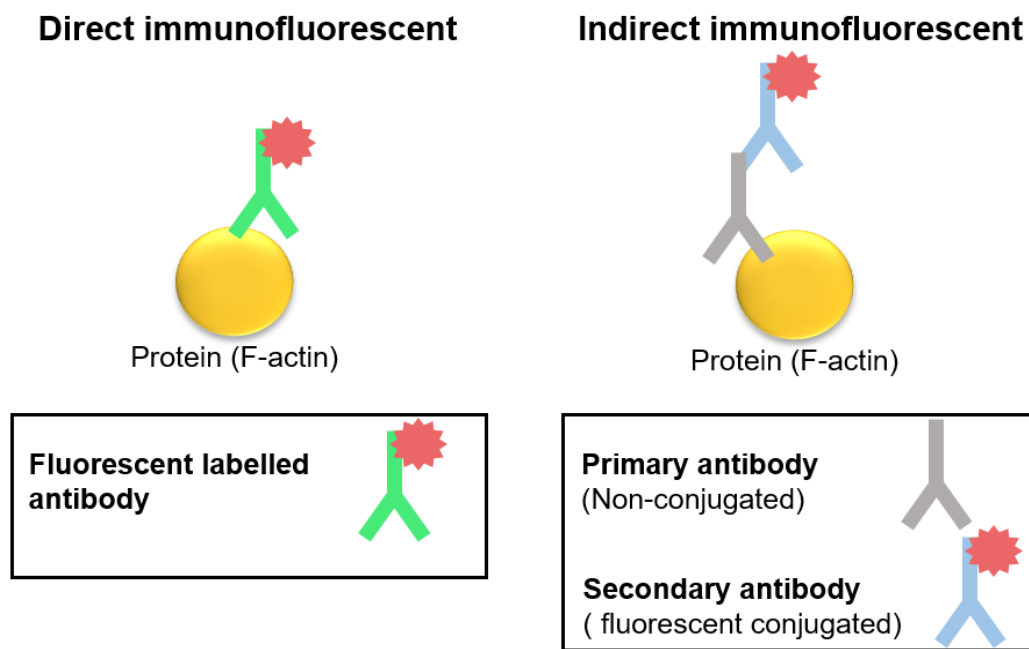
Figure 6-3
Direct versus indirect immunofluorescent assay. For direct method, one single antibody, which is linked to a fluorescent dye, is used to bind to the target protein. Whereas, in an indirect method a secondary fluorescent antibody is used to recognise an unlabelled primary antibody, which has been bound to the target protein.

After 5 days in culture, MIN-6 spheroids were fixed with 10% formalin (Sigma, UK). Samples were then blocked in PBS solution containing 2% BSA and 0.2% Triton X-100 (Sigma, UK) for 1 h. After washing in PBS, fixed cells were stained with Actin-red 555 (F-actin Probe, Life Technologies, UK) for 30 min, followed by several washing steps with PBS. Cell nuclei were also counter-stained using DAPI (1 µg/mL) (Sigma, UK). 3D visualisation of the stained spheroids was undertaken using confocal microscopy (Laser 405 nm: DAPI, Laser 543: Actin-red 555).

6.2.8 Antibody exclusion assay

The permeability of the coated spheroids against large immunologically relevant molecules was evaluated using FITC labelled anti-mouse MHC class II (excitation peak: 490 nm, emission peak: 525 nm). Briefly, cell spheroids with and without coating layers were prepared as described in section 6.2.4. Fifteen MIN-6 spheroids were randomly selected from each group, and 100 µL of 2% BSA in HBSS (blocking buffer) were added to the samples. Cells were incubated for 15 min at 37°C with 1 µL of FITC- antibody. Samples were then washed twice with HBSS and 0.1% Tween-20 to remove any excess antibody. The coated and non-coated spheroids were observed using confocal laser scanning microscopy with an argon laser (wavelength: 488 nm).

6.2.9 Treating MIN-6 cells with cytokines

Groups of coated and non-coated spheroids were treated with a mixture of three cytokines at a final concentration of Interleukin-1β (IL-1β, Sigma, UK) (5 ng/mL), mouse tumour necrosis factor-α (TNF-α, Gibco, Life Technology, UK) (10 ng/mL), and mouse interferon-ɣ (IFN-ɣ, Gibco, Life Technology, UK) (100 ng/mL) in DMEM. All treated samples were incubated overnight at 37°C. The viability of the treated spheroids was measured using the Alamar Blue assay as described previously, and data were normalised to 1000 cells.

6.2.10 Glucose-stimulated insulin secretion assay

To evaluate the function of MIN-6 cells, the amount of insulin secreted from non-coated and coated cells in response to changes in glucose concentration was measured (Section 4.2.12). During the GSIS assay, the cultured supernatant was collected for quantitative evaluation using insulin-ELISA. The colorimetric reaction was then quantified using a plate spectrophotometer at a wavelength of 450 nm.

6.3 Statistical analysis

The student's t-test, assuming equal variance, was used to identify any significant differences between pairs of groups. One-way analysis of variance (ANOVA) was used to identify any significant difference between the means of independent groups. Furthermore, a Bonferroni post-hoc test was performed with ANOVA to find means that were significantly different within groups. A P-value < 0.05 was determined as significant. Results are presented as mean $\pm$ standard deviation unless otherwise stated.

6.4 Results

6.4.1 Formation of uniform MIN-6 spheroids

After 5 days of culturing cells within concave micro-wells, the most robust and uniform shaped MIN-6 spheroids were achieved using 5×10^5 cells/200 µL compared with the other two cell densities (Figure 6-4).
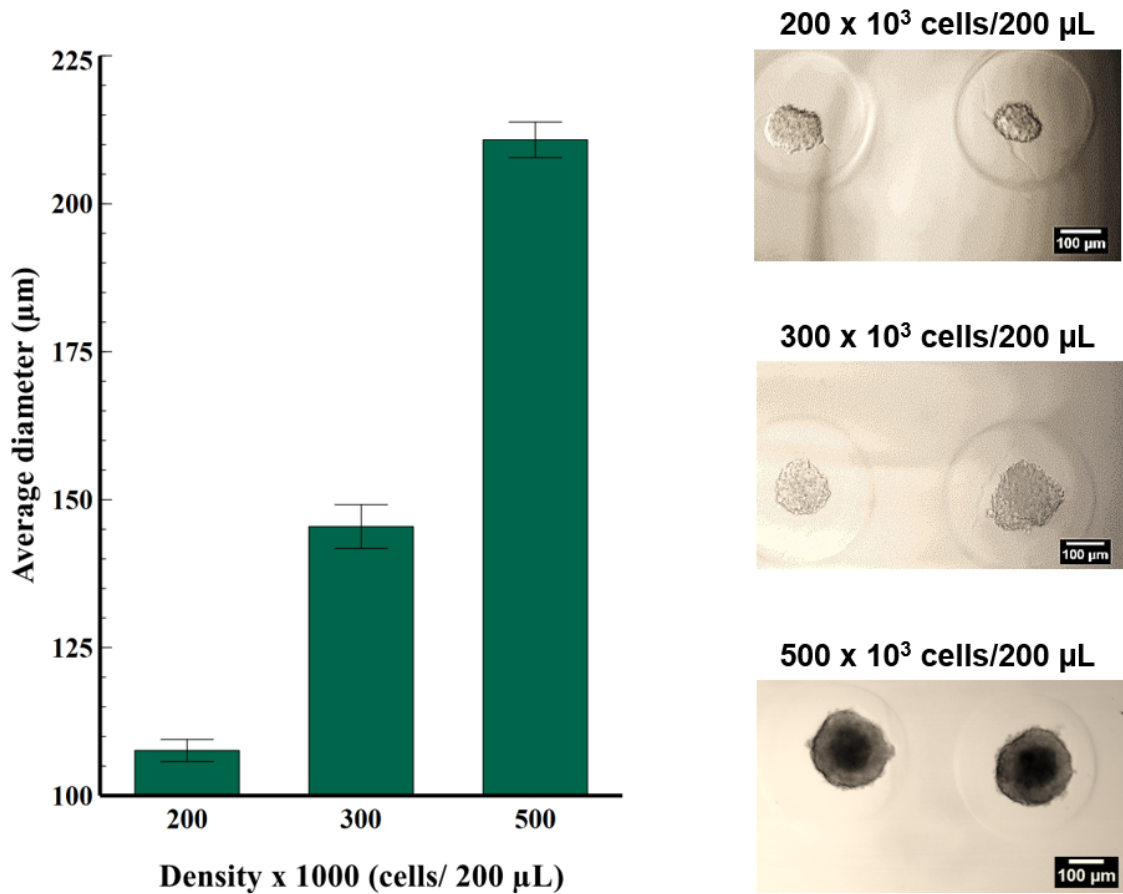
Figure 6-4

Evaluation of MIN-6 spheroids size within micro-wells using different cell seeding densities of 2 x 10^5, 3 x 10^5, and 5 x 10^5 cells/200 µL, (n= 30 spheroids). Scale bars shows 100 µm.

Seeding 5 x 10^5 cells/200 µL, the formation of cell spheroids was observed over time. Figure 6-5 shows cell spheroids were generated in the centre of the concave wells within 24 h due to aggregation of cell population by gravitational force and concave shape of the micro-wells. The majority of cell spheroids formed after one day of culture and only a few micro-wells

remained vacant (<1.5%). It was discovered that 4-5 days of culture was the optimum time period to achieve robust spheroids, which could be easily harvested and used for the coating procedure.

(a)

| Seeding cells on concave micro-well | MIN-6 cells aggregation | Harvesting cell spheroids (After 4-5 days) |

(b)
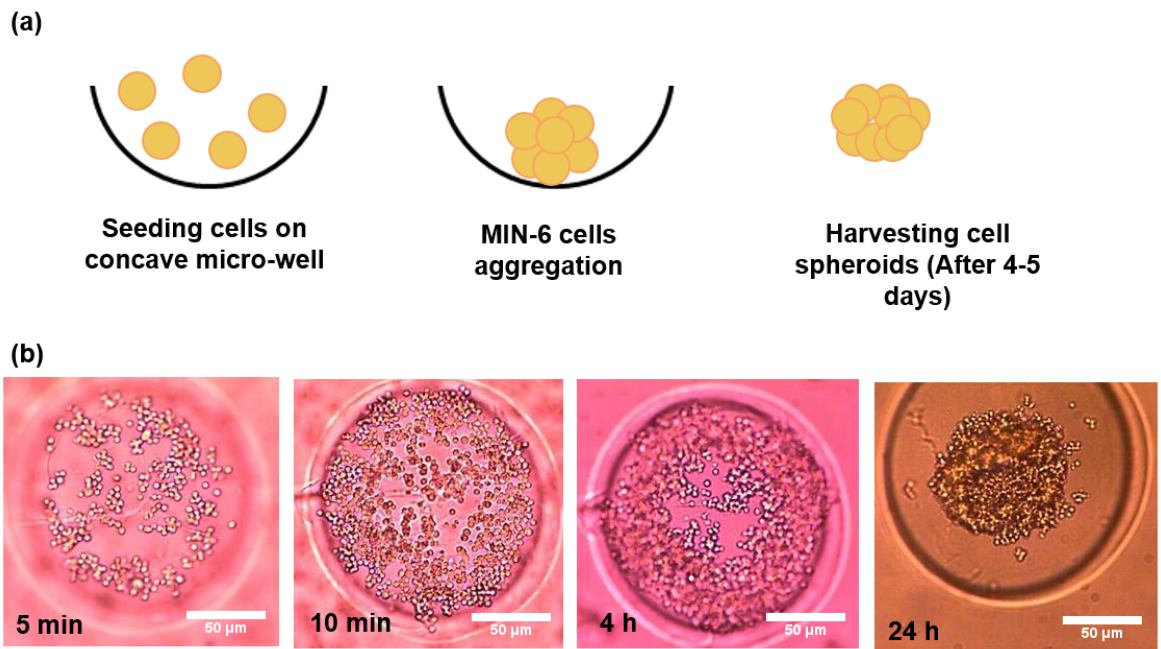
Figure 6-5
Formation of uniform MIN-6 spheroids. (a) Schematic illustration of cell aggregation within agarose-based micro-wells. (b) Light microscopy imaging of cell aggregation in wells during time intervals: 5, 10 min, 4, and 24 h of post-seeding. Scale bars shows 100 µm.

6.4.2 Formation of MIN-6 spheroids in a flat-bottomed plate versus concave micro-wells

To quantify the effect of culturing cells on 3D agarose constructs, the size distribution of 30 spheroids cultured on both a flat-bottomed plate (control) and concave wells were compared

after 7 days of culture. In the case of MIN-6 spheroids in agarose-based wells, their size range was mostly between 200-250 μm with an average of 201 ± 2 μm. However, for the control sample, cells exhibited a wide range of sizes from 50 – 250 μm with an average of 103 ± 49.2 μm (Figure 6-6). Notably, cells within micro-wells exhibited higher viability compared with the cell spheroids formed on the flat culture plate. For the 2D culture, many dead cells were observed within the centre of the aggregates (Figure 6-7).
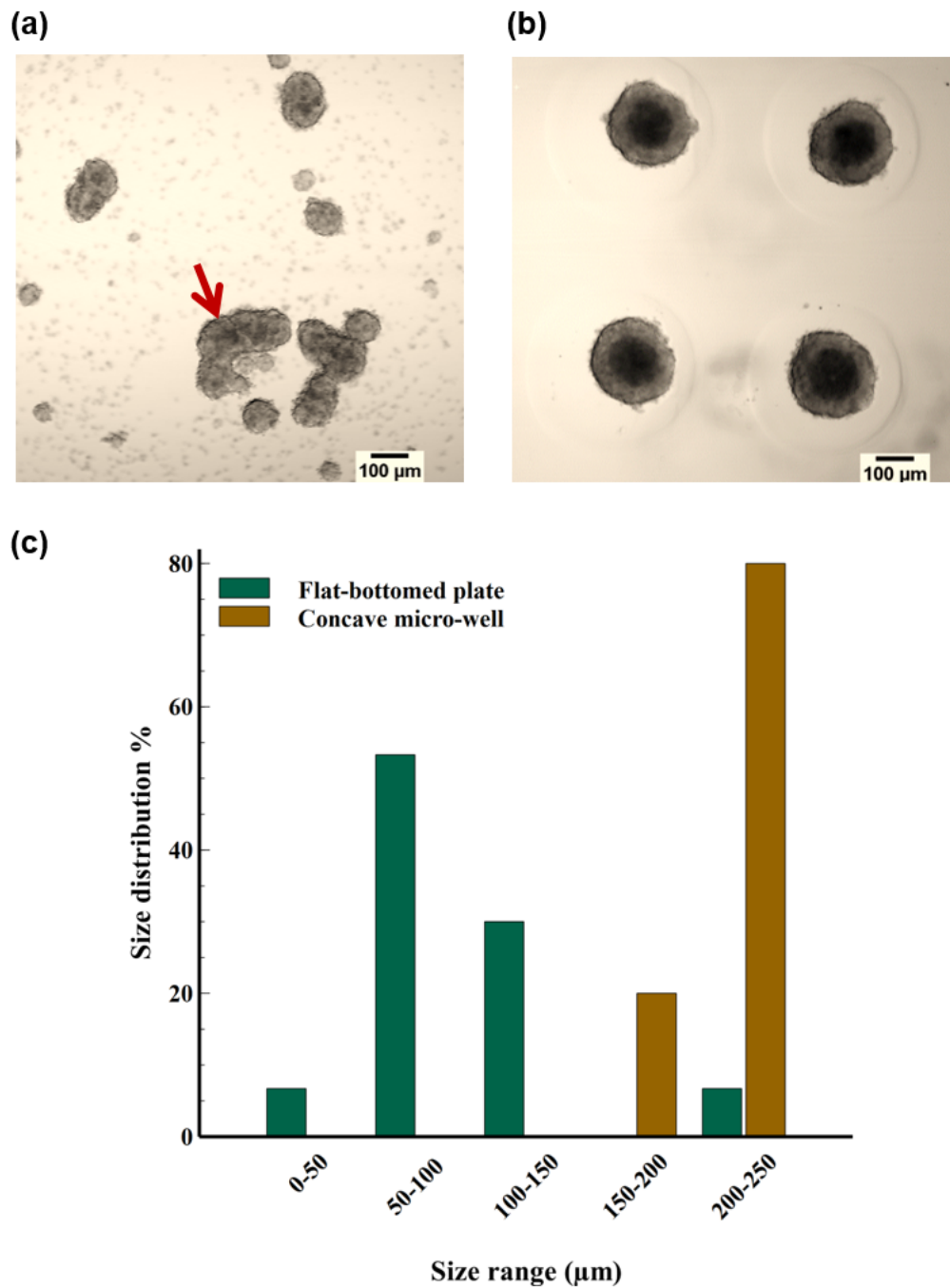
Figure 6-6

Comparison between MIN-6 spheroids cultured on different surfaces. (a) and (b) formation of MIN-6 cell spheroids cultured on flat-bottomed plate and agarose concave micro-wells on day 7, respectively. (c) Comparison between the size distribution of aggregated cells in both flat-bottomed and concave wells (n=30 spheroids), large chain of cell clumps formed in flat-bottomed sample were not analysed in this study (Indicated with an arrow). Scale bars show 100 μm.
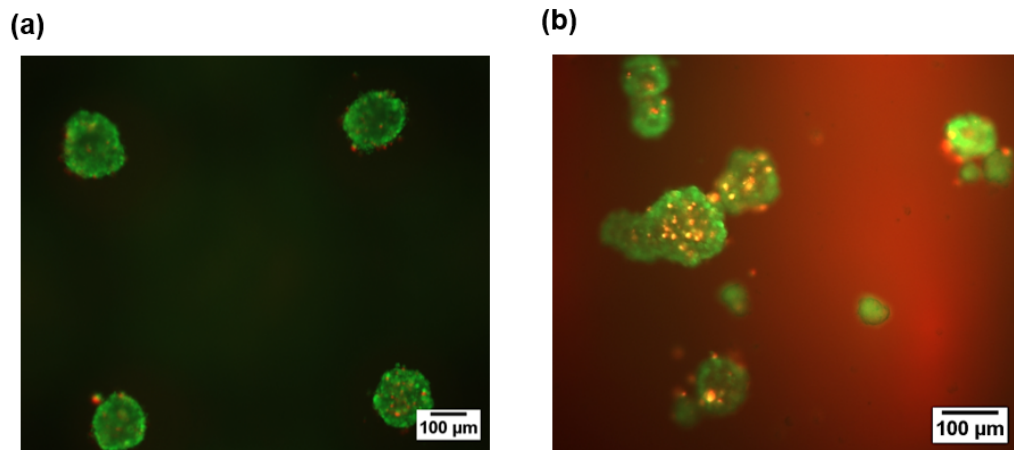
Figure 6-7
Comparison between viability of MIN-6 spheroids cultured on agarose concave micro-wells (a) versus flat-bottomed plate (b) on day 7 using fluorescent microscope. Cells were stained with calcein AM (green: live cells) and PI (red: dead cells). Scale bars show 100 µm.

6.4.3 MIN-6 spheroid morphology

To gain insight in to the influence of 3D culture, immunofluorescent staining of actin filaments and cell nuclei were examined on day 5. Actin filaments are thin fibres with an approximate diameter of 6 nm located within the cytoskeleton of cells. One of the important responsibilities of actin filaments is the organisation of tissues and adhesion among epithelial cells. Therefore, anchorage of actin proteins with the adherent junction exist on the surface of cells plasma membrane permit cell-cell contact between epithelial cells [138, 139].

As expected, fluorescence signals from the filamentous actin (F-actin) cytoskeleton, suggested that the MIN-6 spheroids were adhered to one another, forming a compact

113

structure. DAPI staining showed a large number of freely growing cells on the surface of the MIN-6 spheroids (Figure 6-8).
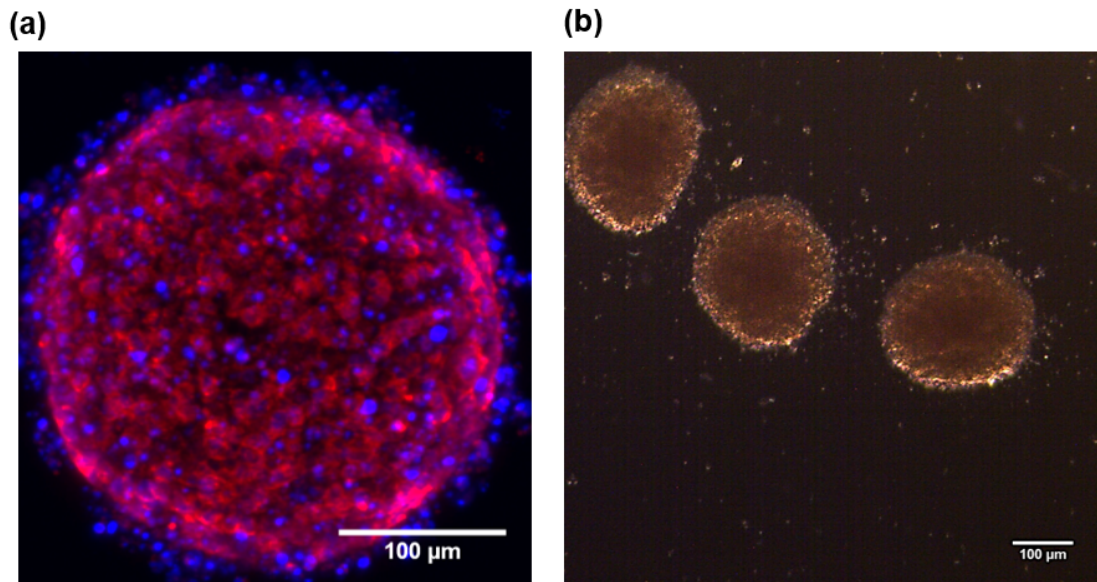
Figure 6-8
MIN-6 spheroids morphology. (a) Direct immunofluorescent staining of MIN-6 spheroids with Actin-Red 555 (F-actin probe, red) and DAPI (cell nuclei probe, blue) for visualisation of cell-cell interaction using CLSM. (b) Phase contrast micrograph of harvested MIN-6 spheroids after 5 days of culture in agarose micro-wells. Scale bars show 100 μm.

6.4.4 Addition of pre-coating step increased cytocompatiblility of coated cells

Coating of MIN-6 spheroids was achieved by subsequent layering of oppositely charged polyelectrolytes; ALG and PLL. After the pre-coating step (pre-conditioning with CaCl$_2$ and deposition of initial ALG layer), each coated spheroid was formed by the alternate deposition of four bilayers (a total of 8 layers) of polyelectrolytes. For all cell spheroids, ALG was chosen as the final polyelectrolyte layer. To investigate whether the pre-coating step was efficient in

reducing the toxic effect of PLL, the viability of the pre-coated cells was compared with MIN-6 spheroids coated directly with PLL. After 8 days of culture, quantitative analysis of the stained cells revealed a significant difference ($p<0.01$) between the viability of cells that were pre-coated (89 ± 6%) and those with an initial layer of PLL (64 ± 11%) (Figure 6-9). The viability of coated MIN-6 cells with calcium pre-conditioning was also observed for another week. More than 90% of coated cells were still viable, shown in Figure 6-10.
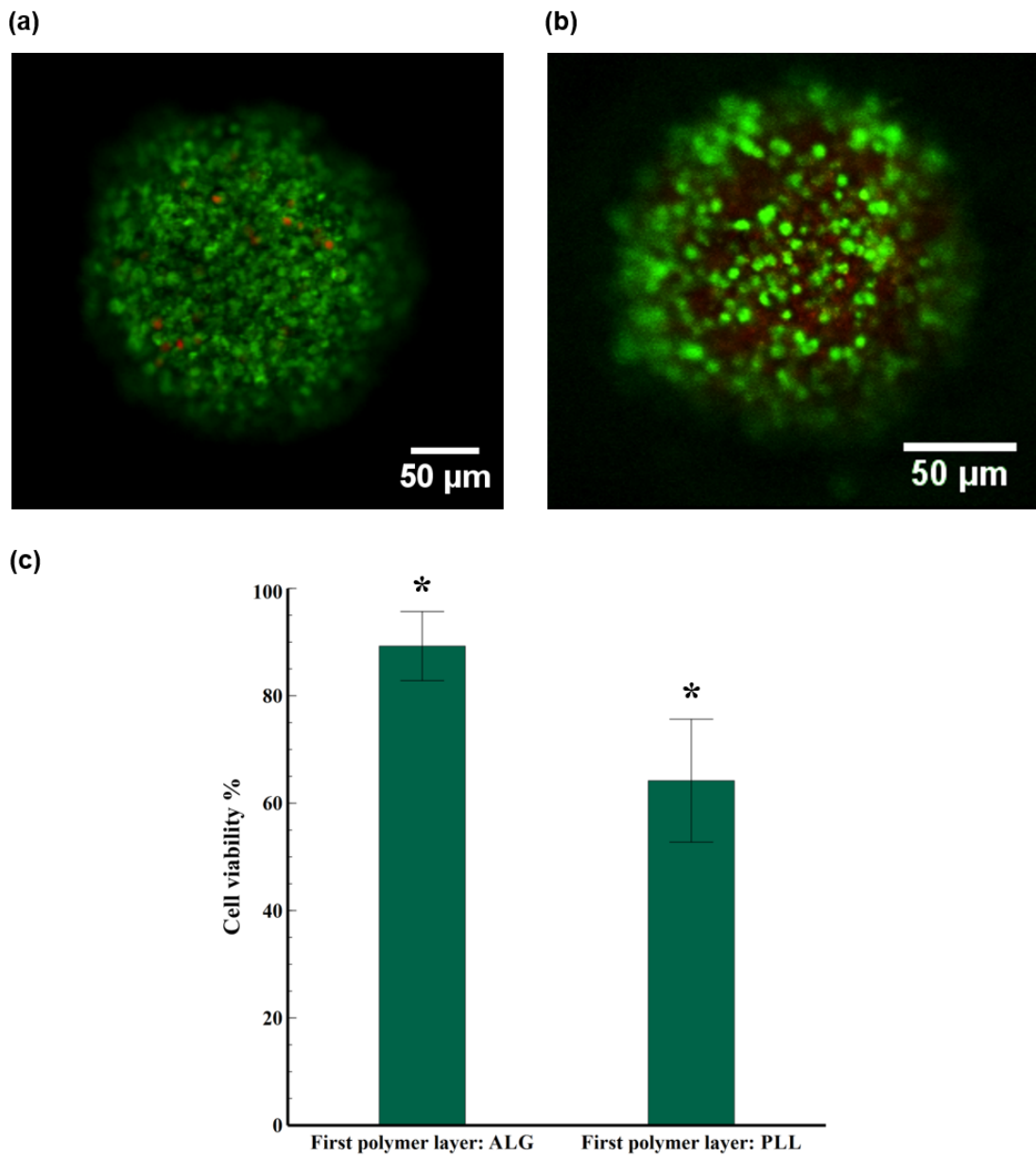
Figure 6-9
Evaluation of viability of MIN-6 spheroids coated with four bilayers of PLL/ALG. (a) Confocal microscopic images of live (green) and dead (red) stained cells coated with initial layer of alginate during the pre-coating step. (b) Cell spheroids coated with PLL as the first coating layer. (c) Quantitative evaluation of live/dead analysis (n=10 spheroids) (*, P<0.01). Scale bars show 50 μm.
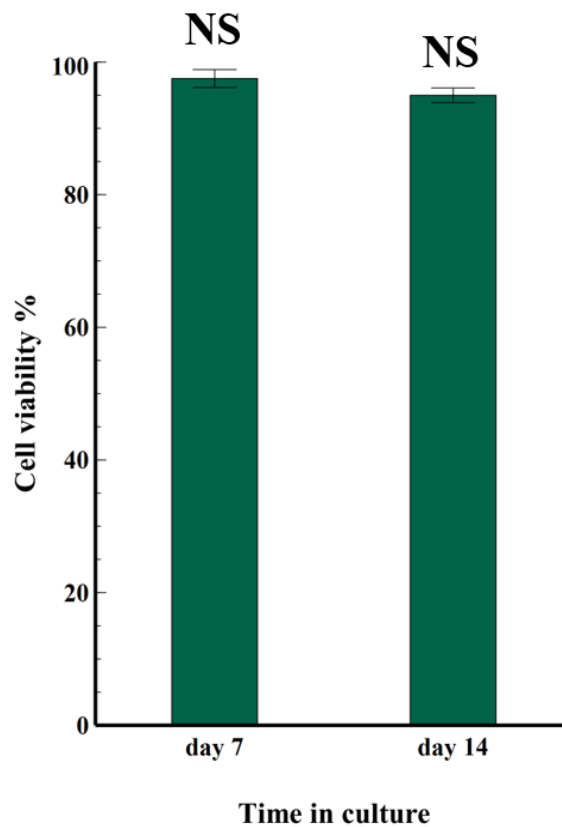
Figure 6-10
Evaluation of viability of coated MIN-6 spheroids with calcium pre-conditioning. Confocal images of live/dead analysis were quantified with imageJ software, (n=10 spheroids), NS= non-significant.

Furthermore, the metabolic activity of coated MIN-6 spheroids (with and without the pre-coating step) was compared with non-coated cells as a control (Figure 6-11). In comparison to pre-coated spheroids (pre-conditioned with calcium) and non-coated cells (control), the ability of non-pre-coated spheroids to reduce the Alamar Blue reagent (metabolic activity indicator) was significantly reduced (p=0.04) after 9 days of culture. This is possibly due to the toxicity of PLL when used in direct contact with MIN-6 cells. Hence, in comparison to the control, the

metabolic activity of cells coated with an initial layer of PLL was reduced by 32%, while for the cells with the addition of pre-coating step there was a smaller reduction of only 13%.
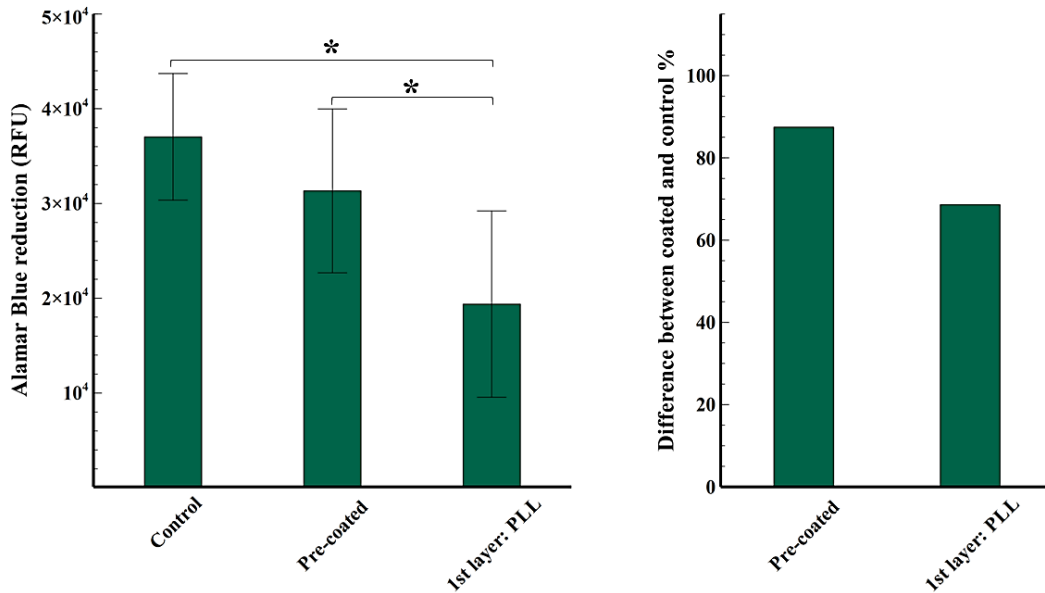
Figure 6-11
Comparison between metabolic activity of MIN-6 coated spheroids with and without pre-coating step, and the control (non-coated spheroids) (n=3), (∗, P<0.05).

6.4.5 Confirmation of coating on cell spheroid surfaces

To demonstrate the deposition of polyelectrolytes on cell spheroids, PLL labelled with Alexa Fluor-647 was used. The fluorescently labelled PLL was then applied to the final bilayer (7th layer) to enable visualisation of coated cells under the confocal microscope. From cross-sectional images obtained at distances of 10 and 30 μ m from the centre of cell spheroid,

using Z-stack imaging technique (Figure 6-12), the fluorescence was mainly located at the peripheries of the coated cells, which indicated successful coating of the entire surface of the cell spheroids.

(a)

(b)

Distance from the core: 10 µm   Distance from the core: 30 µm
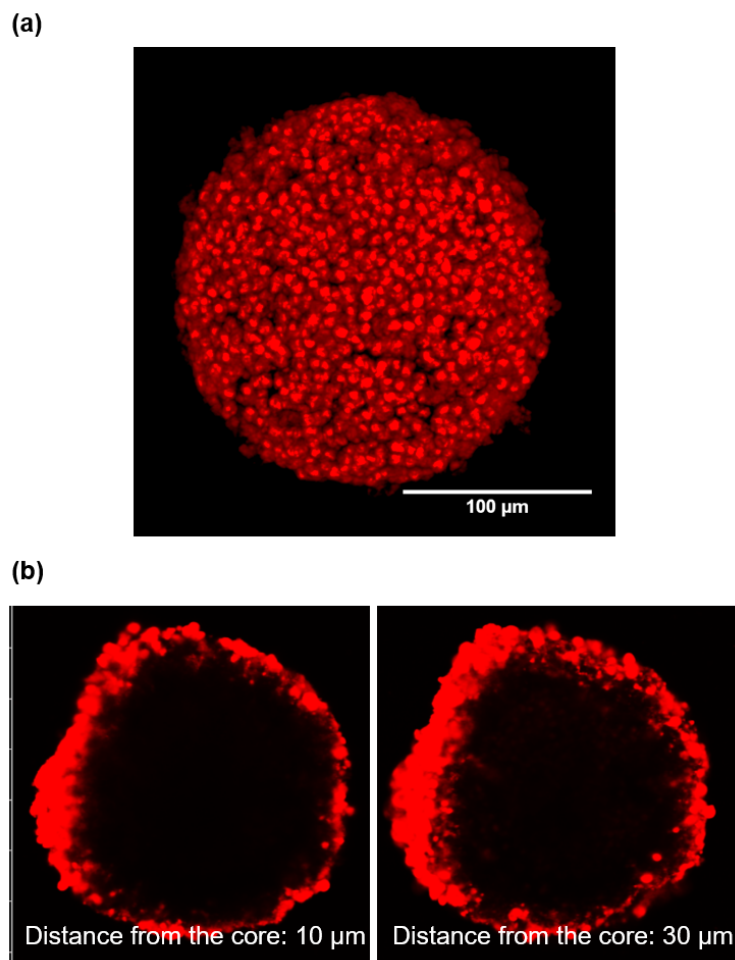
Figure 6-12
Monitoring the ALG/PLL-labelled coating layers on MIN-6 spheroids. (a) Confocal micrograph of a cell spheroids coated with Alexa Fluor-647 labelled PLL (7th layer). (b) Z-stack cross-sections of coated MIN-6 spheroids with labelled-PLL obtained at 10 and 30 µm from the centre of the coated spheroid. Scale bar shows 100 µm.

Also Figure 6-13 demonstrate the difference in behaviour of coated and non-coated spheroids when cultured on a CellBIND tissue culture plate. After 7 days of culture, non-coated spheroids attached to the surface and cells covered and migrated across the whole area, as expected. On the contrary, coated spheroids with 4 bilayers remained suspended in the culture medium confirming that the entire spheroid surface was coated with the polyelectrolytes.
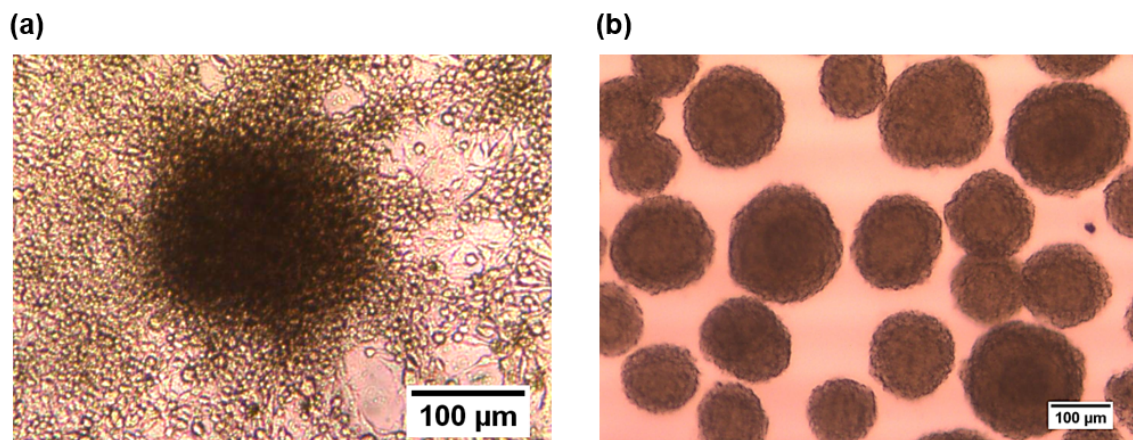
Figure 6-13
Light Micrographs of non-coated (a) and coated cell spheroids (b) in response to cell-attachable surface. Scale bar shows 100 μm.

6.4.6 Coated MIN-6 cells excluded FITC-antibody

To investigate the permeability of coated MIN-6 spheroids to immunologically relevant molecules, samples were exposed to FITC-mouse antibody, which can then target the antigens (MHC class II) that exist on the surface of pancreatic beta cells. The fluorescence intensity emitted from non-coated spheroids was shown to be much greater than coated spheroids (Figure 6-14). Notably, z-stack imaging allowed visualisation of spheroids layers located at the

centre of MIN-6 spheroids, this was used to investigate whether the antibody could diffuse through the bilayers toward the centre of the coated cells or not. This provided evidence that compared with the control (non-coated cells); pre-coating of cells with alginate followed by the deposition of four bilayers of PLL and ALG considerably protected the coated pancreatic beta cells from attaching to the FITC-antibody by covering the surface of spheroids.
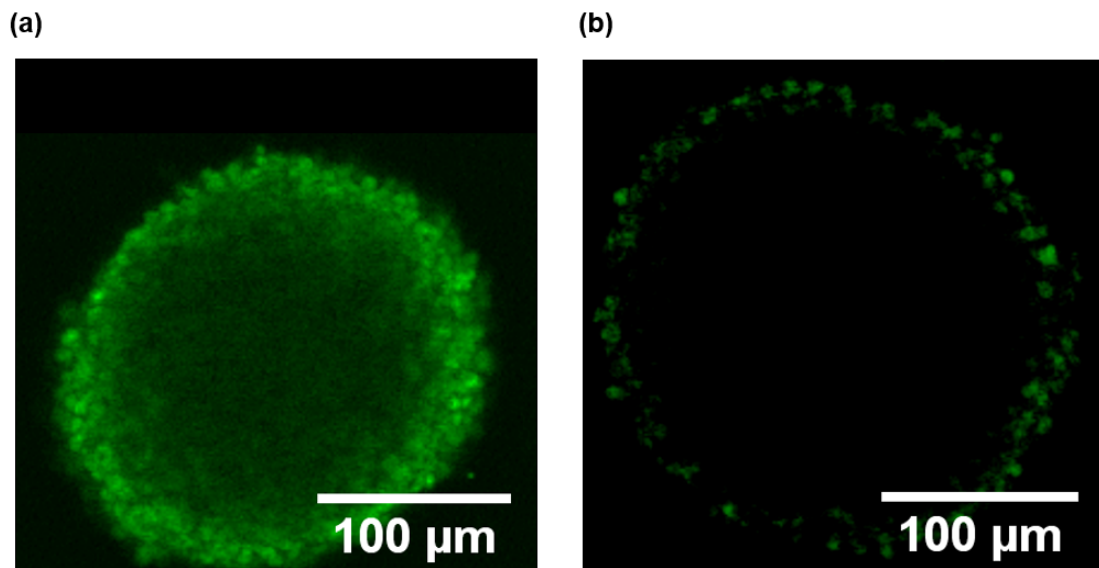
Figure 6-14
Confocal images of MIN-6 spheroids after being exposed to FITC-mouse antibody (150 KDa). (a) Z-stack image of non-coated spheroid using argon laser. (b) Coated spheroid with pre-coating step and 4 bilayers of PLL/ALG, z-stack images were obtained at distance of 5 µm from the centre of both coated and non-coated spheroids. Scale bar shows 100 µm.

6.4.7 Coated cells exhibited higher survival after being exposed to cytokines

To further examine the permeability of coated spheroids against smaller molecules, a mixture of three cytokines: IL-1β (~17 KDa), TNF-α (~17.5 KDa), and IFN-γ (~15 KDa) was added to both non-coated and coated spheroids with 1, 2, and 4 bilayers of polyelectrolytes. As shown in Figure 6-15, after 24 h exposure to cytokines, the metabolic activity of non-coated cell spheroids was notably reduced to 55±2.5 RFU (P-value<0.01). Moreover, the response of MIN-6 spheroids to cytokines after the addition of one bilayer of polyelectrolytes was only slightly different from the non-coated cells. However, deposition of four bilayers of PLL/ALG significantly reduced cytokine damage on pancreatic beta cells survival rate (204 ±3.3 RFU) in comparison with other groups (P-value<0.01).
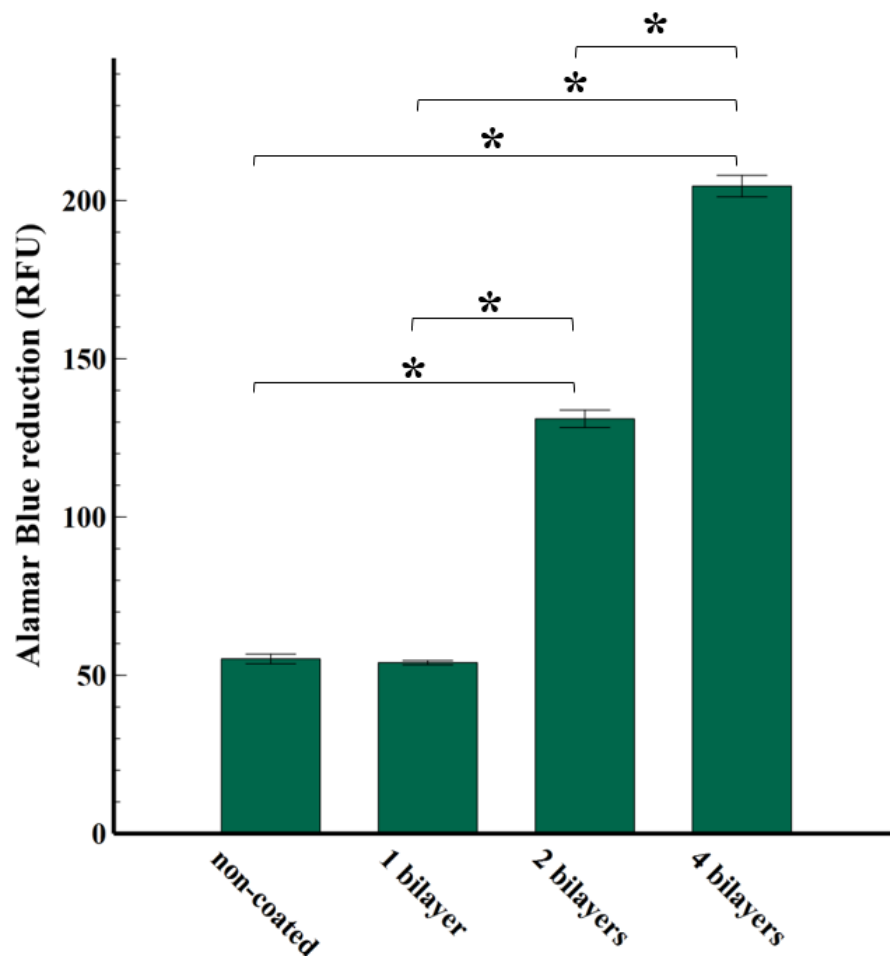
 Figure 6-15
Survival of non-coated and coated MIN-6 spheroids with different numbers of PLL/ALG bilayers after being incubated with a cytokine mixture for 24 h; (n=4), (* P<0.01), and were normalised to 1000 cells.

6.4.8 Coated spheroids remained responsive to the changes in glucose concentrations

After two weeks of culture, insulin secretion from coated and non-coated MIN-6 spheroids in response to glucose was investigated by culturing both samples in a series of basal (2 mM), and stimulatory (20 mM) glucose concentrations. Figure 6-16 showed that after culturing cells for one and two weeks, coated MIN6 cell spheroids retained their insulin secreting ability. The amount of insulin released from the coated spheroids into basal glucose solution was 17.1-±0.1 ng/mL, which was significantly increased to 57.3 ±0.4 ng/mL under a stimulatory glucose concentration (P-value < 0.05) (Figure 6-16: b). In addition, a comparison between the amounts of secreted insulin from both coated and non-coated spheroids showed no significant difference, indicating that the coated MIN-6 cells remained responsive to glucose after applying pre-conditioning step followed by addition of four bilayers of ALG/PLL.

(a)

(b)
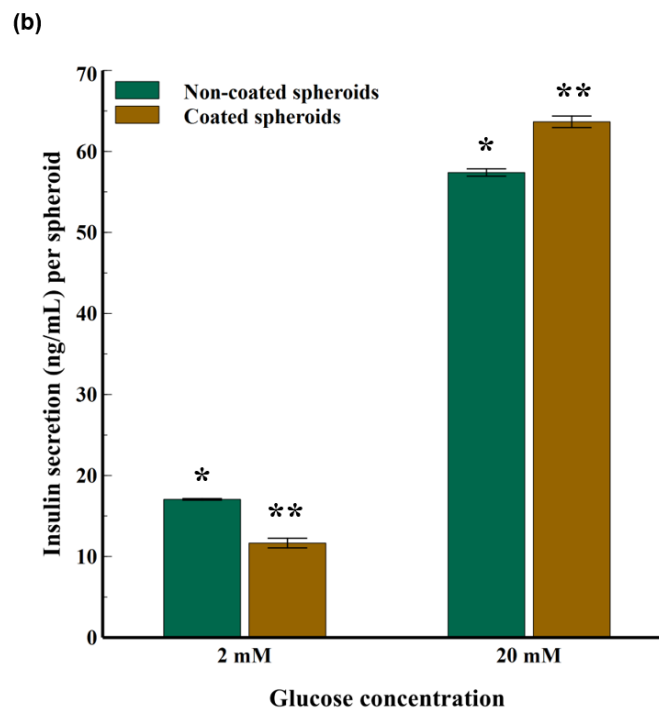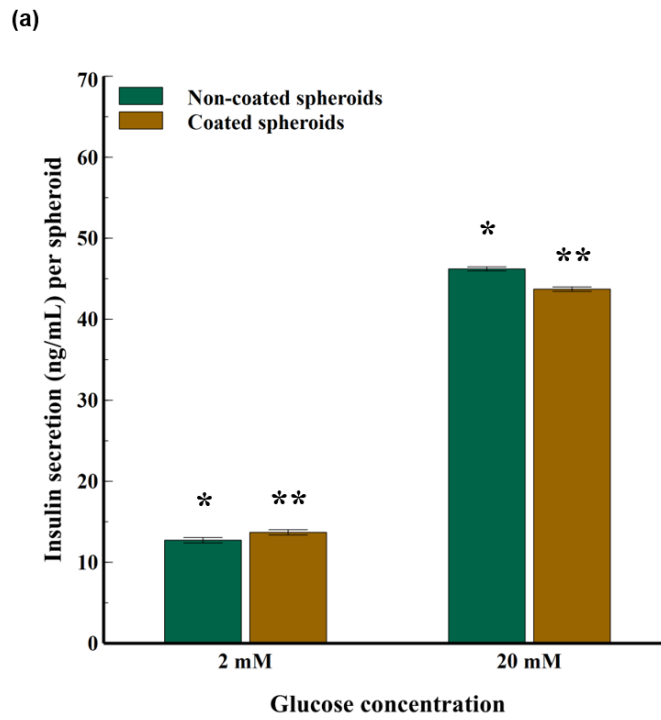
Figure 6-16
Insulin release of non-coated (control) and coated MIN-6 spheroids in response to glucose stimulation (a) After one-week *in vitro* culture. (b) Two-weeks *in vitro* culture. Results are presented as mean ± S.D (n=3), (*, ** P<0.05).

6.5 Discussion

In this study, we have demonstrated the formation of stable and uniformly sized MIN-6 spheroids using agarose-based concave micro-wells. The prepared spheroids were then immunoisolated with ALG and PLL using a novel coating approach. Up to now, several groups have developed polydimethylsiloxane-based micro-molds for creating cell aggregates, however, using this substrate requires further steps for modification of well surfaces and preventing cell adhesion [140-142]. Herein, the formed beta cell spheroids were easily detached and retrieved from the agarose construct without any further need for treatment with trypsin or surface modification. This was an important advantage for preventing damage to cell spheroids during the harvesting and prior to initiating the coating procedure.

Microscopic observation followed by size analysis confirmed that the use of concave micro-wells seeded with 5×10^5 cells/200 µL enabled the formation of uniform MIN-6 spheroids with a size range of 150-250 µm (Figure 6-4), similar to pancreatic islets. In contrast, the diameter of aggregated cells formed on a flat-bottomed plate varied between 50 and 250 µm and resulted in the accumulation of cell chains with non-uniform shape and a broad size distribution (Figure 6-6). As shown in Figure 6-7, the viability of these samples was notably affected, and therefore such shapes were undesirable for coating.

Previous studies have demonstrated that culturing epithelial cells in a 3D environment could improve cell adhesion and intracellular signalling by providing an additional dimension for external cell interactions [143]. As a result, the formation of beta cell spheroids was studied as a means to mimic the real tissue and cell adhesions were observed by direct fluorescent

126

staining of F-actin and cell nuclei of MIN-6 spheroids (Figure 6-8: a). The cell-cell interaction found in this study was also confirmed with beta cells ability to maintain their insulin sensitivity within two weeks of culture, compared with the result established earlier in chapter 4 of this thesis.

For the past two decades, coating bacteria, yeasts, and mammalian cells using a layer-by-layer assembly of polyelectrolytes have been studied as a promising approach to reduce large void volume between the encapsulated cells and the surrounding environment utilising various materials, including both synthetic and natural polymers [131, 144]. However, using this approach and the application of positively charged polymers in direct contact with mammalian cells can be detrimental to cell survival and functionality [95, 135]. Hence several groups have demonstrated the effect of modifying polycations with different materials, including PEG and phosphoro-choline to reduce their toxicity and inflammatory responses [114, 144, 145]. Herein, we chose PLL and ALG as the cationic and anionic polymers, respectively. However, as a novel approach to reduce the toxicity of PLL, cells were first suspended in 100 mM of $CaCl_2$, which enhanced the formation of a layer of ALG prior to the addition of PLL on the cell's surface.

Results from live/dead staining suggested that the coating approach used in this study, enhanced cell survival by 25% in comparison with the conventional LBL procedure after being coated for one week (Figure 6-9).

Furthermore, pre-coated cells were able to maintain higher metabolic activity compared with MIN-6 spheroids coated with an initial layer of PLL (Figure 6-11). Importantly, these studies

confirmed that suspending cells in 100 mM of $CaCl_2$ during the pre-coating step did not induce harmful effects on cell viability, hence it was concluded that with the described coating approach, the toxic effect of PLL was reduced without any further need for surface or chemical modification.

The presence of polyelectrolyte layers on MIN-6 spheroids was confirmed by the means of fluorescently labelled PLL. When Alexa Fluor 647-PLL was applied to the last bilayer, clear fluorescent emission was observed from cross sectional images and Z-stack reconstruction of coated spheroid (Figure 6-12), suggesting the existence and successful deposition of polymeric layers on the surface of the cell spheroids.

Although maintaining a high metabolic activity and survival rate of the encapsulated cells could increase the longevity of transplanted cells, complete success in pancreatic islet implantation relies upon efficient immunoisolation of the cells from recipient immune responses. In this regard, to gain a better insight into the coating approach established in this study, both coated and non-coated cells were exposed to FITC-mouse antibody. The images from spheroids were captured through the Z-axis using confocal microscopy (Figure 6-14). Observation showed a notable prohibition of FITC antibody from attaching to MHC class II antigens on the surface of coated beta cells in comparison to the non-coated cells.

Previous studies have shown that release of the three main pro-inflammatory cytokines (IL-1β, TNF-α, and IFN-γ) from activated T-cells and macrophages could be responsible for dysfunction of beta cells by inducing over expression of inducible nitric oxide synthase (iNOS) [37, 146]. In the present study, we evaluated whether the coated cells could prevent the

diffusion of cytokines to MIN-6 spheroids. Figure 6-15 emphasised that deposition of pre-coating layer and four bilayers of PLL/ALG was effective in inhibiting cytokine damage and hence increasing cell survival compared with non-coated spheroids.

We further demonstrated the MIN-6 spheroid's ability to sense the changes in glucose concentration (2 Vs 20 mM) during the GSIS assay. For both coated and non-coated cells, increasing glucose concentration from basal to stimulatory, significantly increased the amount of insulin secreted by cells (Figure 6-16). Hence, the data showed that suspending cells in $CaCl_2$ solution during the pre-coating step followed by the addition of four bilayers of PLL/ALG, did not affect MIN-6 cells in terms of insulin release.

7 CHAPTER SEVEN

Conclusions

The work reported in this thesis has contributed to further insight into previous research by investigating novel approaches to improve the survival of immunoisolated pancreatic beta cells within a cell-friendly semipermeable membrane. The main conclusions of each experimental chapters are summarised below.

Formation of uniform alginate microcapsules

- In Chapter 4, the development of alginate microcapsules with high uniformity in size and shape (200±19 μm) was established using vibrational nozzle technology.

- Encapsulated pancreatic beta cells within 1% alginate microcapsules were shown to be metabolically active and retain their viability for 30 days *in vitro*. In addition, CLSM images illustrated an even distribution of the cells between the centre and the inner surface of the alginate microcapsules.

- Results from the *in vitro* glucose stimulation assay revealed reduction in the insulin secretion ability of beta cells after 14 days when compared to their insulin sensitivity on day 7. To further explore this observation, a 3D culture method was developed with the aim of improving endocrine beta cells interactions, and hence their insulin secretory response (Chapter 6). However, results achieved in Chapter 4 suggested that the application of vibrational technology has more potential for non-endocrine cell-based therapies by permitting cells to maintain their viability and metabolic activity. The main advantages of this approach in comparison to conventional extrusion method are: (1) a one-step continuous production of uniformly sized microcapsules

with smaller size range, (2) mild gelling conditions for encapsulating live cells, and (3) relatively short production time, which is suitable for scale up.

Microcapsules cultivation in a fluidised-bed bioreactor

- For the first time, the application of a fluidised-bed bioreactor for the cultivation of pancreatic insulin secreting MIN-6 cells was compared to static culture (Chapter 5). Development of alginate cellular microcapsules with high uniformity, which was discussed earlier (Chapter 4), enabled the homogenous fluidisation of microparticles throughout the bioreactor column under a mild fluid flow rate (2 mL/min), which was shown to have no significant effect on the stability of alginate microcapsules.

- In addition to minimal microparticle damage, high beta cell viability and enhanced insulin sensitivity was demonstrated through the use of a fluidised-bed bioreactor. Suggesting that culture of encapsulated cells within this relatively small system could provide a simplistic solution for the current challenges, which exist in transferring encapsulated cells from laboratories to clinical sites. This approach could offer a cost effective solution utilising a sterile fluidised system that eliminates the need for specialised facilities within clinical sites, such as clean rooms, and consequently expands the future application areas of cell-based therapies.

PEM coating of beta cells with calcium pre-conditioning

- Improved cell-cell contact between individual beta cells was achieved using a 3D cell culture approach to form MIN-6 cell spheroids with an average size of 201±2 µm. The

produced cell spheroids were robust enough to be harvested and be used in the development of PEM coating methods.

- In conventional PEM methods cells experience relatively low survival rates due to the toxic effect of the cationic polymer which is in direct contact with living cells. A novel pre-coating step was introduced in Chapter 6 through calcium pre-conditioning of the MIN-6 spheroids, which allowed the addition of anionic polyelectrolyte (alginate) before the deposition of cationic polymer (PLL). This strategy was found to be an effective way for preserving cellular metabolism and viability compared with conventional PEM coating procedures.

- Similar to non-coated beta cell spheroids, coated cell spheroids were shown to respond at a comparative rate to non-coated spheroids. In contrast to microencapsulated beta cells (Chapter 4), the novel PEM coating method developed enabled maintenance of cell insulin sensitivity. Promisingly, incorporation of this pre-coating step followed by four bilayers of ALG and PLL obstructed large immunological molecules as well as cytokines compared to naked spheroids. Consequently, this novel coating method was shown to be a promising immunoisolation therapy, which may be utilised for the treatment of type 1 diabetes and potentially other endocrine diseases.

8 CHAPTER EIGHT

Future work

The study presented here is solely one line of investigation on the beta cell immunoisolated system. Despite the large amount of work within this area, pancreatic cells transplantation is still considered to be in the experimental phase. The resulting PEM coating of pancreatic beta cells reported in this study has a number of improvements when compared with previous microencapsulation methods, including a reduction in graft volume, which enhanced the apparent mass transport limitations. In addition, cells exhibited a greater ability to tolerate direct exposure to the cationic polyelectrolyte. Further, PEM coating provides a possible platform for surface modification using other bioactive compounds, which could extend the clinical application. Future work remains to be conducted to further optimise this coating system. Based on the accomplishments of this thesis the following are recommendations for the direction of future research.

- As was shown in section 6.4.7, deposition of four bilayers of polyelectrolytes provided significantly better protection of beta cells from a mixture of three major destructive cytokines when compared with beta cell spheroids coated with fewer bilayers. However, it is noted that the optimal number of bilayers determined from *in vitro* data may not be representative of the final *in vivo* environment. The *in vitro* results presented in this thesis provide an initial optimisation of the immunoisolated system based on the biological behaviour of pancreatic beta cells, however, at the stage of *in vivo* studies, starting from small animal models and to finally human trials, it will be necessary to re-assess the number of polyelectrolyte bilayers to achieve complete coverage of cells from the host's immune response.

- Currently, a notable variation in the number of pancreatic islets required for the

regulation of blood glucose level has been reported in several transplantation studies, both in animal models and human trials. Previous studies have shown the requirement of second or third transplantation to supplement an unhealthy population of cells, which have lost their functionality after post-transplantation [64, 65, 68]. The quantity of encapsulated cells largely depends on the body mass, insulin requirements, choice of transplantation site, and the characteristic of the immunoisolated system [147]. Therefore, another important investigation related to *in vivo* studies would be discovering the total therapeutic volume of coated spheroids to achieve normoglycaemia. Understanding the optimised amount of encapsulated spheroids via in vivo studies would then enable selection of a fluidised bioreactor with the suitable column length and diameter to achieve the desired transplant volume.

Appendices

Appendix A: Published articles

SCIENTIFIC REPORTS

OPEN

Calcium pre-conditioning substitution enhances viability and glucose sensitivity of pancreatic beta-cells encapsulated using polyelectrolyte multilayer coating method

Niusha Nikravesh, Sophie C. Cox, Gurpreet Birdi, Richard L. Williams & Liam M. Grover

Type I diabetics are dependent on daily insulin injections. A therapy capable of immunoisolating pancreatic beta-cells and providing normoglycaemia is an alternative since it would avoid the late complications associated with insulin use. Here, 3D-concave agarose micro-wells were used to culture robust pancreatic MIN-6 cell spheroids within 24 hours that were shown to exhibit cell-cell contact and uniform size ($201 \pm 2\,\mu m$). A polyelectrolyte multilayer (PEM) approach using alginate and poly-l-lysine was employed to coat cell spheroids. In comparison to conventional PEM, use of a novel Ca^{2+} pre-coating step enhanced beta-cells viability ($89 \pm 6\%$) and metabolic activity since it reduced the toxic effect of the cationic polymer. Pre-coating was achieved by treating MIN-6 spheroids with calcium chloride, which enabled the adhesion of anionic polymer to the cells surface. Pre-coated cells coated with four bilayers of polymers were successfully immunoisolated from FITC-mouse antibody and pro-inflammatory cytokines. Novel PEM coated cells were shown to secret significantly ($P < 0.05$) different amounts of insulin in response to changes in glucose concentration (2 vs. 20 mM). This work presents a 3D culture model and novel PEM coating procedure that enhances viability, maintains functionality and immunoisolates beta-cells, which is a promising step towards an alternative therapy to insulin.

The encapsulation of cells within a polymeric semi-permeable membrane is attractive for various biomedical applications. In particular, this method has been studied to treat endocrine diseases, such as diabetes[1]. Type 1 diabetes, also known as diabetes mellitus, is an autoimmune disease that results from the failure in glucose regulation due to the destruction of pancreatic beta-cells by immune cells[2]. Typically insulin therapies are employed, however, continuous unregulated blood glucose levels can lead to a variety of secondary complications including, cardiovascular disease, blindness, kidney disease, and death[2,3]. Maintaining normoglycaemia would prevent such complications and improve patient's quality of life[1]. A promising alternative therapy is to encapsulate beta-cells so that when transplanted the cells are protected from the host immune system, which would eliminate the need for immunosuppressant drugs. Critically this should be balanced with the diffusion of oxygen, signalling molecules, nutrients, and secreted products, such as insulin[2,4].

Encapsulation of mammalian cells was first described by Lim and Sun, who formed alginate hydrogel micro-capsules embedded with pancreatic islets[5]. Since then, the clinical application of this method has been hampered by various issues, such as poor revascularisation of the constructs after implantation, relatively large diameter microcapsules ($400–800\,\mu m$) in comparison to the transplantation site, and an unfavourable ratio between encapsulated cells volume and overall capsule volume[6,7]. The two latter obstacles are related to the large distance between the encapsulated cells and the surrounding environment, which results in limited mass transfer, hypoxia, and ultimately cell dysfunction and death[1].

School of Chemical Engineering, University of Birmingham, Birmingham, B15 2TT, UK. Correspondence and requests for materials should be addressed to N.N. (email: NXN372@student.bham.ac.uk)
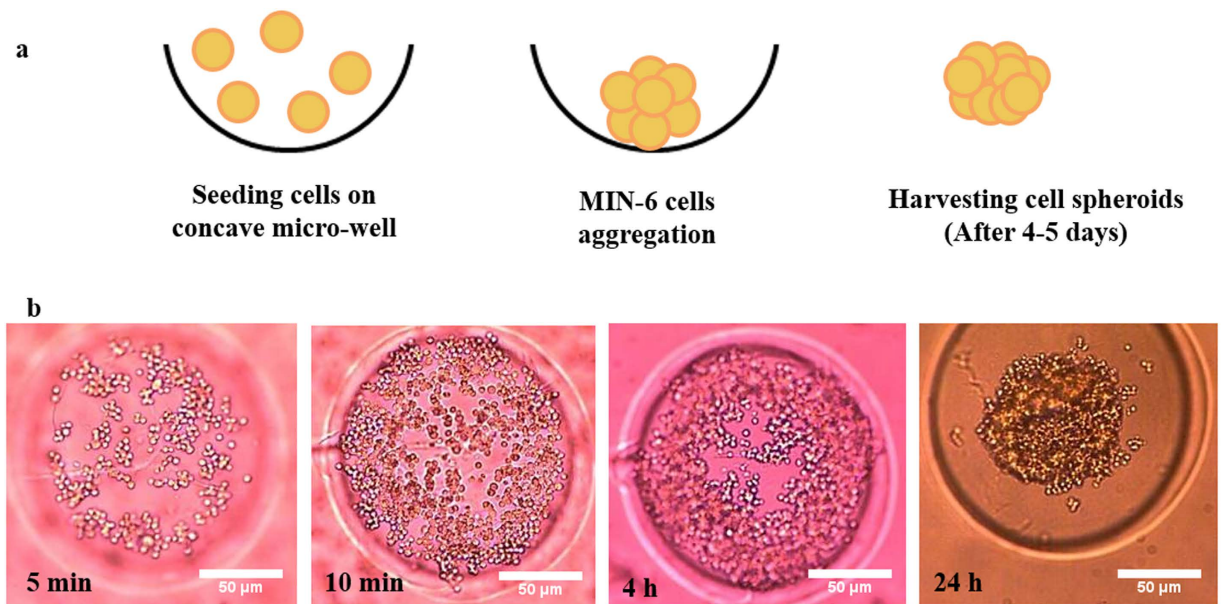
Figure 1. Formation of uniform MIN-6 spheroids. (a) Schematic illustration of cell aggregation within agarose-based micro-wells. (**b**) Light microscopy imaging of cell aggregation in wells during time intervals: 5, 10 min, 4, and 24 h of post-seeding.

A possible solution may be to coat cells with polyelectrolytes rather than embedding cells in a polymeric matrix. This technique, known as layer-by-layer (LBL) or polyelectrolyte multilayer coating (PEM), is based on the alternate deposition of anionic and cationic polymers on to a charged surface[8,9]. This approach limits the gap between the cells and the surrounding environment resulting in a shorter response time to external stimulation[10], while retaining a coating that may prevent immune response. This may allow rapid response to changes in blood glucose and thereby better regulation.

Alginate is the most common and studied material for encapsulation of living cells and therapeutic agents[11]. Alginate is an anionic polymer that can form polyelectrolyte complexes in the presence of polycations, such as poly-l-lysine (PLL) and chitosan. PLL has been used to coat alginate beads as a way of controlling the ingress of biological components harmful to cell survival[12,13]. Owing to the negative charge of cells, PEM coating is initiated by the deposition of a cationic polymer, however, previous studies have shown that when cationic polymers are used in direct contact with cells it increases the possibility of host inflammatory responses and cytotoxic behaviour[1,14].

In this study, a novel pre-coating step was introduced into a conventional PEM coating method to minimise the influence of PLL on cell viability by conditioning the surface of cell aggregates with $CaCl_2$, before exposure to PLL. The resulting spheroids were analysed with respect to viability, functionality, and immunoisolation.

Results

Formation of uniform MIN-6 spheroids.
To achieve uniform aggregation of pancreatic beta-cells prior to the PEM coating process, dispersed MIN-6 cells were seeded on top of agarose-based micro-wells. Cell spheroids with uniform size and shape ($92 \pm 4.9\,\mu m$) were generated in the centre of the concave wells within 24 h due to aggregation of each cell by cell-cell contact and gravitational force (Fig. 1b). The majority of cell spheroids formed after one day of culture and only a few micro-wells remained vacant (<1.5%). It was discovered that 4–5 days of culture was the optimum time period to achieve robust spheroids, which could be easily harvested and used for the coating procedure.

MIN-6 spheroid morphology.
Then to quantify the effect of culturing cells on 3D agarose constructs, the size distribution of 30 spheroids cultured on both a flat-bottomed plate (control) and concave wells were compared after 7 days of culture. In the case of MIN-6 spheroids in agarose-based wells, their size range was mostly between 200–250 μm with an average of $201 \pm 2\,\mu m$. However, for the control sample, cells exhibited a wide range of sizes from 50–250 μm with an average of $103 \pm 49.2\,\mu m$ (Fig. 2a,b,c). To gain insight in to the influence of 3D culture, immunofluorescent staining of actin filaments and cell nuclei were examined on day 5. As expected, fluorescence signals from the filamentous actin (F-actin) cytoskeleton, suggested that the MIN-6 spheroids were adhered to one another, forming a compact structure. DAPI staining showed a large number of freely growing cells on the surface of the MIN-6 spheroids (Fig. 2d).

Addition of pre-coating step increased cytocompatiblility of coated cells.
Coating of MIN-6 spheroids was achieved by subsequent layering of oppositely charged polyelectrolytes; ALG (alginate) and PLL (poly-l-lysine). After the pre-coating step (pre-conditioning with $CaCl_2$ and deposition of initial ALG layer), each coated spheroid was formed by the alternate deposition of four bilayers (a total of 8 layers) of polyelectrolytes. For
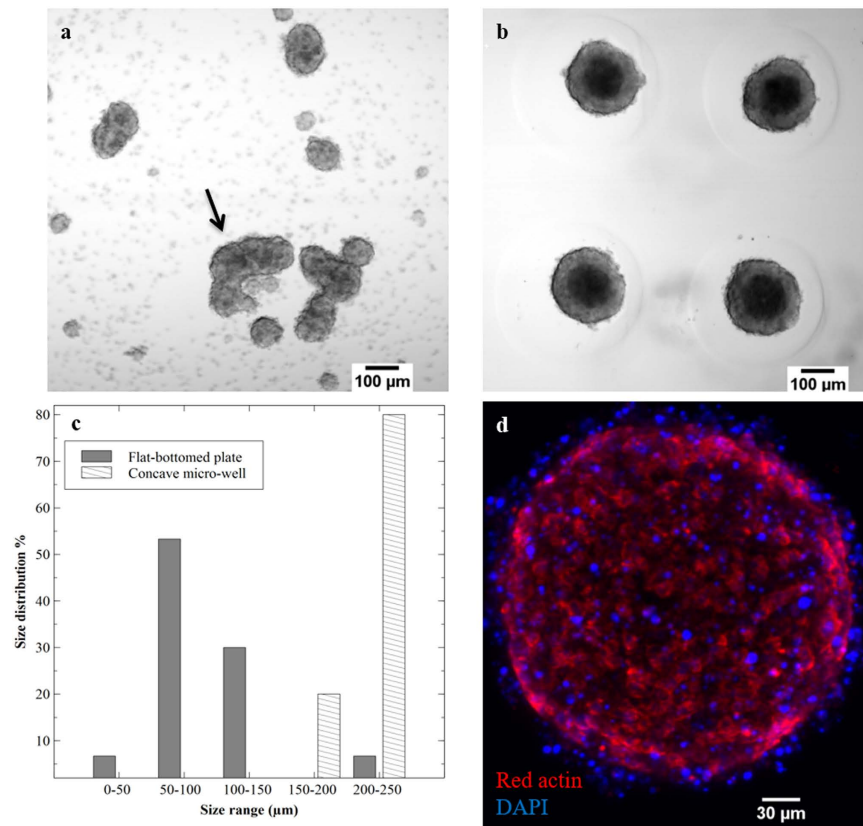
Figure 2. Comparison between MIN-6 spheroids cultured on different surfaces. (**a**) and (**b**) Morphology of MIN-6 cells cultured on flat-bottomed plate and agarose concave micro-wells on day 7, respectively. (**c**) Comparison between the size distribution of aggregated cells in both flat-bottomed and concave wells (n = 30 spheroids), large chain of cell clumps formed in flat-bottomed sample were not analysed in this study (Indicated with an arrow). (**d**) Direct immunofluorescent staining of MIN-6 spheroids with Actin-Red 555 (F-actin probe) and DAPI (cell nuclei probe) for visualisation of cell-cell interaction using CLSM.

all cell spheroids, ALG was chosen as the final polyelectrolyte layer. To investigate whether the pre-coating step was efficient in reducing the toxic effect of PLL, the viability of the pre-coated cells was compared with MIN-6 spheroids coated directly with PLL. After 8 days of culture, quantitative analysis of the stained cells revealed a significant difference (p < 0.01) between the viability of cells that were pre-coated (89 ± 6%) and those with an initial layer of PLL (64 ± 11%) (Fig. 3c).

Furthermore, the metabolic activity of coated MIN-6 spheroids (with and without the pre-coating step) was compared with non-coated cells as a control (Fig. 3d). In comparison to pre-coated spheroids and non-coated cells, the ability of non-pre-coated spheroids to reduce the Alamar Blue reagent (metabolic activity indicator) was significantly reduced (p = 0.04) after 9 days of culture, possibly due to the toxicity of PLL when used in direct contact with MIN-6 cells; Hence in comparison to the control, the metabolic activity of cells coated with an initial layer of PLL was reduced by 32%, while for the cells with pre-coating step there was a smaller reduction of 13%.

Confirmation of coating on cell spheroid surfaces. To demonstrate the deposition of polyelectrolytes on cell spheroids, PLL labelled with Alexa Fluor-647 was used. The FITC labelled PLL was then applied to the final bilayer (7th layer) to enable visualisation of coated cells under confocal microscope. From cross sectional images obtained at distances of 10 and 30 μm from the centre of cell spheroid, using Z-stack imaging technique (Fig. 4a,b), the fluorescent signalling was mainly located at the peripheries of the coated cells, which indicated successful coating of cells with alternate deposition of polyelectrolyte layers. Also Fig. 4d and e demonstrate the difference in behaviour of coated and non-coated spheroids when cultured on a CellBIND tissue culture plate. After 7 days of culture, non-coated spheroids attached to the surface and cells covered and migrated across the whole area, as expected. On the contrary, coated spheroids with 4 bilayers remained suspended in the culture medium confirming that the entire spheroid surface was coated.

Coated MIN-6 cells excluded FITC-antibody. To investigate the permeability of coated MIN-6 spheroids to immunologically relevant molecules, samples were exposed to FITC-mouse antibody which can then target the antigens (MHC class II) that exist on the surface of pancreatic beta-cells. The fluorescence intensity emitted from non-coated spheroids was shown to be much greater than coated spheroids (Fig. 5). This study provided evidence that compared with the control (non-coated cells), pre-coating of cells with alginate followed by the deposition
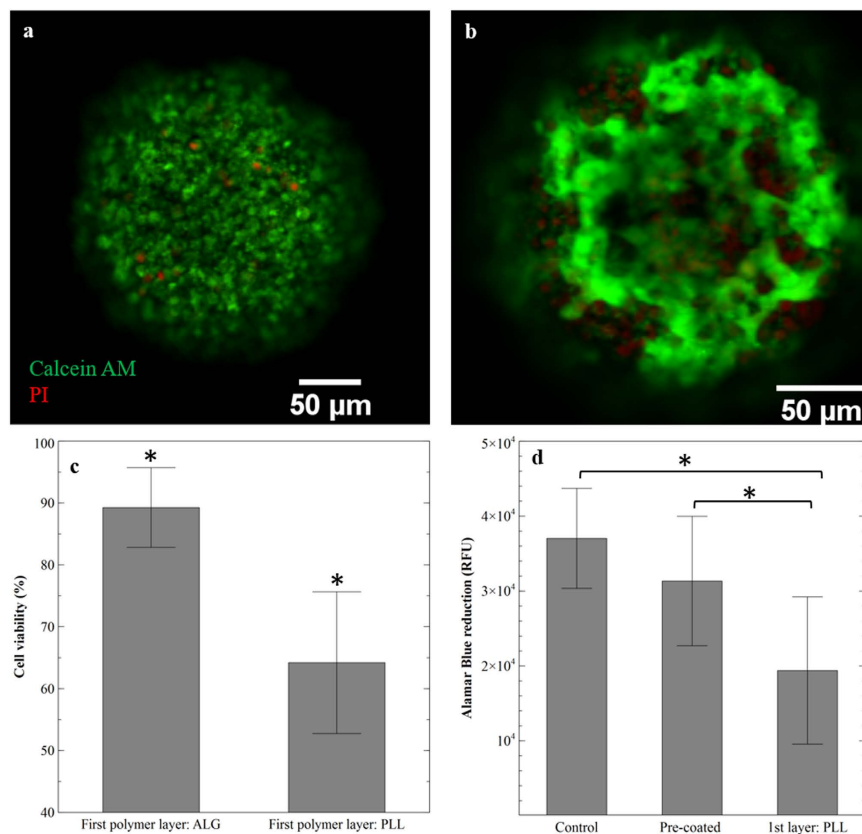
Figure 3. Evaluation of viability and metabolic activity of MIN-6 spheroids coated with four bilayers of PLL/ALG. (**a**) Confocal microscopic images of live (calcein-AM: green) and dead (PI: red) stained cell spheroids coated with initial layer of alginate during the pre-coating step. (**b**) Cells coated with PLL as the first coating layer. (**c**) Quantitative evaluation of live/dead analysis (n = 10 spheroids) (**d**) Comparison between metabolic activity of MIN-6 coated spheroids with and without pre-coating step, and the control (non-coated spheroids) (n = 3), Results are presented as mean ± S.D, (*P < 0.05).
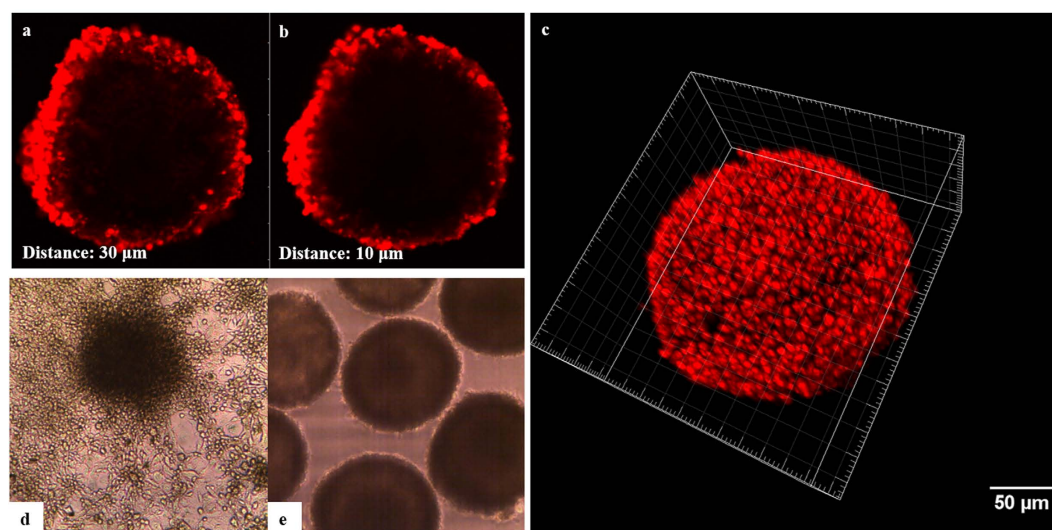
Figure 4. Monitoring the ALG/PLL coating layers on MIN-6 spheroids. (**a**) and (**b**) Z-stack cross-sections of coated MIN-6 spheroids with FITC-PLL obtained at 10 and 30 μm from the centre, respectively. (**c**) 3-D reconstruction of coated spheroid (Raw data from Z-stack was analysed with Imaris software). (**d**) and (**e**) Light Micrographs of coated and non-coated cell spheroids in response to cell-attachable surface, respectively.
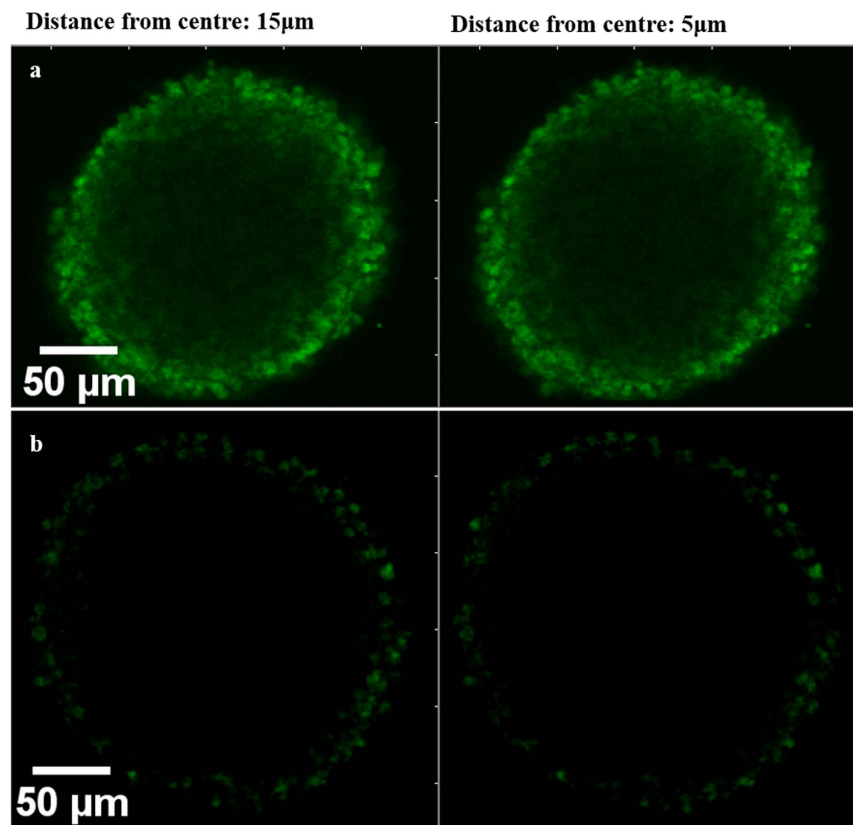
Figure 5. Confocal images of MIN-6 spheroids after being exposed to FITC-mouse antibody (10 KDa). (**a**) Z-stack image of non-coated spheroid using argon laser. (**b**) Coated spheroid with pre-coating step and 4 bilayers of PLL/ALG. Z-stack images were obtained at distance of 5 and 15 μm from the centre of both coated and non-coated spheroids.

of four bilayers of PLL and ALG considerably protected the coated pancreatic beta-cells from attaching to the FITC-antibody by covering the surface of spheroids.

Coated cells exhibited higher survival after being exposed to cytokines. To further examine the permeability of coated spheroids against smaller molecules, a mixture of three cytokines: IL-1β (~17 KDa), TNF-α (~17.5 KDa), and IFN-γ (~15 KDa) was added to both non-coated and coated spheroids with 1, 2, and 4 bilayers of polyelectrolytes. As shown in Fig. 6a, after 24 h exposure to cytokines, the viability and metabolic activity of non-coated cell spheroids were notably reduced to 55 ± 2.5 RFU (P-value < 0.01). Moreover, response of MIN-6 spheroids to cytokines after the addition of one bilayer of polyelectrolytes was only slightly different from the non-coated cells. However, deposition of four bilayers of PLL/ALG significantly reduced cytokine damage on pancreatic beta-cells survival rate (204 ± 3.3 RFU) in comparison with other groups (P-value < 0.01).

Coated spheroids remained responsive to the changes in glucose concentrations. After two weeks of culture, insulin secretion from coated and non-coated MIN-6 spheroids (n = 50) in response to glucose was investigated by culturing both samples in a series of basal (2 mM), and stimulatory (20 mM) glucose concentrations. The amount of insulin released from coated spheroids into basal glucose solution was 17.1 ± 0.1 ng/mL, which was significantly increased to 57.3 ± 0.4 ng/mL under a stimulatory glucose concentration (P-value < 0.05) (Fig. 6b). Also, comparison between the amounts of secreted insulin from both coated and non-coated spheroids showed no significant difference, indicating that the coated MIN-6 cells remained responsive to glucose after applying four bilayers of ALG/PLL.

Discussion

In this study, we have demonstrated the formation of stable and uniformly sized MIN-6 spheroids using agarose-based concave micro-wells. The prepared spheroids were then immunoisolated with ALG and PLL using a novel coating approach. Up to now, several groups have developed polydimethylsiloxane-based micro-molds for creating cell aggregates, however, using this substrate requires further steps for modification of well surfaces and preventing cell adhesion[15–17]. Herein, the formed beta-cell spheroids were easily detached and retrieved from the agarose construct without any further need for treatment with trypsin or surface modification, which was an advantage for preventing damage to cells during the harvesting and coating process.
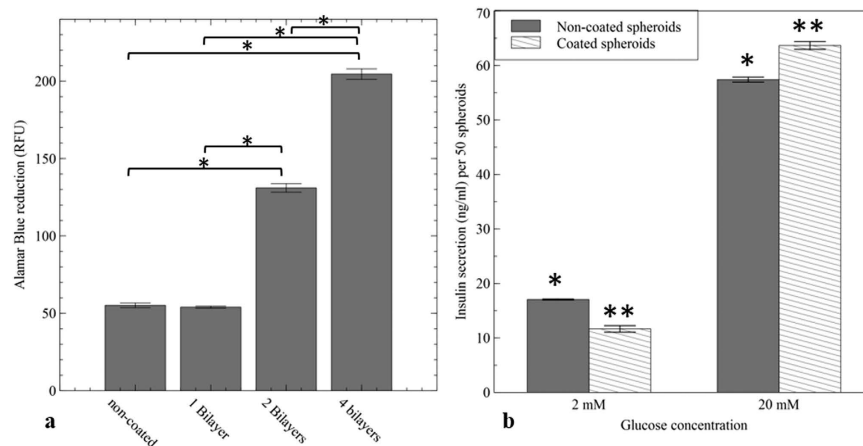
Figure 6. (**a**) Viability of non-coated and coated MIN-6 spheroids with different numbers of PLL/ALG bilayers after being incubated with a cytokine mixture for 24 h; Results are presented as mean ± SEM (n = 4), (*P < 0.01), and were normalised to 1000 cells. (**b**) Insulin release of non-coated (control) and coated MIN-6 spheroids in response to glucose stimulation. Insulin release was normalized against 50 spheroids; Results are presented as mean ± S.D (n = 3), (*, **P < 0.05).

Microscopic observation followed by size analysis confirmed that the use of concave micro-wells facilitated the formation of uniform MIN-6 spheroids with a size range similar to pancreatic islets (150–250 μm) (Fig. 2c). In contrast, the diameter of aggregated cells formed on a flat-bottomed plate varied between 50 and 250 μm, and also resulted in accumulation of cell chains with non-uniform shape and a broad size distribution (Fig. 2a). The viability of these samples was notably affected and therefore such shapes are undesirable for coating. Previous studies have shown that culturing epithelial cells in a 3D environment could improve cell adhesion and intra-cellular signalling by providing an additional dimension for external cell interactions[18]. As a result, formation of beta-cell spheroids were studied as a means to mimic the real tissue and cell adhesions were observed by direct fluorescent staining of F-actin and cell nuclei of MIN-6 spheroids (Fig. 2d).

For the past two decades, coating mammalian cells using a layer-by-layer assembly of polyelectrolytes has been studied as a promising approach to reduce large void volume between the encapsulated cells and the surrounding environment utilising various materials, including both synthetic and natural polymers[9,19]. However, using this approach and the application of positively charged polymers in direct contact with cells can be detrimental to cell survival and functionality[13]. Hence several groups have demonstrated the effect of modifying polycations with different materials, including poly(ethylene) glycol and phosphoro-choline to reduce their toxicity and inflamma-tory responses[19–21]. Herein, we chose PLL and ALG as the cationic and anionic polymers, respectively. However, as a novel approach to reduce the toxicity of PLL, cells were first suspended in 100 mM of $CaCl_2$, which enhanced the formation of a layer of ALG prior to the addition of PLL on the cell's surface. Results from live/dead staining suggested that the coating approach used in this study, enhanced cell survival by 25% in comparison with the conventional LBL procedure after being coated for 8 days (Fig. 3c). Also, a possibility for the clusters of dead cells observed in Fig. 3b might be secretion of harmful chemicals, associated with dead cells.

Furthermore, pre-coated cells were able to maintain higher metabolic activity compared with MIN-6 sphe-roids coated with an initial layer of PLL (Fig. 3D). Importantly, these studies confirmed that suspending cells in 100 mM of $CaCl_2$ during the pre-coating step did not induce harmful effect on cell viability, hence it was con-cluded that with the described coating approach the toxic effect of PLL was reduced without any further need for surface or chemical modification.

The presence of polyelectrolyte layers on MIN-6 spheroids was confirmed by the means of FITC labelled PLL. When FITC-PLL was applied to the last bilayers, clear fluorescent emission was observed from cross sectional images and Z-stack 3D reconstruction of coated spheroid (Fig. 4a,b,c), suggesting the existence and successful deposition of polymeric layers on the surface of cell spheroids.

Although maintaining a high metabolic activity and survival rate of the encapsulated cells could increase the longevity of transplanted cells, complete success in pancreatic islet implantation relies upon efficient immu-noisolation of the cells from recipient immune responses. In this regard, to gain a better insight into the coating approach established in this study, both coated and non-coated cells were exposed to FITC-mouse antibody. The images from spheroids were captured through the Z-axis using confocal microscopy (Fig. 5). Observation showed a notable prohibition of FITC antibody from attaching to MHC class II antigens on the surface of coated beta-cells in comparison to the non-coated cells.

Previous studies have shown that release of the three main pro-inflammatory cytokines (IL-1β, TNF-α, and IFN-γ) from activated T-cells and macrophages could be responsible for dysfunction of beta-cells by inducing over expression of inducible nitric oxide synthase (iNOS)[22,23]. In the present study, we evaluated whether the coated cells could prevent the diffusion of cytokines to MIN-6 spheroids. Figure 6a, emphasised that deposition of pre-coating layer and four bilayers of PLL/ALG was effective in inhibiting cytokine damage and hence increasing cell viability compared with naked spheroids.

We further demonstrated the MIN-6 spheroid's ability to sense the changes in glucose concentration (2 Vs. 20 mM) during the GSIS assay. For both coated and non-coated cells, increasing glucose concentration from basal to stimulatory, significantly increased the amount of insulin secreted by cells (Fig. 6b). Hence the data showed that suspending cells in $CaCl_2$ solution during the pre-coating step followed by the addition of 4 bilayers of PLL/ALG, did not affect MIN-6 cells in terms of insulin release.

In conclusion, we developed uniform sized and shaped MIN-6 spheroids using an agarose construct with the advantage of forming robust 3D cell spheroids that may be easily harvested. The feasibility of the reported novel calcium pre-coating approach to enhance cell survival and functionality of pancreatic beta-cells was demonstrated using various assays. Use of this pre-coating step was found to be an effective way for preserving MIN-6 cellular metabolism and viability compared with conventional PEM coating procedures. Similar to non-coated cells, coated pancreatic beta-cells allowed a rapid response to external glucose changes. Promisingly, incorporation of this pre-coating step followed by four bilayers of ALG and PLL obstructed large immunological molecules as well as cytokines compared to naked spheroids. In summary, this novel coating method was shown to be a promising immunoisolation therapy which may be utilised for the treatment of type 1 diabetes and potentially other endocrine diseases.

Methods

Cell culture.
MIN-6 cells (AddexBio, San Diego, USA) were cultured in Dulbecco's modified eagle medium (DMEM, 4500 mg/L glucose, Sigma, UK) supplemented with 15% fetal bovine serum (FBS, Sigma, UK), 2 mM L-glutamine (Sigma, UK) and 0.05 mM 2-mercaptoethanol (Sigma, UK)[22]. Since mouse pancreatic beta-cells have limited ability to tolerate oxidative stresses, 2-mercaptoethanol was added to the cell culture medium to aid in maintaining a reducing environment; limiting toxic oxygen radicals. All cultures were incubated at 37 °C with 5% CO_2 until they reached 70–80% confluency. Culture medium was changed every other day to enhance cell growth and viability.

Seeding beta-cells within micro-wells.
Micro-molds (Sigma-Aldrich, UK) were used for casting 3-dimensional (3D) culture plates by adding 500 μL of 2 w/v% agarose solution into each mold. The final transparent agarose culture plate with 400 μm diameter micro-wells (number of micro-wells per mold: 256) were removed from the mold after being cooled. Cells were first trypsinized with trypsin-EDTA (Sigma, UK), and counted with a haemocytometer. MIN-6 cells suspended in supplemented DMEM, at a density of 5×10^5 cells/200 μL, were seeded on top of the concave agarose micro-wells. Spheroid formation was observed daily using an inverted microscope (Olympus Co., Germany), and formed spheroids were used for further studies after being cultured for 4–5 days (Fig. 1a).

Size analysis of MIN-6 spheroids.
The size of the MIN-6 cell spheroids formed in micro-wells were compared with the same concentration of cells (2.5×10^6 cells/mL) seeded on flat-bottomed non-attachable culture plates. The average diameters of the two groups were determined on day 7 of culture from thirty randomly selected samples, which were observed using a light microscope (Olympus Co., Germany). Quantitative data was determined using Image J software (NIH, Bethesda, MD, USA).

Coating MIN-6 spheroids with multi-polyelectrolyte layers.
After 4–5 days of culture, cell spheroids were retrieved from the agarose micro-wells using a plate shaker (Grant-bio, PMS-1000i, UK) (450 rpm). Solutions of alginate (1 mg/mL) (ALG, medium viscosity (≫20,000 cP, Sigma, UK) and Poly-l-lysine (1 mg/mL) (PLL, MW: 30,000–70,000, Sigma, UK) were prepared in deionised water and Phosphate buffered saline (PBS, Fisher Scientific, UK), respectively. All solutions were sterile filtered using a 0.22 μm syringe filter (Millipore, USA) and UV sterilised overnight. Contrary to the conventional layer-by-layer deposition, before starting the coating process cell spheroids were first suspended in 200 μl of $CaCl_2$ (100 mM). After washing with PBS, 200 μL of alginate was added to minimise the potential toxicity of direct contact between cells surface and cationic polymer (PLL). Alternating layers of PLL and alginate were then applied according to conventional LBL methods[24,25]. Briefly, 200 μl of PLL was added to the pre-coated spheroids, after 4 min deposition time, cells were washed twice in 500 μl PBS to remove any unbound PLL, followed by the addition of the anionic polymer (alginate) with the same procedure. The last two steps were repeated to achieve the desired number of layers. Finally, cells were washed three times with DMEM and were incubated at 37 °C for further studies.

Fluorescent labelling of PLL.
To prepare the fluorescently labelled PLL, 0.1 mg of Alexa Fluor 647NHS ester (Succinimidyl Ester) (Thermo Fisher, UK) was dissolved in 1 mL of dimethyl sulfoxide (DMSO, Sigma, UK). 100 μL of the dye was added to 1 mL of PLL stock solution with a concentration of 2 mg/mL. The solution was incubated at room temperature for 6 h under continuous stirring. To remove the excess dye, the solution was then dialyzed for 24 h against deionised water. The final solution was then kept in the dark at 4 °C until needed.

Assessment of cell viability and metabolic activity.
Viability of coated MIN-6 cells using different coating deposition sequence was evaluated using a live/dead staining kit. Briefly on the day of experimentation, 1 μL of calcein acetoxymethylester (Calcein AM (662 Da), indicator for live cells, Invitrogen, USA) and 5 μL of propidium iodide (PI (668 Da), indicator for dead cells, Invitrogen, UK) were added to a 200 μL suspension of coated spheroids in cell culture medium. Cells were incubated in the dark at 37 °C for 30 min. Stained cells were then visualised using confocal laser scanning microscopy (Olympus FV1000, Multiple Ar laser, Germany), and images were analysed using ImageJ software (NIH, USA).

The metabolic activities of coated and non-coated (control) MIN-6 cells were assessed using the Alamar Blue cell proliferation assay (Thermo Fisher, UK). The assay reagent reduces from a non-fluorescent blue colour to a fluorescent red form, during cellular metabolism. Hence, the amount of assay reagent reduction is proportional

to cell number (presuming equal metabolic activity). Briefly, 20 μL of Alamar Blue reagent were added to 200 μL of cell spheroids suspension in DMEM, followed by incubating for 4 h at 37 °C. The fluorescence was then read (590 nm emission and 560 nm excitation) using a microplate reader (GloMax-Multi+, Promega, USA). The results were reported as percentage reduction between the coated and the control sample.

Immunofluorescent staining. After 5 days in culture, MIN-6 spheroids were fixed with 10% formalin (Sigma, UK). Samples were then blocked in PBS solution containing 2% bovine serum albumin (BSA, Sigma, UK) and 0.2% Triton X-100 (Sigma, UK) for 1 h. After washing in PBS, fixed cells were stained with Actin-red 555 (F-actin Probe, Life Technologies, UK) for 30 min, followed by several washing steps with PBS. Cell nuclei were also counter-stained using DAPI (1 μg/mL) (Sigma, UK). 3D visualisation of the stained spheroids was undertaken using confocal microscopy (Laser 405 nm: DAPI, Laser 543: Actin-red 555).

Antibody exclusion assay. The permeability of the coated spheroids against large immunologically relevant molecules was evaluated using FITC labelled anti-mouse MHC class II (eBioscience, UK). Briefly, cell spheroids with and without coating layers were prepared as described previously. Fifteen MIN-6 spheroids were randomly selected from each group, and 100 μL of 2% BSA and Hanks' balanced salt solution (HBSS, blocking buffer, Sigma, UK) were added to the samples. Cells were incubated for 15 min at 37 °C with 1 μL of FITC- antibody. Samples were then washed twice with HBSS and 0.1% Tween-20 to remove any excess antibody. The coated and non-coated spheroids were observed using confocal laser scanning microscopy with an argon laser.

Treating MIN-6 cells with cytokines. Groups of coated and non-coated spheroids were treated with a mixture of three cytokines at a final concentration of Interleukin-1β (IL-1β, Sigma, UK) (5 ng/mL), mouse tumour necrosis factor-α (TNF-α, Gibco, Life Technology, UK) (10 ng/mL), and mouse interferon-ϒ (IFN-ϒ, Gibco, Life Technology, UK) (100 ng/mL) in DMEM. All treated samples were incubated overnight at 37 °C. The viability of the treated spheroids was measured using the Alamar Blue assay as described previously, and data were normalised to 1000 cells.

Glucose-stimulated insulin secretion (GSIS) assay. To evaluate the function of MIN-6 cells, the amount of insulin secreted from non-coated and coated cells in response to changes in glucose concentration was measured. Briefly, samples were washed and pre-incubated in Krebs-Ringer bicarbonate buffer (KRBH: 125 mM NaCl, 1.2 mM MgSO$_4$, 1.2 mM CaCl$_2$, 22 mM NaHCO$_3$, 10 mM HEPES, 1.19 mM KH$_2$PO$_4$) + 0.1% BSA with glucose concentration of 2 mM for 2 h. Then, samples underwent a static incubation for 1 h with low (2 mM) glucose concentration in KRBH + 0.1% BSA followed incubation for a further hour in high (20 mM) glucose concentration KRBH + 0.1% BSA as the stimulator. For each incubation period the cultured supernatant was collected for insulin assay and diluted to the appropriate range based on the assay standard curve. The secreted insulin was measured using an Enzyme-linked immunosorbent assay (ELISA) kit (Millipore, UK), and the colorimetric reaction was quantified using a plate spectrophotometer (GloMax-Multi + Mictoplate Multimode reader, Promega, USA) at a wavelength of 450 nm.

Statistical analysis. The student's t-test, assuming equal variance, was used to identify any significant differences between pairs of groups. One-way analysis of variance (ANOVA) was used to identify any significant difference between the means of independent groups. Furthermore, a Bonferroni post-hoc test was performed with ANOVA to find means that were significantly different within groups. A P-value < 0.05 was determined as significant. Results are presented as mean ± standard deviation unless otherwise stated.

References

1. Gasperini, L., J. F. Mano & R. L. Reis. Natural polymers for the microencapsulation of cells. *Journal of The Royal Society Interface* **11(100),** 20140817 (2014).
2. Pagliuca, F. W. & D. A. Melton. How to make a functional β-cell. *Development*, **140(12),** 2472–2483 (2013).
3. Ashcroft, F. M. & P. Rorsman. Diabetes mellitus and the β cell: the last ten years. *Cell*. **148(6),** 1160–1171 (2012).
4. Colton, C. K. Oxygen supply to encapsulated therapeutic cells. *Advanced drug delivery reviews*. **67,** 93–110 (2014).
5. Lim, F. & A. M. Sun. Microencapsulated islets as bioartificial endocrine pancreas. *Science*. **210(4472),** 908–910 (1980).
6. Davis, N. E. *et al.* Enhanced function of pancreatic islets co-encapsulated with ECM proteins and mesenchymal stromal cells in a silk hydrogel. *Biomaterials*. **33(28),** 6691–6697 (2012).
7. de Groot, M., T. A. Schuurs & R. van Schilfgaarde. Causes of limited survival of microencapsulated pancreatic islet grafts. *Journal of Surgical Research*. **121(1),** 141–150 (2004).
8. Diaspro, A. *et al.* Single living cell encapsulation in nano-organized polyelectrolyte shells. *Langmuir*. **18(13),** 5047–5050 (2002).
9. Picart, C. Polyelectrolyte multilayer films: from physico-chemical properties to the control of cellular processes. *Current medicinal chemistry*. **15(7),** 685–697 (2008).
10. Frezza, C. *et al.* Metabolic profiling of hypoxic cells revealed a catabolic signature required for cell survival. *PloS one*. **6(9),** e24411 (2011).
11. de Vos, P. *et al.* Alginate-based microcapsules for immunoisolation of pancreatic islets. *Biomaterials*. **27(32),** 5603–5617 (2006).
12. Cui, W. *et al.* A membrane-mimetic barrier for islet encapsulation. In *Transplantation proceedings*. Elsevier (2004).
13. Kozlovskaya, V. *et al.* Hydrogen-bonded LbL shells for living cell surface engineering. *Soft Matter*. **7(6),** 2364–2372 (2011).
14. Gribova, V., R. Auzely-Velty & C. Picart. Polyelectrolyte multilayer assemblies on materials surfaces: from cell adhesion to tissue engineering. *Chemistry of Materials*. **24(5),** 854–869 (2011).
15. Jun, Y. *et al.* 3D co-culturing model of primary pancreatic islets and hepatocytes in hybrid spheroid to overcome pancreatic cell shortage. *Biomaterials*. **34(15),** 3784–3794 (2013).
16. Lee, S.-A. *et al.* Functional 3D human primary hepatocyte spheroids made by co-culturing hepatocytes from partial hepatectomy specimens and human adipose-derived stem cells (2012).
17. Wong, S. F. *et al.* Concave microwell based size-controllable hepatosphere as a three-dimensional liver tissue model. *Biomaterials*. **32(32),** 8087–8096 (2011).
18. Griffith, L. G. & M. A. Swartz. Capturing complex 3D tissue physiology *in vitro*. *Nature reviews Molecular cell biology*. **7(3),** 211–224 (2006).

19. Kizilel, S. *et al.* Encapsulation of pancreatic islets within nano-thin functional polyethylene glycol coatings for enhanced insulin secretion. *Tissue Engineering Part A.* **16(7),** 2217–2228 (2010).
20. Bhaiji, T., Z. L. Zhi & J. C. Pickup. Improving cellular function and immune protection via layer-by-layer nanocoating of pancreatic islet β-cell spheroids cocultured with mesenchymal stem cells. *Journal of Biomedical Materials Research Part A.* **100(6),** 1628–1636 (2012).
21. Wilson, J. T., W. Cui & E. L. Chaikof. Layer-by-layer assembly of a conformal nanothin PEG coating for intraportal islet transplantation. *Nano letters.* **8(7),** 1940–1948 (2008).
22. Fu, Z., E. R. Gilbert & D. Liu. Regulation of insulin synthesis and secretion and pancreatic Beta-cell dysfunction in diabetes. *Current diabetes reviews.* **9(1),** 25 (2013).
23. Barshes, N. R., S. Wyllie & J. A. Goss. Inflammation-mediated dysfunction and apoptosis in pancreatic islet transplantation: implications for intrahepatic grafts. *Journal of leukocyte biology.* **77(5),** 587–597 (2005).
24. Costa, R. R. & J. F. Mano. Polyelectrolyte multilayered assemblies in biomedical technologies. *Chemical Society Reviews.* **43(10),** 3453–3479 (2014).
25. Hajicharalambous, C. S. *et al.* Nano-and sub-micron porous polyelectrolyte multilayer assemblies: biomimetic surfaces for human corneal epithelial cells. *Biomaterials.* **30(23),** 4029–4036 (2009).

Author Contributions

N.N. undertook the majority of experimental work and wrote the initial manuscript. S.C. advised on the work, and read and modified the final manuscript. G.B., and R.W. assisted with the work and helped in the proof-reading of the manuscript. L.M.G. planned and supervised the research, and read and modified the final manuscript.

Additional Information

How to cite this article: Nikravesh, N. *et al.* Calcium pre-conditioning substitution enhances viability and glucose sensitivity of pancreatic beta-cells encapsulated using polyelectrolyte multilayer coating method. *Sci. Rep.* **7**, 43171; doi: 10.1038/srep43171 (2017).

Publisher's note: Springer Nature remains neutral with regard to jurisdictional claims in published maps and institutional affiliations.

"Encapsulation and fluidisation maintains the viability and glucose sensitivity of beta-cells"

Niusha Nikravesh[1*], Sophie C. Cox[1], Marianne J. Ellis[2], and Liam M. Grover[1]

Affiliations:
[1] School of Chemical Engineering, University of Birmingham, Birmingham, B15 2TT, UK
[2] School of chemical engineering, University of Bath, Bath, BA2 7AY
* Corresponding author, Email: nxn372@student.bham.ac.uk

Abstract

This study presents experimental data of a fluidised-bed bioreactor for the cultivation of encapsulated pancreatic beta-cells. The fluidisation quality for the bioreactor was evaluated at different flow rate using bed-expansion parameters. Homogeneous distribution of microcapsules was achieved at a flow rate of 2000 μL/min. This enabled efficient contact between the encapsulated cells and medium, which contributed to high cell viability. Microcapsule breakage was < 4% on day 7 and confirmed the stability of encapsulated systems under fluidised culture. Importantly, endocrine beta-cells cultured in the bioreactor were shown to be dramatically more responsive to changes in glucose concentration compared to static culture (P< 0.001). Based on these results, cultivation of encapsulated cells in a fluidised bioreactor, especially for pancreatic beta-cells that are limited in supply, is a promising approach to address the lack of a safe method for storage and handling of cells between laboratories and clinical sites prior to transplantation.

Keywords: microcapsules, endocrine beta-cells, bioreactor, viability, fluidisation, insulin secretion.

Appendix B: List of achievements

<u>Conference presentations</u>

- EPS research conference; University of Birmingham, UK; **Poster title**: "Coating of pancreatic beta cells with calcium preconditioning", 2016.

- 10th world Biomaterial Congress (WBC); Montréal, Canada; **Oral presentation**: "A novel method for the coating of pancreatic beta-cell spheroids", 2016.

- 27th annual conference of European Society of Biomaterials (ESB); Krakow, Poland; **Poster title**: "Microencapsulation and nano coating of pancreatic beta cells", 2015.

<u>Published research articles and abstracts</u>

Abstract:

Nikravesh, N., et al., A novel method for the coating of pancreatic beta-cell spheroids. Frontiers in Bioengineering and Biotechnology.

Research articles:

- **Nikravesh, N**. et al. Calcium pre-conditioning substitution enhances viability and glucose sensitivity of pancreatic beta cells encapsulated using polyelectrolyte multilayer coating method. Sci.Rep. 7, 43171; doi: 10.1038/srep43171 (2017).

- **N. Nikravesh**, S.C Cox, M.J Ellis, and L.M Grover. Encapsulation and fluidization

maintains the viability and glucose sensitivity of beta cells. ACS Biomaterials Science & Engineering, (**Accepted paper, June 2017)**.

References

1. Ashcroft, F.M. and P. Rorsman, *Diabetes mellitus and the β cell: the last ten years.* Cell, 2012. **148**(6): p. 1160-1171.

2. Pagliuca, F.W. and D.A. Melton, *How to make a functional β-cell.* Development, 2013. **140**(12): p. 2472-2483.

3. Ratner, F. and M. Kaufman, *Type 1 diabetes mellitus.* Pediatrics in Review, 2003. **24**(9): p. 291.

4. O'Sullivan, E.S., et al., *Islets transplanted in immunoisolation devices: a review of the progress and the challenges that remain.* Endocrine reviews, 2011. **32**(6): p. 827-844.

5. Steele, J., et al., *Therapeutic cell encapsulation techniques and applications in diabetes.* Advanced drug delivery reviews, 2014. **67**: p. 74-83.

6. Lysy, P.A., G.C. Weir, and S. Bonner-Weir, *Concise review: pancreas regeneration: recent advances and perspectives.* Stem cells translational medicine, 2012. **1**(2): p. 150-159.

7. Beck, J., et al., *Islet encapsulation: strategies to enhance islet cell functions.* Tissue engineering, 2007. **13**(3): p. 589-599.

8. Gasperini, L., J.F. Mano, and R.L. Reis, *Natural polymers for the microencapsulation of cells.* Journal of The Royal Society Interface, 2014. **11**(100): p. 20140817.

9. Rother, K.I. and D.M. Harlan, *Challenges facing islet transplantation for the treatment of type 1 diabetes mellitus.* The Journal of clinical investigation, 2004. **114**(7): p. 877-883.

10. de Groot, M., T.A. Schuurs, and R. van Schilfgaarde, *Causes of limited survival of microencapsulated pancreatic islet grafts.* Journal of Surgical Research, 2004. **121**(1): p. 141-150.

11. Kang, A., et al., *Cell encapsulation via microtechnologies.* Biomaterials, 2014. **35**(9): p. 2651-2663.

12. Song, S. and S. Roy, *Progress and challenges in macroencapsulation approaches for type 1 diabetes (T1D) treatment: Cells, biomaterials, and devices.* Biotechnology and bioengineering, 2016.

13. Swioklo, S. and C.J. Connon, *Keeping cells in their place: the future of stem cell encapsulation*. 2016, Taylor & Francis.

14. Weir, G., *Islet encapsulation: advances and obstacles.* Diabetologia, 2013. **56**(7): p. 1458-1461.

15. Nafea, E., et al., *Immunoisolating semi-permeable membranes for cell encapsulation: focus on hydrogels.* Journal of Controlled Release, 2011. **154**(2): p. 110-122.

16. Murua, A., et al., *Cell microencapsulation technology: towards clinical application.* Journal of controlled release, 2008. **132**(2): p. 76-83.

17. Schweicher, J., C. Nyitray, and T.A. Desai, *Membranes to achieve immunoprotection of transplanted islets.* Frontiers in bioscience (Landmark edition), 2014. **19**: p. 49.

18. Barkai, U., A. Rotem, and P. de Vos, *Survival of encapsulated islets: More than a membrane story.* World journal of transplantation, 2016. **6**(1): p. 69.

19. Lim, F. and A.M. Sun, *Microencapsulated islets as bioartificial endocrine pancreas.* Science, 1980. **210**(4472): p. 908-910.

20. Davis, N.E., et al., *Enhanced function of pancreatic islets co-encapsulated with ECM proteins and mesenchymal stromal cells in a silk hydrogel.* Biomaterials, 2012. **33**(28): p. 6691-6697.

21. Khajehdehi, M., et al., *Function of Rat Diabetic Islets Improved By Coculturing with Pancreatic Mesenchymal Stromal Cells.* J Stem Cell Res Transplant, 2015. **2**(1): p. 1016.

22. Wang, Z. and D.C. Thurmond, *Mechanisms of biphasic insulin-granule exocytosis–roles of the cytoskeleton, small GTPases and SNARE proteins.* Journal of cell science, 2009. **122**(7): p. 893-903.

23. Fotino, N., C. Fotino, and A. Pileggi, *Re-engineering islet cell transplantation.* Pharmacological Research, 2015.

24. Muoio, D.M. and C.B. Newgard, *Molecular and metabolic mechanisms of insulin resistance and β-cell failure in type 2 diabetes.* Nature reviews Molecular cell biology, 2008. **9**(3): p. 193-205.

25. Krishnan, R., et al., *Noninvasive evaluation of the vascular response to transplantation of alginate encapsulated islets using the dorsal skin-fold model.* Biomaterials, 2014. **35**(3): p. 891-898.

26. Qi, M., *Transplantation of encapsulated pancreatic islets as a treatment for patients with type 1 diabetes mellitus.* Advances in Medicine, 2014. **2014**.

27. Whiting, D.R., et al., *IDF diabetes atlas: global estimates of the prevalence of diabetes for 2011 and 2030.* Diabetes research and clinical practice, 2011. **94**(3): p. 311-321.

28. Park, J.H., et al., *Nanocoating of Single Cells: From Maintenance of Cell Viability to Manipulation of Cellular Activities.* Advanced Materials, 2014. **26**(13): p. 2001-2010.

29.   Scharp, D.W. and P. Marchetti, *Encapsulated islets for diabetes therapy: history, current progress, and critical issues requiring solution.* Advanced drug delivery reviews, 2014. **67**: p. 35-73.

30.   Banting, F., et al., *Pancreatic extracts in the treatment of diabetes mellitus.* Canadian Medical Association Journal, 1922. **12**(3): p. 141.

31.   Li, N., et al., *The preservation of islet with alginate encapsulation in the process of transportation.* Biotechnology and applied biochemistry, 2015.

32.   Marchioli, G., et al., *Fabrication of three-dimensional bioplotted hydrogel scaffolds for islets of Langerhans transplantation.* Biofabrication, 2015. **7**(2): p. 025009.

33.   Shapiro, A.J., et al., *International trial of the Edmonton protocol for islet transplantation.* New England Journal of Medicine, 2006. **355**(13): p. 1318-1330.

34.   Naftanel, M.A. and D.M. Harlan, *Pancreatic islet transplantation.* PLoS Med, 2004. **1**(3): p. e58.

35.   Kojima, N., S. Takeuchi, and Y. Sakai. *Engineering of pseudoislets: effect on insulin secretion activity by cell number, cell population, and microchannel networks*. in *Transplantation proceedings*. 2014. Elsevier.

36.   Kulkarni, R.N., *The islet β-cell.* The international journal of biochemistry & cell biology, 2004. **36**(3): p. 365-371.

37.   Fu, Z., E.R. Gilbert, and D. Liu, *Regulation of insulin synthesis and secretion and pancreatic Beta-cell dysfunction in diabetes.* Current diabetes reviews, 2013. **9**(1): p. 25.

38.   Grapin-Botton, A., *Ductal cells of the pancreas.* The international journal of biochemistry & cell biology, 2005. **37**(3): p. 504-510.

39. Saito, H., et al., *Generation of glucose-responsive functional islets with a three-dimensional structure from mouse fetal pancreatic cells and iPS cells in vitro.* PloS one, 2011. **6**(12): p. e28209.

40. Hwang, J.W., et al., *Functional clustering of pancreatic islet cells using concave microwell array.* Macromolecular Research, 2011. **19**(12): p. 1320-1326.

41. Korsgren, O., et al., *Optimising islet engraftment is critical for successful clinical islet transplantation.* Diabetologia, 2008. **51**(2): p. 227-232.

42. NIH. *National institute of diabetes and digestive and kidney disease*. [cited 2016 20 December]; Available from: https://www.niddk.nih.gov/health-information/diabetes.

43. research, H.f.f.p.c. *Pancreas and nearby organs*. [cited 2016 20 December]; Available from: http://pancreatic.org/pancreatic-cancer/about-the-pancreas/the-pancreas/.

44. Jansson, L., et al., *Pancreatic islet blood flow and its measurement.* Upsala journal of medical sciences, 2016: p. 1-15.

45. Giraldo, J.A., J.D. Weaver, and C.L. Stabler, *Enhancing Clinical Islet Transplantation through Tissue Engineeering Strategies.* Journal of diabetes science and technology, 2010. **4**(5): p. 1238-1247.

46. Skelin, M., M. Rupnik, and A. Cencic, *Pancreatic beta cell lines and their applications in diabetes mellitus research.* Altex, 2010. **27**(2): p. 105-113.

47. Alismail, H. and S. Jin, *Microenvironmental stimuli for proliferation of functional islet β-cells.* Cell & bioscience, 2014. **4**(1): p. 12.

48. Ciszak, E., et al., *Role of C-terminal B-chain residues in insulin assembly: the structure of hexameric Lys B28 Pro B29-human insulin.* Structure, 1995. **3**(6): p. 615-622.

49.   Weiss, M., D.F. Steiner, and L.H. Philipson, *Insulin Biosynthesis, Secretion, Structure, and Structure-Activity Relationships.* 2009.

50.   Dreamstime. *Structure of human insulin diagramed in two different ways*. [cited 2017 10 January]; Available from: https://www.dreamstime.com/stock-images-structure-human-insulin-image27081204.

51.   Olson, A.L., *Regulation of GLUT4 and insulin-dependent glucose flux.* ISRN Molecular Biology, 2012. **2012**.

52.   Kim, K.A. and M.S. Lee, *Role and mechanism of pancreatic β-cell death in diabetes: The emerging role of autophagy.* Journal of diabetes investigation, 2010. **1**(6): p. 232-238.

53.   Cnop, M., et al., *Mechanisms of pancreatic β-cell death in Type 1 and Type 2 diabetes many differences, few similarities.* Diabetes, 2005. **54**(suppl 2): p. S97-S107.

54.   Mathis, D., L. Vence, and C. Benoist, *β-Cell death during progression to diabetes.* Nature, 2001. **414**(6865): p. 792-798.

55.   Wang, C., Y. Guan, and J. Yang, *Cytokines in the progression of pancreatic β-cell dysfunction.* International journal of endocrinology, 2010. **2010**.

56.   Pagliuca, F.W., et al., *Generation of functional human pancreatic β cells in vitro.* Cell, 2014. **159**(2): p. 428-439.

57.   Millman, J.R., et al., *Generation of stem cell-derived [beta]-cells from patients with type 1 diabetes.* Nature communications, 2016. **7**.

58.   Melton, D.A., *Chapter Four-Applied Developmental Biology: Making Human Pancreatic Beta Cells for Diabetics.* Current topics in developmental biology, 2016. **117**: p. 65-73.

59.   Chick, W.L., et al., *Artificial pancreas using living beta cells:. effects on glucose homeostasis in diabetic rats.* Science, 1977. **197**(4305): p. 780-782.

60.   Kepsutlu, B., et al., *Design of bioartificial pancreas with functional micro/nano-based encapsulation of islets.* Current pharmaceutical biotechnology, 2014. **15**(7): p. 590-608.

61.   Colton, C.K., *Oxygen supply to encapsulated therapeutic cells.* Advanced drug delivery reviews, 2014. **67**: p. 93-110.

62.   Soon-Shiong, P., et al., *Insulin independence in a type 1 diabetic patient after encapsulated islet transplantation.* The Lancet, 1994. **343**(8903): p. 950-951.

63.   Calafiore, R., et al., *Microencapsulated Pancreatic Islet Allografts Into Nonimmunosuppressed Patients With Type 1 Diabetes First two cases.* Diabetes Care, 2006. **29**(1): p. 137-138.

64.   Tuch, B.E., et al., *Safety and viability of microencapsulated human islets transplanted into diabetic humans.* Diabetes care, 2009. **32**(10): p. 1887-1889.

65.   Jacobs-Tulleneers-Thevissen, D., et al., *Sustained function of alginate-encapsulated human islet cell implants in the peritoneal cavity of mice leading to a pilot study in a type 1 diabetic patient.* Diabetologia, 2013. **56**(7): p. 1605-1614.

66.   Meier, R., et al., *Survival of free and encapsulated human and rat islet xenografts transplanted into the mouse bone marrow.* PloS one, 2014. **9**(3): p. e91268.

67.   de Vos, P., et al., *The association between in vivo physicochemical changes and inflammatory responses against alginate based microcapsules.* Biomaterials, 2012. **33**(22): p. 5552-5559.

68.   Lee, B.R., et al., *In situ formation and collagen-alginate composite encapsulation of pancreatic islet spheroids.* Biomaterials, 2012. **33**(3): p. 837-845.

69.   Dufrane, D., et al., *Six-month survival of microencapsulated pig islets and alginate biocompatibility in primates: proof of concept.* Transplantation, 2006. **81**(9): p. 1345-1353.

70.   Qi, C., et al., *Biomaterials as carrier, barrier and reactor for cell-based regenerative medicine.* Protein & cell, 2015. **6**(9): p. 638-653.

71.   de Vos, P., et al., *Polymers in cell encapsulation from an enveloped cell perspective.* Advanced drug delivery reviews, 2014. **67**: p. 15-34.

72.   Juárez, G.A.P., et al., *Immunological and technical considerations in application of alginate-based microencapsulation systems.* Frontiers in bioengineering and biotechnology, 2014. **2**.

73.   Orive, G., et al., *Cell encapsulation: technical and clinical advances.* Trends in pharmacological sciences, 2015. **36**(8): p. 537-546.

74.   Krishnan, R., et al., *Islet and stem cell encapsulation for clinical transplantation.* The review of diabetic studies: RDS, 2014. **11**(1): p. 84.

75.   Lee, K.Y. and D.J. Mooney, *Alginate: properties and biomedical applications.* Progress in polymer science, 2012. **37**(1): p. 106-126.

76.   Sarker, B., et al., *Alginate-based hydrogels with improved adhesive properties for cell encapsulation.* International journal of biological macromolecules, 2015. **78**: p. 72-78.

77.   Mazzitelli, S., et al., *Preparation of cell-encapsulation devices in confined microenvironment.* Advanced drug delivery reviews, 2013. **65**(11): p. 1533-1555.

78. Rokstad, A.M.A., et al., *Advances in biocompatibility and physico-chemical characterization of microspheres for cell encapsulation.* Advanced drug delivery reviews, 2014. **67**: p. 111-130.

79. Vo, T.S., et al., *The beneficial properties of marine polysaccharides in alleviation of allergic responses.* Molecular nutrition & food research, 2015. **59**(1): p. 129-138.

80. Montanucci, P., et al., *Insights in behavior of variably formulated alginate-based microcapsules for cell transplantation.* BioMed research international, 2015. **2015**.

81. Rezende, R., et al., *Experimental characterisation of the alginate gelation process for rapid prototyping.* Chem. Eng. Trans., 2007. **11**: p. 509-514.

82. Kashima, K. and M. Imai, *Advanced membrane material from marine biological polymer and sensitive molecular-size recognition for promising separation technology*. 2012: INTECH Open Access Publisher.

83. Whelehan, M. and I.W. Marison, *Microencapsulation using vibrating technology.* Journal of microencapsulation, 2011. **28**(8): p. 669-688.

84. Prüsse, U., et al., *Comparison of different technologies for alginate beads production.* Chemical Papers, 2008. **62**(4): p. 364-374.

85. Mazzitelli, S., et al., *Encapsulation of eukaryotic cells in alginate microparticles: cell signaling by TNF-alpha through capsular structure of cystic fibrosis cells.* Journal of cell communication and signaling, 2011. **5**(2): p. 157-165.

86. Herrero, E., E.M. Del Valle, and M. Galan, *Development of a new technology for the production of microcapsules based in atomization processes.* Chemical Engineering Journal, 2006. **117**(2): p. 137-142.

87. Gryshkov, O., et al., *Process engineering of high voltage alginate encapsulation of mesenchymal stem cells.* Materials Science and Engineering: C, 2014. **36**: p. 77-83.

88. Wilson, J.T. and E.L. Chaikof, *Challenges and emerging technologies in the immunoisolation of cells and tissues.* Advanced drug delivery reviews, 2008. **60**(2): p. 124-145.

89. Sakata, N., et al., *Encapsulated islets transplantation: past, present and future.* World journal of gastrointestinal pathophysiology, 2012. **3**(1): p. 19.

90. Li, W., et al., *The effect of layer-by-layer assembly coating on the proliferation and differentiation of neural stem cells.* ACS applied materials & interfaces, 2015. **7**(5): p. 3018-3029.

91. Gormley, A.J., et al., *Layer-by-layer self-assembly of polymer films and capsules through coiled-coil peptides.* Chemistry of Materials, 2015. **27**(16): p. 5820-5824.

92. Costa, R.R. and J.F. Mano, *Polyelectrolyte multilayered assemblies in biomedical technologies.* Chemical Society Reviews, 2014. **43**(10): p. 3453-3479.

93. Joseph, N., et al., *Layer-by-layer preparation of polyelectrolyte multilayer membranes for separation.* Polymer Chemistry, 2014. **5**(6): p. 1817-1831.

94. Decher, G., *Fuzzy nanoassemblies: toward layered polymeric multicomposites.* science, 1997. **277**(5330): p. 1232-1237.

95. Wilson, J.T., et al., *Cell surface engineering with polyelectrolyte multilayer thin films.* Journal of the American Chemical Society, 2011. **133**(18): p. 7054-7064.

96. Zhi, Z.-L., F. Khan, and J.C. Pickup, *Multilayer nanoencapsulation: a nanomedicine technology for diabetes research and management.* Diabetes research and clinical practice, 2013. **100**(2): p. 162-169.

97.   Zhi, Z.-l., et al., *Nano-scale encapsulation enhances allograft survival and function of islets transplanted in a mouse model of diabetes.* Diabetologia, 2012. **55**(4): p. 1081-1090.

98.   Gribova, V., R. Auzely-Velty, and C. Picart, *Polyelectrolyte multilayer assemblies on materials surfaces: from cell adhesion to tissue engineering.* Chemistry of Materials, 2011. **24**(5): p. 854-869.

99.   Moussallem, M.D., et al., *Smooth muscle cell phenotype modulation and contraction on native and cross-linked polyelectrolyte multilayers.* Biomacromolecules, 2009. **10**(11): p. 3062-3068.

100.   Zhou, T.C., et al., *Bioreactors, cell culture, commercial production.* Encyclopedia of Industrial Biotechnology, 2010.

101.   Pörtner, R., et al., *Fixed bed reactors for the cultivation of mammalian cells: design, performance and scale-up.* Open Biotechnol J, 2007. **1**(1): p. 41-46.

102.   Wang, D., et al., *The bioreactor: a powerful tool for large-scale culture of animal cells.* Current pharmaceutical biotechnology, 2005. **6**(5): p. 397-403.

103.   Martin, I., D. Wendt, and M. Heberer, *The role of bioreactors in tissue engineering.* TRENDS in Biotechnology, 2004. **22**(2): p. 80-86.

104.   Storm, M.P., et al., *Hollow Fiber Bioreactors for In Vivo-like Mammalian Tissue Culture.* Journal of visualized experiments: JoVE, 2016(111).

105.   Philippsen, C.G., A.C.F. Vilela, and L. Dalla Zen, *Fluidized bed modeling applied to the analysis of processes: review and state of the art.* Journal of Materials Research and Technology, 2015. **4**(2): p. 208-216.

106. Brotherton, J.D. and P.C. Chau, *Modeling of Axial-Flow Hollow Fiber Cell Culture Bioreactors.* Biotechnology progress, 1996. **12**(5): p. 575-590.

107. Huang, K.-S., et al., *Electrostatic droplets assisted synthesis of alginate microcapsules.* Drug delivery and translational research, 2011. **1**(4): p. 289-298.

108. Bhujbal, S.V., et al., *A novel multilayer immunoisolating encapsulation system overcoming protrusion of cells.* Scientific reports, 2014. **4**.

109. Hoesli, C.A., et al., *Pancreatic cell immobilization in alginate beads produced by emulsion and internal gelation.* Biotechnology and bioengineering, 2011. **108**(2): p. 424-434.

110. Lange-Asschenfeldt, S., et al., *Applicability of confocal laser scanning microscopy for evaluation and monitoring of cutaneous wound healing.* Journal of biomedical optics, 2012. **17**(7): p. 0760161-07601610.

111. Roessner, E.D., M. Vitacolonna, and P. Hohenberger, *Confocal laser scanning microscopy evaluation of an acellular dermis tissue transplant (Epiflex®).* PloS one, 2012. **7**(10): p. e45991.

112. Rossetti, F.b.C., L.v.V. Depieri, and M.V.r.L.B. Bentley, *Confocal laser scanning microscopy as a tool for the investigation of skin drug delivery systems and diagnosis of skin disorders*, in *Confocal Laser Microscopy-Principles and Applications in Medicine, Biology, and the Food Sciences*. 2013, InTech.

113. BitesizeBio. *Microscopy & Imaging.* [cited 2017 25 April]; Available from: http://bitesizebio.com/19958/what-is-confocal-laser-scanning-microscopy/.

114. Bhaiji, T., Z.L. Zhi, and J.C. Pickup, *Improving cellular function and immune protection via layer-by-layer nanocoating of pancreatic islet β-cell spheroids cocultured with*

mesenchymal stem cells. Journal of Biomedical Materials Research Part A, 2012. **100**(6): p. 1628-1636.

115. Mueller, K.R., et al., *Differences in glucose-stimulated insulin secretion in vitro of islets from human, nonhuman primate, and porcine origin.* Xenotransplantation, 2013. **20**(2): p. 75-81.

116. Hals, I., et al., *Alginate microencapsulation of human islets does not increase susceptibility to acute hypoxia.* Journal of diabetes research, 2013. **2013**.

117. Goosen, M.F., *Fundamentals of animal cell encapsulation and immobilization.* 1992: CRC Press.

118. Orive, G., et al., *Survival of different cell lines in alginate-agarose microcapsules.* European journal of pharmaceutical sciences, 2003. **18**(1): p. 23-30.

119. de Haan, B.J., M.M. Faas, and P. de Vos, *Factors influencing insulin secretion from encapsulated islets.* Cell transplantation, 2003. **12**(6): p. 617-625.

120. Wung, N., et al., *Hollow fibre membrane bioreactors for tissue engineering applications.* Biotechnology letters, 2014. **36**(12): p. 2357-2366.

121. Lu, J., et al., *A New Fluidized Bed Bioreactor Based on Diversion-Type Microcapsule Suspension for Bioartificial Liver Systems.* PloS one, 2016. **11**(2): p. e0147376.

122. Al-Zahrani, A. and M. Daous, *Bed expansion and average bubble rise velocity in a gas-solid fluidized bed.* Powder technology, 1996. **87**(3): p. 255-257.

123. Abreu, F.O., et al., *Influence of the composition and preparation method on the morphology and swelling behavior of alginate–chitosan hydrogels.* Carbohydrate Polymers, 2008. **74**(2): p. 283-289.

124. Spier, M.R., et al., *APPLICATION OF DIFFERENT TYPES OF BIOREACTORS IN BIOPROCESSES.* 2011.

125. Zhao, J., et al., *Bioreactors for tissue engineering: An update.* Biochemical Engineering Journal, 2016. **109**: p. 268-281.

126. Bancroft, G.N., V.I. Sikavitsas, and A.G. Mikos, *Technical note: Design of a flow perfusion bioreactor system for bone tissue-engineering applications.* Tissue engineering, 2003. **9**(3): p. 549-554.

127. Goldbach, H.E. and M.A. Wimmer, *Boron in plants and animals: Is there a role beyond cell-wall structure?* Journal of Plant Nutrition and Soil Science, 2007. **170**(1): p. 39-48.

128. Yang, Q., et al., *Fluidized-bed bioartificial liver assist devices (BLADs) based on microencapsulated primary porcine hepatocytes have risk of porcine endogenous retroviruses transmission.* Hepatology international, 2010. **4**(4): p. 757-761.

129. Chang, Y. and H.A. Chase, *Development of operating conditions for protein purification using expanded bed techniques: the effect of the degree of bed expansion on adsorption performance.* Biotechnology and bioengineering, 1996. **49**(5): p. 512-526.

130. Diaspro, A., et al., *Single living cell encapsulation in nano-organized polyelectrolyte shells.* Langmuir, 2002. **18**(13): p. 5047-5050.

131. Picart, C., *Polyelectrolyte multilayer films: from physico-chemical properties to the control of cellular processes.* Current medicinal chemistry, 2008. **15**(7): p. 685-697.

132. Frezza, C., et al., *Metabolic profiling of hypoxic cells revealed a catabolic signature required for cell survival.* PloS one, 2011. **6**(9): p. e24411.

133. de Vos, P., et al., *Alginate-based microcapsules for immunoisolation of pancreatic islets.* Biomaterials, 2006. **27**(32): p. 5603-5617.

134. Cui, W., et al. *A membrane-mimetic barrier for islet encapsulation*. in *Transplantation proceedings*. 2004. Elsevier.

135. Kozlovskaya, V., et al., *Hydrogen-bonded LbL shells for living cell surface engineering.* Soft Matter, 2011. **7**(6): p. 2364-2372.

136. Hajicharalambous, C.S., et al., *Nano-and sub-micron porous polyelectrolyte multilayer assemblies: biomimetic surfaces for human corneal epithelial cells.* Biomaterials, 2009. **30**(23): p. 4029-4036.

137. Sitbon, M., et al., *Use of a focal immunofluorescence assay on live cells for quantitation of retroviruses: distinction of host range classes in virus mixtures and biological cloning of dual-tropic murine leukemia viruses.* Virology, 1985. **141**(1): p. 110-118.

138. O'Connor, C.M., J.U. Adams, and J. Fairman, *Essentials of cell biology.* Cambridge: NPG Education, 2010.

139. Cooper, G.M. and R.E. Hausman, *The cell*. 2000: Sinauer Associates Sunderland.

140. Jun, Y., et al., *3D co-culturing model of primary pancreatic islets and hepatocytes in hybrid spheroid to overcome pancreatic cell shortage.* Biomaterials, 2013. **34**(15): p. 3784-3794.

141. Lee, S.-A., et al., *Functional 3D human primary hepatocyte spheroids made by co-culturing hepatocytes from partial hepatectomy specimens and human adipose-derived stem cells.* 2012.

142. Wong, S.F., et al., *Concave microwell based size-controllable hepatosphere as a three-dimensional liver tissue model.* Biomaterials, 2011. **32**(32): p. 8087-8096.

143. Griffith, L.G. and M.A. Swartz, *Capturing complex 3D tissue physiology in vitro.* Nature reviews Molecular cell biology, 2006. **7**(3): p. 211-224.

144.   Kizilel, S., et al., *Encapsulation of pancreatic islets within nano-thin functional polyethylene glycol coatings for enhanced insulin secretion.* Tissue Engineering Part A, 2010. **16**(7): p. 2217-2228.

145.   Wilson, J.T., W. Cui, and E.L. Chaikof, *Layer-by-layer assembly of a conformal nanothin PEG coating for intraportal islet transplantation.* Nano letters, 2008. **8**(7): p. 1940-1948.

146.   Barshes, N.R., S. Wyllie, and J.A. Goss, *Inflammation-mediated dysfunction and apoptosis in pancreatic islet transplantation: implications for intrahepatic grafts.* Journal of leukocyte biology, 2005. **77**(5): p. 587-597.

147.   Corrêa-Giannella, M.L. and A.S.R. do Amaral, *Pancreatic islet transplantation.* Diabetology & metabolic syndrome, 2009. **1**(1): p. 9.